People's Democratic Republic of Algeria
Ministry of Higher Education and Scientific Research
University of 8 May 1945 Guelma

Faculty of Sciences and Technology
Department of Process Engineering
Laboratory of Industrial Analysis and Materials Engineering (LAIGM)

Thesis

Submitted in Candidacy for the Degree of *Doctorate in Third Cycle*

Field: Sciences and Technology Stream: Process Engineering

Speciality: Chemical Engineering

Presented by:

GHEDIRI Dalia

Title

Design and development of a screen-printed sensor modified with Ru nanoparticles for the detection of dopamine and paracetamol

Defended on: 13/01/2026 Composition of the jury:

Full name	Rank	University	
BENHAMZA Mohamed El Hocine	Professor	Univ. of 8 mai 1945 Guelma	President
CHELAGHMIA Mohamed Lyamine	Professor	Univ. of 8 mai 1945 Guelma	Supervisor
NACEF Mouna	Professor	Univ. of 8 mai 1945 Guelma	Co- supervisor
BERREDJEM Yamina	Professor	Univ. Badji Mokhtar of Annaba	Examiner
KOUADRI Imane	MCA	Univ. of 8 mai 1945 Guelma	Examiner

Academic year: 2025-2026

République Algérienne Démocratique et Populaire
Ministère de l'Enseignement Supérieur et de la Recherche Scientifique
Université 8 Mai 1945 Guelma

Faculté des Sciences et de la Technologie
Département de Génie des procédés
Laboratoire d'Analyses Industrielles et Génie des Matériaux (LAIGM)

THÈSE

En Vue de l'Obtention du Diplôme de Doctorat en Troisième Cycle

Domaine : Sciences et Technologie Filière : Génie des procédés

Spécialité : Génie Chimique

Présentée par

GHEDIRI Dalia

Intitulée

Conception et développement d'un capteur sérigraphié modifié par des nanoparticules de Ru pour la détection de la dopamine et du paracétamol

Soutenue le : 13/01/2026 Composition du jury:

Nom et Prénom	Grade	Université	
BENHAMZA Mohamed El Hocine	Professeur	Univ. de 8 mai 1945 Guelma	Président
CHELAGHMIA Mohamed Lyamine	Professeur	Univ. de 8 mai 1945 Guelma	Encadreur
NACEF Mouna	Professeur	Univ. de 8 mai 1945 Guelma	Co-encadreur
BERREDJEM Yamina	Professeur	Univ. de Badji Mokhtar Annaba	Examinatrice
KOUADRI Imane	MCA	Univ. de 8 mai 1945 Guelma	Examinatrice

Année Universitaire: 2025-2026

Dedication

I dedicate this work to all those who have lefit their mark on my journey:

To the one who taught me a letter

To all those with whom I have had the honor ofi sharing the benches ofi learning

To those who have instilled in me the love ofi science and have awakened the

scientifiic curiosity necessary fior any research activity

To those who have given me their support and instilled hope in me, to those

who have loved me.

Thank you firom the bottom ofi my heart

Ghediri Dalia

Acknowledgments

First and foremost, I extend my limitless gratitude to Allah, the Ever Magnificent, the Ever Thankful, for His divine guidance, help, and blessings that enabled me to complete these endless years of study.
At the completion of the long and winding road this thesis has been, I would like to thank:

My thesis supervisor

I would like to extend my sincere thanks to my thesis director, Professor **Mohamed Lyamie CHELAGHMIA** without whom this thesis would not have been realized. These five years working at your side have been truly enriching. Above all ,thank you for welcoming me into your research team, thanks for your encouragement, particularly when I was unwell, and also for your valuable advice, your motivation, your criticisms, and your always relevant remarks. Your extensive knowledge has been of precious help to me. I also thank you for your ongoing availability, even during weekends and holidays.

My co-thesis supervisor

I would also like to thank my second thesis supervisor, Professor **Mouna NACEF**. You always smile and have energy. Thank you for your presence in this thesis, for your goodness. Thank you also for your unconditional and punctual support, as well as for your unfaltering optimism, especially during the time I was ill, which enabled me to successfully finalize this work.

Jury Members

I would like to thank all the jury members for accepting to evaluate the work which has been done in this thesis.

I would also like to thank Professor **Mohamed El Hocine BENHAMZA**, as well as Professor **Abed Mohamed AFFOUNE**, Successive directors of the LAIGM laboratory, for having taken me into their laboratory. Thank you for welcoming me in your team and more importantly for having allowed me to use the facilities of the LAIGM laboratory.

Colleagues and friends of the laboratory

I would also like to thank the people I encountered on a daily basis throughout my doctoral life. To begin with, I would like to thank **Houda BOUKHDENNA** in particular. I am truly grateful for your attentiveness and for all the times that I went to your office in a frustrated despair state to complain and announce my weariness. Thank you for being ever willing to listen without ever getting tired of my complaints. Thanks also to **Nahla KADRI** for the coffee breaks, for all the solutions that were prepared and for all the cleaned glassware. Thanks for all the nice moments shared together.

I also keep remembering all those individuals who are not formally under the tutelage of this thesis but who have played a key role in its completion :

My Family

To my family who have always supported me in all my endeavors, and most especially to my parents, I am thankful.

To my mother, for all the pride I see in your eyes, for your unconditional support, and for always helping me get through the tough times, I appreciate how you have always been so devoted to my wants, and how you have always respected my decisions. Thank you, Mom.

To my father, I appreciate how you have always inspired me to do better. You have taught me the value of perseverance and perfectionism. This drive to better myself has brought me so far, and I owe it all to you.

To my brothers **Ahmed** and **Mohamed**, my unwavering pillars, and the ones life has allowed me as support. Thank you for the moments we have shared and for our complicity. I am proud to be your sister.
To my best cousins **Asma** and **Ihssen,** thank you for all the support during the doctoral training period. I really appreciate all your support and for everything you tried to help me with.
To **Hanna** and **Katia**, thank you for all the laughter and happiness we have shared, and for all the time spent together. I know there are even more to come!

My companions

To **Dounia**, Thank you for your friendship, thank you for your support, thank you for being there in the most difficult moments. Thank you for every night you spent with me, for taking care of me at the university residence. Thank you for your presence, and for all the good and bad times shared together.

I think this paragraph is even harder to write than the introduction.....

To my friends, thank you for your presence in the wonderful moments and the super difficult moments. I appreciate you being my haven of love and solace.I want to express my gratitude to **Anissa** for being a part of my everyday life for so many years and for always supporting me in everything I do.I'll censor the majority of what I want to say to **Anfel**. Please don't thank me; I am the one who sincerely appreciates your unwavering love and every moment you have looked out for me.
It's a pleasure to have gone through the doctoral journey with **Rania** and **Rayane**. I appreciate you being there with me everywhere. Thank you for all the memories we made together.

To **Rayane,** you are the greatest, I appreciate your positive energy that has always made me feel better and your presence in reminding me of what really matters.Thank you for your patience with my many complaints, and your unwavering support.
To **Rania**, I express my gratitude for our more than 17 year friendship, for bringing joy into my life when I needed it most, and for your invaluable assistance.

Finally, I extend my profound gratitude to the person who accompanied me throughout this journey, **my doctor**. A huge thank you to the one who supports me. Thank you for your attentive listening, even in moments of fatigue, for your repeated efforts to understand my thesis subject, as well as for your unwavering support and your patience. I hope I can be of support to you, just as you have been to me.

Abstract

The careful use of drug doses administered in therapeutic or surgical environments is essential since even minor variations may have catastrophic health implications. Some drugs can cause permanent damage to organs through overdose, which may necessitate transplantation or compromise the functions of vital physiological systems. Paracetamol is a notable example of an analgesic and antipyretic drug, as its misuse or overdose may lead to acute liver toxicity as well as renal damage. Simultaneously, a sensitive monitoring of some physiological parameters is needed, as their non-pathological levels are generally in accordance with the pathogenesis or development of disease. Fluctuations in brain dopamine are directly implicated in neurodegenerative illnesses like Parkinson's disease and schizophrenia. Clinically relevant evaluation, drug management with therapeutic intervention, and proactive health care thus demand accurate and reproducible quantitation of these bioactive molecules.

A selective and simple electrochemical technique was created for the simultaneous analysis of paracetamol (PA) and dopamine (DA). The technique utilized a commercially available screen printed electrode (SPE), that was electrochemically activated in 1.0 M H_2SO_4 via cyclic voltammetry and modified with ruthenium nanoparticles. Electrochemical behavior before and after modification was investigated using electrochemical impedance spectroscopy (EIS) and cyclic voltammetry (CV).. The findings indicate that both electrochemical activation and ruthenium nanoparticle electrodeposition enhance the conductivity and surface area of the screen-printed electrode**.** The structural and interfacial properties of the nanocomposite were also examined using scanning electron microscopy (SEM), transmission electron microscopy (TEM), energy-dispersive X-ray spectroscopy (EDX), X-ray diffraction (XRD), fourier transform infrared spectroscopy (FT-IR), and atomic force microscopy (AFM).

The detection of both dopamine and paracetamol was assessed through cyclic voltammetry, electrochemical impedance spectroscopy, and square wave voltammetry (SWV). Under optimized conditions, it was found that the developed sensor was able to detect dopamine and paracetamol efficiently through the three methods. In the case of single analyte detection, SWV and EIS showed better performance, with SWV presenting the best sensitivity (1.93 and 1.06 μA mM^{-1} cm^{-2}) and lowest detection limits (0.11 μM for DA and 0.17 μM for PA). However, CV was found to be better for simultaneous detection as it presented wider linear ranges (1.0–300 μM for DA and 1.0–400 μM for PA). Moreover, the RuNPs/ASPE sensor also exhibited good repeatability, reproducibility, stability, and selectivity. The sensor was successfully utilized for PA and DA determination in pharmaceutical preparations and human blood serum samples with good recovery percentages.

Keywords: Activated screen-printed electrode ,Graphite sensor, Dopamine, Paracetamol, Simultaneous determination, Pharmaceutical formulations.

Résumé

L'utilisation prudente des doses de médicaments administrées dans des environnements thérapeutiques ou chirurgicaux est essentielle, car même des légères variations peuvent avoir des implications catastrophiques pour la santé. Certains médicaments peuvent causer des dommages permanents aux organes en cas de surdosage, ce qui peut nécessiter une transplantation ou compromettre les fonctions des systèmes physiologiques vitaux. Le paracétamol est un exemple notable de médicament analgésique et antipyrétique, dont l'usage inapproprié ou le surdosage peut entraîner une hépatotoxicité aiguë ainsi que des atteintes rénales. Simultanément, une surveillance sensible de certains paramètres physiologiques est nécessaire, car leurs niveaux non pathologiques sont généralement en accord avec la pathogenèse ou le développement de la maladie. Les fluctuations de la dopamine cérébrale sont directement impliquées dans les maladies neurodégénératives comme la maladie de Parkinson et la schizophrénie. L'évaluation cliniquement pertinente, la gestion des médicaments avec intervention thérapeutique et les soins de santé proactifs exigent donc une quantification précise et reproductible de ces molécules bioactives.

Une technique électrochimique sélective et simple a été créée pour l'analyse simultanée du paracétamol (PA) et de la dopamine (DA). La technique utilise une électrode sérigraphiée (SPE) disponible dans le commerce, qui a été activée électrochimiquement dans 1,0 M H_2SO_4 par voltamétrie cyclique et modifiée avec des nanoparticules de ruthénium. Le comportement électrochimique avant et après modification a été étudié à l'aide de la spectroscopie d'impédance électrochimique (EIS) et de la voltampérométrie cyclique (CV). Les résultats indiquent que l'activation électrochimique et l'électrodéposition de nanoparticules de ruthénium améliorent la conductivité et la surface active de l'électrode sérigraphiée**.** Les propriétés structurelles et interfaciales du nanocomposite ont également été examinées en utilisant la microscopie électronique à balayage à émission (MEB), la microscopie électronique à transmission (MET), la spectroscopie de dispersion d'énergie des rayons X (SDX), la diffraction des rayons X (DRX), la spectroscopie infrarouge à transformée de Fourier (IRTF) et la microscopie à force atomique (MFA).

La détection à la fois de la dopamine et du paracétamol a été évaluée par voltamétrie cyclique, spectroscopie d'impédance électrochimique et voltamétrie à ondes carrées (SWV). Dans des conditions optimisées, il a été constaté que le capteur développé était capable de détecter la dopamine et le paracétamol efficacement à travers les trois méthodes. Dans le cas de la détection d'un seul analyte, SWV et EIS ont montré de meilleures performances, avec SWV présentant la meilleure sensibilité (1,93 et 1,06 μA mM^{-1} cm^{-2}) et les limites de détection les plus basses (0,11 μM pour DA et 0,17 μM pour PA). Cependant, la CV s'est avérée meilleure pour la détection simultanée car elle présentait des plages linéaires plus larges (1,0–300 μM pour la DA et 1,0–400 μM pour la PA). De plus, le capteur RuNPs/ASPE a également montré une bonne répétabilité, reproductibilité, stabilité et sélectivité. Le capteur a été utilisé avec succès pour la détermination de PA et de DA dans des préparations pharmaceutiques et des échantillons de sérum sanguin humain avec de bons pourcentages de récupération.

Mots-clés : Électrode activée, Electrode sérigraphiée, Capteur de graphite, Dopamine, Paracétamol, Détermination simultanée, Formulations pharmaceutiques.

ملخص

الاستخدام الحذر لجرعات الأدوية المُعطاة في البيئات العلاجية أو الجراحية أمر ضروري، إذ إن حتى التغيرات البسيطة قد تترتب عليها عواقب صحية كارثية. فبعض الأدوية يمكن أن تُسبب أضرارًا دائمة للأعضاء عند تناول جرعات زائدة، مما قد يستدعي إجراء عملية زرع أو يُعرّض وظائف الأنظمة الحيوية الأساسية للخطر. الباراسيتامول مثال على دواء مسكن وخافض للحرارة، و لكن سوء استخدامه أو تناول جرعة زائدة قد يسبب أضرارًا للكبد والكلى .وفي الوقت نفسه، هناك حاجة لمراقبة دقيقة لبعض المؤشرات الفسيولوجية، إذ إن مستوياتها غير المرضية غالبًا ما تكون مرتبطة بآليات نشوء المرض أو تطوره. على سبيل المثال، فإن تقلبات الدوبامين في الدماغ ترتبط بشكل مباشر بالأمراض التنكسية العصبية مثل مرض باركنسون والفصام. وبالتالي، فإن التقييم السريري الدقيق، وإدارة الأدوية بالتدخل العلاجي، والرعاية الصحية الاستباقية تتطلب قياسًا كميًا دقيقًا وقابلًا للتكرار لهذه الجزيئات النشطة بيولوجيًا.

تم ابتكار تقنية كهروكيميائية انتقائية وبسيطة للتحليل المتزامن لكل من الباراسيتامول (PA) والدوبامين (DA). تعتمد هذه التقنية على قطب مطبوع تجاريًا (SPE) تم تفعيله كهروكيميائيًا في 1.0 M H_2SO_4 باستخدام الفولتمترية الدورية (CV) ،ثم تم تعديله بجسيمات نانوية من الروثينيوم. تمت دراسة السلوك الكهروكيميائي قبل وبعد التعديل باستخدام مطيافية المقاومة الكهروكيميائية (EIS) والفولطامترية الدورية (CV). تشير النتائج إلى أن التنشيط الكهروكيميائي والترسيب الكهروكيميائي لجسيمات الروثينيوم النانوية يحسّنان الموصلية والمساحة السطحية النشطة للقطب المطبوع بالشاشة . كما جرى فحص الخصائصالبنائية والسطحية البينية لهذا المركب النانوي باستخدام المجهر الإلكتروني الماسح (SEM)، والمجهر الإلكتروني النافذ (TEM) ، ومطيافية الأشعة السينية المشتتة للطاقة (EDX)، وحيود الأشعة السينية (XRD)، ومطيافية الأشعة تحت الحمراء بتحويل فوريه (FTIR)، والمجهر القوة الذرية (AFM).

تم تقييم الكشف عن كل من الدوبامين والباراسيتامول باستخدام الفولتمترية الدورية، ومطيافية الممانعة الكهروكيميائية، والفولتمترية المربعة الموجة (SWV). وتحت ظروف مثالية، تبيّن أن المستشعر المطوَّر قادر على الكشف عن الدوبامين والباراسيتامول بكفاءة باستخدام الطرق الثلاث.في حالة الكشف عن محلل واحد، أظهرت كل من تقنية (SWV) و (EIS) أداءً أفضل، حيث قدّمت تقنية (SWV) أفضل حساسية ($1.06\ \mu A\ mM^{-1}\ cm^{-2}$, 1.93) وأدنى حدود للكشف (0.11 µM for DA and 0.17 µM for PA) . و مع ذلك، وُجد أن تقنية (CV) أفضل للكشف المتزامن،إذ قدّمت نطاقات خطية أوسع (1.0–300 µM DA) و (1.0–400 µM PA) . بالإضافة إلى ذلك، أظهر حساس RuNPs/ASPE تكرارية جيدة، وقابلية لإعادة الإنتاج، وثباتاً وانتقائية مميزة. وقد استُخدم الحساس بنجاح في تحديد (DA) و (PA) في المستحضرات الدوائية وعينات مصل الدم البشري مع نسب استرجاع جيدة.

الكلمات المفتاحية: قطب مفعل كيميائيًا كهربائيًا، قطب كهربائيً مطبوع بالشاشة، مستشعر جرافيتي، دوبامين، باراسيتامول، تحديد متزامن، تركيبات صيدلانية

Table of contents

Chapter II

Advances in modified screen printed sensors

Chapter III

Characterisation methods and experimental protocols

Part B

Impedimetric detection of dopamine and paracetamol

General conclusion

List of figures

Chapter I

Chapter II

Chapter III

Chapter IV

Part A

Part B

List of tables

Chapter I

Chapter II

Chapter III

Chapter IV
Part A

Chapter IV
Part B

List of abbreviations and symbols

Abbreviation	Significance
AA	Ascorbic acid
ABS	Acetate buffer solution
AFM	Atomic force microscopy
Amp	Amperometry
AuNPs	Gold nanoparticles
AgNPs	Silver nanoparticles
BPEI	branched polyethyleneimine
CNTs	Carbon nanotubes
CP	Conducting polymer
COVID-19	Coronavirus disease 2019
CA19–9	carbohydrate antigen 19–9
CEA	carcinogenic embryonic antigen
CV	Cyclic voltammetry
CA	Chronoamperometry
CE	Counter electrode
CAF	Caffeine
CPE	Carbon paste electrode
DA	Dopamine
DOPAC	3,4-Dihydroxyphenylacetic acid
DOX	Doxorubicin
DNA	Deoxyribonucleic Acid
DMSO	dimethyl sulfoxide
DPV	Differential pulse voltammetry
DPASV	Differential pulse anodic stripping voltammetry
EIS	Electrochemical impedance spectroscopy
EP	Epinephrine
FTIR	Fourier-transform infrared spectroscopy
Glu	Glucose
HPLC	High-performance liquid chromatography
INN	International non-proprietary name
ITO	Tin oxide
LOD	Limits of detection
L-DOPA	L-3,4-dihydroxyphenylalanine
MWCNTs	Multiwall carbon nanotubes
MIPs	Molecularly imprinted polymers
NSAIDs	Non-Steroidal Anti-Inflammatory Drugs
NAPQI	N-acetyl-p-benzo-quinone imine
NB	Note well
OTC	Over-the-counter

PA	Paracetamol
PtNPs	Platinum nanoparticles
PPy	Polypyrrole
PANI	Polyaniline
PTs	Polythiophene
PEDOT	Poly(3,4-ethylenedioxythiophene)
PET	polyethylene terephthalate
PBS	Phosphate buffer solution
Pd NPs	Palladium nanoparticles
RE	Reference electrode
RNA	Ribonucleic Acid
rGO	Reduced graphene oxide
SPEs	Screen-printed electrodes
SPIDEs	Screen-printed interdigitated electrodes
SWCNT	Single-walled carbon nanotube
SWV	Square wave voltammetry
SEM	Scanning electron microscopy
TEM	Transmission electron microscopy
UA	Uric acid
WE	Working electrode
XRD	X-ray diffraction

Symbols

Symbol	Significance
A	Electroactive surface area of the working electrode
C	Concentration of the analyte
$\mathbf{C}_{dl}$	Double layer capacitor
$\mathbf{C}_{\mathbf{PE}}$	Constant phase element
D	Diffusion coefficient
D	Interatomic distance
E	Potential
$\mathbf{E}_{\mathbf{Pa}}$	Oxidation peak potential
$\mathbf{E}_{\mathbf{Pc}}$	Reduction peak potential
$\mathbf{E}_{1/2}$	Half-wave potential
ΔEp	Anodic and cathodic peak potential difference
F	Faraday constant
I	Currents
$\mathbf{i}_{\mathbf{pa}}$	Anodic peak currents
$\mathbf{i}_{\mathbf{pc}}$	Cathodic peak currents
$\mathbf{k}^{\mathbf{o}}$	Electron transfer rate constant
L	Inductance
$\boldsymbol{n}$	Number of exchanged electrons
R	Universal gas constant
Rct	Charge transfer resistance
Rs	Solution resistance
t	Time
T	Temperature
τ	Period
υ	Scan rate
|Z|	Impedance
Zw	Warburg simulating element
$\mathbf{Z}_{\mathbf{L}}$	Impedance of an inductor
Λ	X-ray wavelength
θ	Incidence angle
ϕ	Phase shift
σ	Warburg coefficient.
ω	Angular frequency

General introduction

General introduction

Dopamine, a low molecular weight catecholamine neurotransmitter, is synthesized by a minority of neurons and plays a role in the central nervous system. Though occurring in relatively low concentrations in the brain, dopamine controls a wide variety of neuronal processes and modulates critical cognitive and motor processes. Dysregulation of dopamine is implicated in numerous disorders, including Parkinson's disease, schizophrenia, Tourette's syndrome, and hyperprolactinemia, leading to motor impairment, mood alterations, and motivational impairments. Thus, precise quantitation of the concentration of dopamine in biological samples is essential for correct neurological and medical diagnoses **[1].**

Paracetamol is an analgesic and antipyretic drug that is extensively employed. At therapeutic doses, paracetamol does not produce any side effects in human health. But liver damage, nephrotoxicity, and pancreatitis result from excessive intake **[2],** long-term administration, or co-administration with other drugs, emphasizing the need for proper regulation and quality control. International consumption of painkillers has increased dramatically, with paracetamol prescription in a decade doubling its rate to become one of the world's most consumed drugs.

It is therefore important to make concomitant measurements of both constituents because an investigation of their potential correlations can provide better understanding of brain and body functions and allow for the development of novel methods to study and recommend therapeutic interventions into illnesses.

While sensitive methods are needed for correct measurement of paracetamol and dopamine, existing pharmaceutical analysis techniques such as high-performance liquid chromatography**[3],** capillary electrophoresis**[4],** fluorescence spectrometry**[5],** all suffer severe limitations. Including low specificity, high cost, time-consuming protocols, and need for skilled operators, as well as interference from other processes and drug treatment effects, all of which are difficult to interpret. Electrochemical methods, however, provide a better, uncomplexed, and effective approach **[6].**

Electrochemistry underlies numerous industrial chemical processes and increasingly plays a vital role across an enormous spectrum of industries, including health and life sciences, materials science, renewable energy, pharmaceuticals, environmental sectors. Electrochemical sensors, for example, are extremely effective for substance detection due to the rapid response rate and convenience of use. Advances in recent years allowed developing miniaturized sensors based on disposable screen-printed carbon electrodes (SPCEs) possess numerous benefits over

traditional techniques, such as simple activation, disposability, smallness, high chemical stability, portability, broad electrochemical window, and affordability, all without the requirement for elaborate preparation. Moreover, the ability to modify the SPCE surface enormously increases its specificity and sensitivity, which illustrates the significance of material selection in maximizing their performance **[7].**

The advancements in nanotechnology have inspired the development of multi-billion dollar industries, allowing for novel methodologies in the synthesis of materials with unique properties. Carbon nanomaterials, polymer based nanocomposites and metal nanoparticles are under increasing scrutiny for their potential applications, particularly in electrochemical sensing. Metallic nanoparticles like gold, platinum, palladium, copper, nickel, and ruthenium possess distinct physicochemical and electronic properties compared to their bulk counterparts due to their nanoscale dimensions and distinctive structures. The metallic nanoparticles are the primary building blocks for developing novel materials, providing increased sensitivity, selectivity, and lower detection limits. Their inherent catalytic and conductive characteristics make them valuable as electronic mediators, facilitating improved electron transfer between redox sites on electrode surfaces and as catalysts to facilitate electrochemical reactions **[8].**

Ruthenium possesses a broad array of significant physical and chemical properties, which are the cause of its widespread application in industry and extensive research in the scientific community **[9-11].** This thesis presents ruthenium and its applications in industry. Along with this, recent progress in the production of ruthenium based electrochemical sensors for pharmaceutical sensing is highlighted.

This thesis aims at contributing to the development of novel functional materials for analytical electrochemistry. The study deals with the development and characterization of screen-printed graphite electrode based electrochemical sensors that are activated and decorated with ruthenium nanomaterials. The sensor was then employed for the monitoring and detection of biologically significant compounds.

On this basis, the four chapters of this thesis are structured as follows:

Chapter I provides an exhaustive bibliographic review of dopamine and paracetamol, with special emphasis on their biological significance and electrochemical behavior. Furthermore, it deals with the topic of electrochemical sensors, with special focus placed on screen-printed electrodes (SPEs) as promising alternatives to conventional analytical procedures for the sensing of these molecules.

Chapter II gives a wide overview of functional materials, and mostly nanoparticles. The chapter describes the role of nanotechnology in the evolution of electrochemical sensors and reviews different classes of nanomaterials and nanocomposites that have been used in the last few years for electrode modification. Their structural features, history, and synthesis methods are expounded in detail. Special focus is laid on ruthenium nanoparticles and their increasing importance in many areas, particularly the creation of electrochemical sensors. An overview of the current literature is also presented.

Chapter III is devoted to the theoretical background of surface analysis and the electrochemical techniques employed in this research work for characterization of the produced sensor. It also describes experimental setup associated with these techniques, as well as the detailed experimental protocols followed for electrode preparation.

Chapter IV is structured into two distinct parts:

Part A gives an account of the physicochemical characterization of unmodified screen-printed electrodes and electrodes modified with Ru nanoparticles. The electrochemical behavior of the electrodes was investigated by cyclic voltammetry and square wave voltammetry, allowing for the individual and simultaneous determination of dopamine and paracetamol, as well as real tests are studied by SWV in this chapter.

Part B describes the electrochemical characterization of the new sensor using an equivalent circuit model, Also the electrochemical activity of the new sensor toward dopamine and paracetamol oxidation was examined by EIS.

Finally, a general conclusion will summarize all the results and present the perspectives of this work.

References

[1]Chen C, Ren J, Zhao P, et al (2023) A novel dopamine electrochemical sensor based on a β-cyclodextrin/Ni-MOF/glassy carbon electrode. Microchemical Journal 194:109328.

[2] Annadurai K, Sudha V, Murugadoss G, Thangamuthu R (2021) Electrochemical sensor based on hydrothermally prepared nickel oxide for the determination of 4-acetaminophen in paracetamol tablets and human blood serum samples. Journal of Alloys and Compounds 852:156911.

[3] Zhang S, Li C, Zhou G, Che G, You J, Suo Y. Determination of the carbohydrates from Notopterygium forbesii Boiss by HPLC with fluorescence detection. Carbohydr Polym. 2013; 97(2):794–9.

[4] Wu P, Zhao X, Ding Y, et al (2023) Self-assembled multilayer Nb2C MXene/MnFe2O4 electrochemical sensor with Schottky junctions for the detection of acetaminophen and dopamine. Colloids and Surfaces A: Physicochemical and Engineering Aspects 667:131377.

[5] Kader Mohiuddin A, Shamsuddin Ahmed M, Jeon S (2022) Palladium doped α-MnO2 nanorods on graphene as an electrochemical sensor for simultaneous determination of dopamine and paracetamol. Applied Surface Science 578:152090.

[6] Wu G, Wu L, Zhang H, et al (2024) Research progress of screen-printed flexible pressure sensor. Sensors and Actuators A: Physical 374:115512.

[7] Abedeen MZ, Sharma M, Singh Kushwaha H, Gupta R (2024) Sensitive enzyme-free electrochemical sensors for the detection of pesticide residues in food and water. TrAC Trends in Analytical Chemistry 176:117729.

[8] O. F. Oluoch, Synthesis and characterization of bimetallic silver and platinum nanoparticles as electrochemical sensor for nevirapine, an anti-HIV drug, PhD thesis, Cape Peninsula University of Technology, Faculty of Applied Sciences, Chemistry, South Africa, (2019)

[9] Asran AM, Mohamed MA, Eldin GMG, et al (2021) Self-assembled ruthenium decorated electrochemical platform for sensitive and selective determination of amisulpride in presence of co-administered drugs using safranin as a mediator. Microchemical Journal 164:106061.

[10] Duraisamy M, Elancheziyan M, Eswaran M, et al (2023) Novel ruthenium-doped vanadium carbide/polymeric nanohybrid sensor for acetaminophen drug detection in human blood. International Journal of Biological Macromolecules 244:125329.

[11] Ikram M, Munawar A, Kalyar AA, et al (2024) Ruthenium decorated V@WO3 nanocomposites heterostructures for selective detection of sulfonamide in honey samples. Journal of Food Composition and Analysis 126:105842.

Chapter I
Literature Review on Dopamine, Paracetamol, and Sensor technologies

I.1. Introduction

Dopamine is a principal catecholamine neurotransmitter that has a vital function in the functioning of the mammalian central nervous system. It must be in balance because an imbalance will result in a large variety of disorders. Low dopamine levels are associated with diseases such as Parkinson's disease, schizophrenia, and Alzheimer's, while high levels will result in increased heart rate, high blood pressure, and addiction.

Paracetamol is an effective analgesic and antipyretic but lacks anti-inflammatory properties. Paracetamol is now the preferred treatment due to its proven effectiveness and enhanced safety record, particularly if used under strict medical supervision. Long-term use or overdoses of paracetamol, however, can result in severe liver and kidney damage.

Therefore, the identification and quantification of dopamine and paracetamol concentration in biological samples through a sensitive method are required for diagnostic purposes.

This chapter highlights the importance of dopamine and paracetamol detection and it delves into electrochemical sensors, with a specific focus on screen printed electrode technology.

I.2. Dopamine

I.2.1. History of dopamine

Dopamine, the most recently discovered of the catecholamines, was discovered to exist naturally in mammalian tissues. It has since achieved phenomenal scientific advancement since its discovery.*J.Ewens, G. Barger*, and *H. Dale* first isolated dopamine in 1910, which they subsequently identified as a straightforward precursor in the biosynthesis of noradrenaline and adrenaline from tyrosine **[1].** However, it was not until 1951 that dopamine was discovered in mammalian tissues specifically the adrenal medulla and sheep heart, by *Goodall* **[2].** In 1957 *A.Carlsson et al* in Lund, Sweden, in collaboration with *Montagu* at the Runwell Hospital outside London gained insights into dopamine's role as a neurotransmitter in the central nervous system **[3]**.The following year, *A.Carlsson* and colleagues demonstrated dopamine’s function as a neurotransmitter, a discovery that earned *Carlsson* the Nobel Prize in physiology and medicine in 2000 **[4].**

In the early 1960s, *Hornykiewicz et al.* characterized pathologically low dopamine levels in patients with Parkinson's disease, involving dopamine in a central role in motor control **[5,6].** These fundamental discoveries prompted the initial clinical trials of the dopamine precursor L-DOPA in patients with Parkinson's **[7,8].** Then, in 1967, *G. Cotzias* in New York pioneered a high-dose oral DOPA therapy, a major advance in the management of parkinson's disease. Dopamine within a few years , transformed from being relatively obscure to being essential to life as we know it **[9].**

I.2.2. Biosynthesis and metabolism of dopamine

Catecholamines, including dopamine, norepinephrine, and epinephrine, are synthesized from the amino acid tyrosine. Biosynthesis begins with the action of tyrosine hydroxylase on tyrosine to produce L-DOPA, which is rapidly converted to dopamine by DOPA decarboxylase (Figure I.1). Dopamine concentrations in nerve terminals are regulated by vesicular monoamine transporters, and its degradation is blocked by monoamine oxidases **[10].**

Upon arrival of an action potential at the nerve terminal, dopamine is released into the synaptic cleft and binds to postsynaptic receptors. Dopaminergic autoreceptors on the presynaptic terminal regulate this release. Following action, dopamine can either be metabolized or returned to the presynaptic terminal by dopamine transporters, which utilize the energy of the Na^+/K^+ ATPase pump to regulate its level and action on receptors **[11].**

Reuptaken dopamine into the presynaptic neuron can either be stored into synaptic vesicles for future release or degraded into DOPAC by intraneuronal monoamine oxidase. Dopamine remaining in the synaptic cleft is initially transformed into 3-methoxytyramine, then into homovanillic acid by the enzymatic actions of catechol-O-methyltransferase and extrasynaptic monoamine oxidase **[12].**

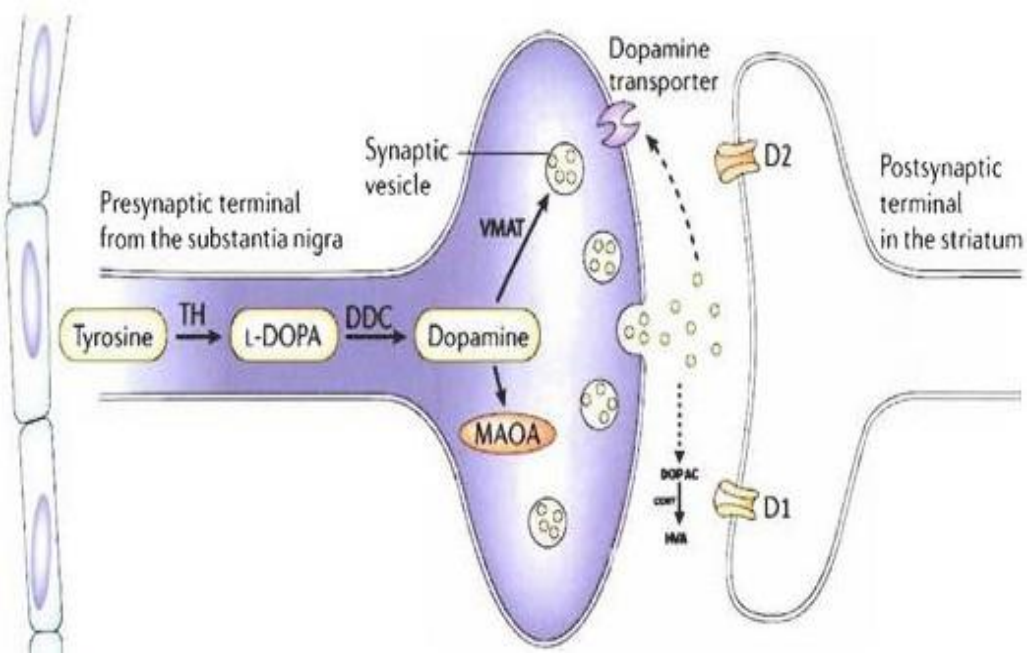

Figure I.1. Pathways for synthesis of dopamine **[13].**

I.2.3. Chemical structure and physicochemical properties of dopamine

The molecule known as dopamine is made up of a benzene ring with two hydroxyl (-OH) groups next to it, creating a catechol structure. An amine group is part of the ethylamine side chain that is joined to this ring at the first position. Dopamine is the most basic catecholamine and a substituted phenethylamine due to its structure **[14].**

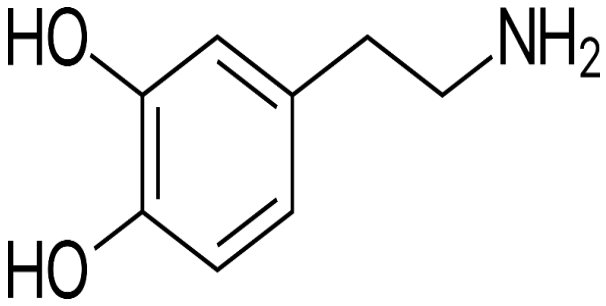

Figure I.2. Chemical structure of dopamine.

The subsequent **table I.1** outlines the fundamental physicochemical features of dopamine.

Table I.1. Physicochemical properties of dopamine [15].

Name of the Drug Substance	Dopamine
Chemical Name	4-(2-aminoethyl) benzene-1,2-diol
Molecular Weight	153.18 g/mol
Molecular Formula	$C_8H_{11}NO_2$
Solubility	It dissolves easily in water, methanol, and hot 95% ethanol, but shows very little solubility in ether, petroleum ether, chloroform,benzene and toluene.
Aspects	White powder

I.2.4. Pharmacodynamic properties of dopamine

When dopamine is administered pharmacologically to humans, its effects are primarily peripheral. These effects are also transient, generally lasting only 1 to 2 minutes.

I.2.4.1. Cardiovascular effects of dopamine

The most notable effects stem from the activation of particular dopaminergic receptors, and to a lesser extent, certain adrenergic receptors. Dopamine's influence on these receptors is dose dependent, with dopamine acting as a weak agonist.

I.2.4.2. Other effects of dopamine

Within the intestine, dopamine exerts its influence by inhibiting the cholinergic system. This inhibition leads to gastric stasis accompanied by pylorus and duodenum spasms, ultimately resulting in constipation **[15].**

I.2.5. Roles of dopamine in learning and motivation

I.2.5.1. Learning

Ventral tegmental area and substantia nigra pars compacta dopamine neurons are briefly activated when they respond to rewarding stimuli.Their activation is also toggled on the

appearance of cues that predict upcoming rewards **[16].** If the predicted reward does not materialize, however, these dopamine neurons reduce their activity, reporting a 'prediction error' that encodes the difference between expected and actual rewards **[17].** This is in line with the hypothesis that learning is guided by dopamine through synaptic plasticity **[18,19].** There is evidence in the present, in dopamine deficient mice, that dopamine may affect the expression of learning, rather than the learning itself **[20].** This is evidenced by restoration of learning after dopamine agonist treatment with L-dopa or caffeine **[21,22].** Additionally, under varying states of dopaminergic, a differential rate of learning has been demonstrated **[23,24],** with hyperdopaminergic mice exhibiting increased lever pressing behavior, albeit without related increase in speed of learning **[25].** These findings propose that dopamine may have greater effect on performance than on the learning process itself and may be responsible for associating learned cues with "incentive motivation" **[26,27].**

I.2.5.2. Motivation

Empirical evidence reveals basal levels of dopamine play a role in regulating the rate and strength of voluntary.It has been revealed by research that dopamine regulates motivational effort and vigor of actions and when depleted, is revealed to decrease motivation to employ effort for rewards under difficult reinforcement conditions **[28,29],** and conversely, elevated levels of dopamine revealed to enhance invigoration of behaviors **[30].**

The levels of the neurotransmitter dopamine modify the desire of an organism to work for a reward, changing its response patterns **[29,31].**Computational models from theoretical neuroscience propose that tonic levels of dopamine represent the rate of environmental rewards.Under conditions of elevated dopamine, the rate of reward receipt is enhanced, in that delays in reward acquisition are more costly, and thus engender quicker action at greater energetic costs **[29,32].**This is supported by the incentive salience theory which proposes that dopamine confers motivational value to reward cues **[26].**

I.2.6. Roles of dopamine in neurological and psychiatric disorders

I.2.6.1. Parkinson's disease

Parkinson's disease is defined by the degeneration of the nigrostriatal pathway and presents with a combination of motor and non-motor manifestations, primarily attributed to dysregulation of the dopaminergic system, although other neurotransmitters such as

acetylcholine, noradrenaline, and serotonin also play a role **[33,34].** Dopaminergic therapy has been shown to enhance motor function; however, neuropsychiatric conditions such as anxiety and depression are associated with dopamine deficits in the limbic region. Accordingly, dopaminergic interventions have been proposed as a potential treatment strategy for depression in Parkinson's disease patients **[34,35].** These interventions can partially ameliorate deficits in reward sensitivity and motivation, but increased dopamine signaling may adversely impact cognitive control in certain individuals **[36].** Levodopa and dopamine agonist medications augment receptor activation in the dorsal striatal region **[37].**Dopamine therapy affected how patients learned from rewards and penalties.When taking dopamine drugs, patients were better at choosing high-reward options, but worse at avoiding low-reward options. This pattern reversed when patients were not taking the medication. This suggests that reward learning is improved when on the drugs, while penalty learning is enhanced when off the drugs **[38].** Dopamine agonists increased novelty-driven and reward-based behaviors, but impaired punishment processing **[39]**, although these findings were not consistently replicated. Levodopa enhanced saccadic amplitude but slowed prosaccadic responses compared to the "OFF" state **[40,41].** In contrast, antisaccadic accuracy improved in the "ON" levodopa condition **[42].** Individuals without a history of movement disorders developed neuroleptic induced parkinsonism, suggesting an underlying genetic susceptibility **[43].**

I.2.6.2. Schizophrenia

Schizophrenia is a prevalent and serious psychiatric disorder. It is characterized by hallucinations,thought dysfunction, and memory impairment. The disorder results in excessive unemployment and reduced life expectancy, resulting from suicidal potential. Dysregulation of dopamine signaling is central to the etiology of schizophrenia.The dopamine hypothesis suggests that schizophrenia is related to D2 blocking of dopamine receptors. Existing antipsychotic medications still function as D2 blockers. Additionally, some drugs like amphetamines and L-DOPA can worsen the symptoms or cause schizophrenia like symptoms.Studies have also found increased levels of dopamine and its metabolites in postmortem brain tissue of people with schizophrenia **[44].**

I.2.6.3. Dopamine in other nervous disorders

The dysregulation of dopaminergic neurotransmission has also been associated with the pathophysiology of numerous psychiatric disorders, including depression, attention

deficit/hyperactivity disorder, personality disorders, bipolar disorder, and obsessive compulsive disorder. These psychiatric disorders are believed to involve altered levels or modulation of the neurotransmitter dopamine within the brain, which is significant in the regulation of mood, attention and motor function. Further, antipsychotic medications have their primary therapeutic effects mediated by blockade of dopamine receptors, quite literally governing dopaminergic activity. Similarly, attention deficit/hyperactivity disorder and restless legs syndrome are suspected to be linked to reduced dopaminergic activity in specific brain regions, which leads to the characteristic symptoms of these conditions **[45].**

I.2.7. Indications

I.2.7.1. Shocks

Dopamine exhibits a unique profile among amines when used to treat shock. Unlike other treatments, it primarily enhances cardiac output without significantly affecting heart rate or excitability. Notably, it maintains blood flow to vital organs, especially the kidneys, making it suitable for low output shock cases with compromised renal function. Dopamine allows for individualized perfusion adjustments, necessitating careful monitoring. Despite these advantages, clinical outcomes have been less promising than expected.

I.2.7.2. Heart failure

In instances of edematous asystole where cardiac tonics and diuretics have proven ineffective, low dose dopamine administration may be considered.

I.2.8. Adverse effects

The adverse effects of dopamine are numerous, very common, sometimes severe, and in some cases fatal. **The table I.2** summarizes some of these side effects.

Table I.2. Adverse effects of dopamine [46].

SYSTEMS	EFFECTS
Cardiovascular system	Arterial hypotension (low blood pressure) Peripheral vasoconstriction Cardiac conduction disorder Arterial hypertension (high blood pressure) Palpitation Gangrene Bradycardia (slow heart rate) Arrhythmia (irregular heartbeat) Extrasystole (premature heartbeat) Tachycardia (fast heart rate)
Digestive System	Vomiting Nausea
Respiratory system	Dyspnea
Nervous System	Headache Tremor
Urology, Nephrology	Polyuria
Ophthalmology	Mydriasis

I.3. Paracetamol

I.3.1. History of paracetamol

The prehistory of paracetamol is complex and complicated. Paracetamol is the only survivor of the once-so-called " aniline derivatives " paracetamol like compounds were first described in the 1880s when acetanilide was erroneously given to a patient instead of naphthalene at a Strasbourg clinic, an error with long lasting consequences **[47,48].** Acetanilide was unexpectedly found to have antipyretic (fever reducing) effects. Following this discovery, it was introduced by *Kalle* and Company for clinical use under the name 'antifebrin' **[47,49].** Not long after its introduction, the drug was found to have unacceptable toxicity effects that were characterized by cyanosis caused by methemoglobinemia, a side effect of aniline derivatives. It was already known to cause hematotoxic (blood related) effects. Thus, an effort to create safer chemical derivatives began. Two compounds that appeared to meet the safety tests were soon evident: N-acetyl-p-aminophenol and phenacetin. These were first synthesized by *Harmon N. Morse* at Johns Hopkins University in 1878 and were found to have antipyretic and, eventually, analgesic (pain relieving) properties **[50].** *J.V.Mering*, a renowned pharmacologist in Strasbourg, clinically utilized paracetamol in 1887. *V.Mering*, however, concluded that paracetamol possessed a toxicity similar to that of

the parent drug acetanilide and was more toxic than phenacetin, a conclusion that proved to be erroneous. Thus, paracetamol led the way for the widespread use of phenacetin, the first derivative to be used clinically and which became phenomenally popular for a few decades. When phenacetin was discovered to be nephrotoxic and fell out of clinical use, interest again turned to paracetamol as an analgesic alternative, which was launched in the market in 1893 **[51].** In 1948, *Brodie* and *Axelrod* conducted a study in New York in which it was demonstrated that paracetamol is the primary active metabolite of phenacetin and acetanilide without the same toxicity **[52].** This discovery marked the beginning of paracetamol's rise to becoming a worldwide utilized analgesic and antipyretic drug. In the following years, paracetamol was introduced and marketed as a prescription-only drug for children, initially by McNeil Laboratories in the USA in 1955, and then by *F. Stearns & Co.* in the UK in 1956 under the brand name panadol **[53].** Paracetamol is today available in many forms such as tablets, effervescent tablets, suspensions, powders (sachets), and rectal suppositories and has become the most prescribed non-narcotic analgesic drug. It is renowned for analgesic and antipyretic effects comparable to those of nonsteroidal anti-inflammatory drugs but lacks the anti-inflammatory action. Paracetamol's limited side effects and minimal drug interactions have assisted it in attaining widespread worldwide use and popularity, particularly in the pediatric population **[54, 55].**

I.3.2. Denomination of paracetamol

Paracetamol or N-acetyl-p-aminophenol, is an organic chemical compound with the formula $C_8H_9NO_2$. As any other drug, acetaminophen comes into contact with both a brand name and an International Nonproprietary Name (INN):

i. The World Health Organization (WHO) suggests "Paracetamol" as the INN, which is used in Europe and the rest of the world, while "Acetaminophen" is the principal name used in the United States and Canada, regardless of the laboratory that markets it **[15].**
ii. Paracetamol is available under a number of tradename preparations, which correspond to specific product presentations, dosages, or pharmaceutical forms. These include Dafalgan, Doliprane, Efferalgan, Mylan, Perdolan, Sandoz, Tylenol, Panadol and Ratiopharm.These trade-name products are present in various dosages and in various forms,e.g.tablet, capsule, or liquid suspension, to accommodate different patient needs and preferences.

iii. Paracetamol is also marketed under other brand names, when it is normally manufactured in combination with other active ingredients such as caffeine (Claradol cafeine, Exidol, and Theinol,) or aspirine (Novacetol) **[56].**

I.3.3. Synthesis of paracetamol

The initial report of the synthesis of paracetamol was made in 1878 by *H.N. Morse.* The initial step is the reduction of para-nitrophenol to para-aminophenol using tin in glacial acetic acid. The resulting para-aminophenol is then acylated with acetic acid to give paracetamol. *Vignolo* adapted this process using starting material para-aminophenol and requiring only one acylation step, which was simpler. *Friedlander* also adapted the synthesis by conducting the acylation of para-aminophenol from para-nitrophenol through acetic anhydride instead of acetic acid with an improved yield **[57,58].**

I.3.4. Chemical structure and physicochemical properties of paracetamol

Paracetamol is a derivative of acylated aromatic amide. Its chemical composition is a benzene ring with two significant functional groups attached in the para position: a hydroxyl group and an amide group (**Figure I.3**).This molecule has no asymmetric carbon atoms, and thus no stereoisomers are present.carbonyl carbon's *p*-orbital, the lone pair of the nitrogen atom, the benzene ring, and one lone pair of the oxygen atom on the hydroxyl group are all implicated in the formation of a conjugated system. This conjugation diminishes the basicity of the nitrogen and oxygen atoms, making the hydroxyl group more acidic, an in phenols, through delocalization of charges on a phenolate ion **[59].**

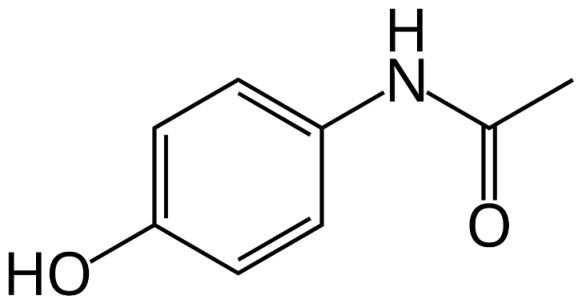

Figure I.3. Chemical structure of paracetamol.

The table I.3 below details the principal physicochemical properties of paracetamol

Table I.3. Physicochemical properties of paracetamol **[60].**

Name of the Drug Substance	Acetaminophen
Chemical Name	N-acetyl-p-aminophenol, 4'-hydroxyacetanilide and N-(4-hydroxyphenyl) acetamide
Molecular Weight	151.2 g/mol
Molecular Formula	$C_8H_9NO_2$
Solubility	Slightly soluble in cold water, dissolves readily in boiling water, easily soluble in alcohol; very soluble in chloroform and ether
Aspects	White odourless crystalline powder with a slightly bitter taste

Stability and degradation conditions

i. Paracetamol exhibits limited solubility in fats but demonstrates stability in aqueous solutions. When stored under typical conditions, shielded from light, it maintains its integrity in both aqueous and dry forms for up to five years. Following administration, paracetamol is absorbed swiftly and almost completely within the small intestine through a passive transport process **[61,62].**

ii. Paracetamol is prone to hydrolysis in humid conditions, particularly in aqueous solutions. This process leads to the formation of para-aminophenol, a primary degradation product, which can further degrade into secondary products like quinoneimine.

iii. Paracetamol's degradation accelerates with higher temperatures and exposure to light. Consequently, it's crucial to shield it from air to prevent any interaction with environmental humidity **[63].**

iv. Paracetamol's breakdown via hydrolysis in water is accelerated by both acidic and basic conditions. The compound's instability in aqueous solutions is significantly influenced by pH levels **[64].**

v. Paracetamol in aqueous solution is known to be unstable, with hydrolysis being the primary degradation pathway. Findings indicate that this degradation is minimized when the pH is approximately 6, resulting in a degradation half-life of 21.8 years at 25°C **[65].**

I.3.5. Indications

Paracetamol is categorized as a non-opioid molecule with analgesic and antipyretic properties. Firstly, paracetamol in its various formulations is considered a primary treatment option for managing a variety of acute painful conditions, such as those caused by headaches including during pregnancy, muscle aches, sprains, flu, cold, osteoarthritic pain, back pain, toothaches, and postoperative pain **[66].** This preference is due to its lower risk of adverse effects and fewer interactions when combined with other medications such as tramadol, in the case of intense pain at therapeutic doses **[67]**. Moreover, paracetamol is often the preferred analgesic option over aspirin, especially for patients with coagulation abnormalities, a history of peptic ulcers, or an inability to tolerate aspirin **[60]**. Secondly, similar to its analgesic (pain relieving) action, paracetamol is one of the oldest treatments for fever worldwide **[68],** especially for treating fever in children **[69].**

I.3.6. Contraindications and take precautions

Paracetamol is not recommended for certain individuals and it should not be used in cases of:

- Hypersensitivity to paracetamol or any other drug.
- Liver or kidney disorders (this includes individuals with acute porphyria and Gilbert's syndrome).

Also Paracetamol should be used with caution in cases of:

- Glucose-6-Phosphate Dehydrogenase (G6PD) deficiency.
- Weighing less than 50 kg.
- Chronic alcoholism.
- Anorexia, bulimia, or cachexia **[70,15]**.
- Pregnancy considerations.
- Breastfeeding considerations **[59,71]**.

I.3.7. Tolerance and posology

The doses (**Table I.4**) are adjusted according to the patient's weight and age.

Table I.4. Recommended dosing protocols for the use of paracetamol **[59].**

Individual	The recommended dosage	The maximum recommended single dosage	The maximum daily dosage
Adolescents and adults with a body mass of ≥50 kg	650 mg every 4 hours or 1000 mg every 6 hours	Should not surpass 1000mg	Should not exceed 4000mg
Adolescents and adults with a body mass of <50Kg	12.5 mg/kg every 4 hours or 15 mg/kg every 6 hours	Should not surpass15 mg/kg	75 mg/kg, up to a maximum of 3750 mg.
Children aged 2 to 12 years	12.5mg/kg every 4 hours or 15 mg/kg every 6 hours	should not surpass 15mg/kg	75 mg/kg
Older patients	325 to 500 mg every 4 hours or 500 to 1 g every 6 hours	For those with liver dysfunction or a history of alcohol abuse, the maximum dose should be reduced by 50% to 75%	4 g

I.3.8. Adverse effects

Generally the safest painkiller, paracetamol nonetheless contains many side effects including:

- Increased cardiovascular risk associated with long-term paracetamol use **[72].**
- Paracetamol is also able to trigger gastrointestinal bleeding as an unwanted effect. In addition, there have been studies linking use of paracetamol and the development of nausea and indigestion **[73,74].**
- Paracetamol has a significant potential to trigger asthma in children **[75].**
- Paracetamol is associated with a substantially high risk of impaired kidney function among adult participants **[76].**
- Paracetamol has been reported as a probable risk factor associated with the development of liver cancer **[77].**

- Maternal use of paracetamol during early pregnancy is associated with an increased risk of cryptorchidism, or undescended testes, in boys **[78].**
- Paracetamol hypersensitivity is commonly presented with the formation of uncomplicated cutaneous eruptions, such as erythema and urticarial **[79].**

I.3.9. Pharmaceutical interactions

i. **Warfarin:** Paracetamol will enhance warfarin's anticoagulant effect. The interaction rarely causes clinically significant bleeding when added to an increased INR (International Normalized Ratio). Interaction is also possible with other oral anticoagulants. Interaction is more likely with paracetamol doses greater than 2 g daily for longer than a week. In these cases, INR monitoring is advised for the week of initiation or stopping paracetamol **[80].**

ii. **NSAIDs:** Paracetamol and non-steroidal anti-inflammatory drug combination administration simultaneously has been shown to provide better pain relief than paracetamol alone, regardless of route of administration. Combination therapy has also been associated with a lower postoperative requirement for morphine.

iii. **Flucloxacillin:** Paracetamol combined with flucloxacillin is cautioned against due to the risk of increased production of metabolic acidosis with a raised anion gap.

iv. **Alcohol:** Risk of paracetamol toxicity is promoted by long-term alcohol use through depletion of hepatic glutathione, and suppression of NAPQI detoxification. It may also suppress glucuronidation, increase oxidation, and block biliary excretion **[81].**

I.3.10. Toxicity

Paracetamol, though once regarded as a fairly innocuous drug, actually has a narrow therapeutic range, which predisposes it to accidental and intentional overdosage. Endless academic discussion has pervaded its ability to cause hepatic toxicity, renal and hematologic side effects.

I.3.10.1. Liver toxicity (hepatotoxicity)

The paracetamol toxic metabolite, N-acetyl-p-benzoquinone imine is usually detoxified by the body's intrinsic antioxidant, hepatic glutathione. This guards against any danger at the

recommended therapeutic doses **[82,83].** But an overdose scenario can overwhelm the liver's detox mechanism and exhaust its glutathione reserves, ultimately to cause liver toxicity. Severity of liver damage is determined by the quantity of paracetamol taken **[47].** Paracetamol acute poisoning can result in severe hepatitis, possible necrosis, and irreversible liver damage. The toxic metabolite causes production of injurious metabolites, disruption of intracellular calcium homeostasis, and lipolysis, resulting in cell necrosis and hepatitis **[84].** Extensive paracetamol abusers have a sequence of clinical stages. No symptomatic presentations at the onset of this process exist. These are preceded by vomiting, nausea, diarrhoea, and abdominal pain, which are typically self-limiting within 48 hours.Symptoms of liver failure, such as hepatomegaly, jaundice, and elevated liver enzymes, develop after 3 to 4 day and may lead to liver failure and coma **[85].** N-acetylcysteine, the antidote, enables repair of oxidative damage from the toxic metabolite directly or by promoting glutathione synthesis. Severe liver damage may necessitate a liver transplant **[86, 87].**

I.3.10.2. Kidney toxicity (nephrotoxicity)

The kidney is a secondary target of paracetamol toxicity. At overdoses greater than the therapeutic range, paracetamol is also capable of producing severe renal necrosis in animals and man **[88].**This nephrotoxicity observed is largely a direct result of local generation of NAPQI, which may exert its action in much the same way as its hepatotoxic effect **[47,89].** Alternatively, the nephrotoxin 4-aminophenol, produced by deacetylation of paracetamol, may decrease renal glutathione levels **[84].** While renal impairment, if it occurs, only becomes evident after 1 week and recovers in 2 to 3 weeks **[85,86],** long term toxicity studies show that paracetamol is unlikely to be nephrotoxic compared to aspirin and other non-steroidal anti-inflammatory analgesics **[90].**However, paracetamol does possess the ability to cause severe renal damage, especially at high doses or prolonged administration. Proper dosing and monitoring are essential to minimize the potential for paracetamol induced nephrotoxicity.

I.3.11. Epidemiology

Paracetamol overdose is the most common cause of ALF (Acute Liver Failure) in USA. Females are more likely to be poisoned **[91,92].** Drug-induced hepatitis due to acetaminophen is the cause of approximately 39% of acute hepatitis cases.This is based on epidemiological studies thet report paracetamol overdose results in approximately 56,000 to 78,000 emergency room visits, 26,000 to 34,000 hospitalizations, and approximately 500 deaths per

year in the United States: this is due to the fact that it is an over the counter drug with no medical prescription that exposes patients to abuse **[93,94].**

Paracetamol is the second most frequently prescribed molecule, after benzodiazepines. Admission for paracetamol poisoning accounts for approximately 4-13% of drug poisoning admissions to hospitals: it is the eighth most frequent reason for intensive care unit admission **[71].**

I.4. Significance of dopamine and paracetamol detection

Dopamine, while present in small quantities in the body, is essential for neurological health, and its imbalance can lead to various disorders. Similarly, the metabolism of paracetamol, if not properly regulated, can result in harmful effects on the liver and kidneys. Thus, developing sensitive detection systems for both dopamine levels and paracetamol metabolites is crucial for the early diagnosis and management of related health issues.

As highlighted above, the need for quick and accurate identification of trace amounts of certain molecules is most critical in the preservation of organism health.Conventional analysis methods, including push-pull methods, microdialysis **[95],** capillary electrophoresis **[96,97],** and high-performance liquid chromatography **[98,99],** as well as UV-visible spectrophotometry **[100,101],** have been extensively employed in the determination of dopamine and paracetamol levels in a wide range of biological specimens, water, and drug matrices. Despite all these, there are several disadvantages with these techniques, including the need for expensive equipment. They are very time consuming and sophisticated, based on sample preparation, to the point that they require vast amounts of organic solvents in some instances, which can lead to secondary contamination. These methods also lack high sensitivity and selectivity, limiting their use in routine analysis.

On the other hand electrochemical technology, especially sensors, has been suggested as a solution to the obstacles previously mentioned, owing to its intrinsic merits. These include sensitivity and high selectivity, portability, time efficiency, simplicity, cost-effectiveness, exceptional reliability, accuracy, and notably, a low detection threshold for the analysis and detection of organic molecules such as dopamine and paracetamol **[102-104].**

I.5. Electrochemical sensors

I.5.1. A Comprehensive overview and advantages

A sensor functions as a device that transforms a non-electrical measurable quantity into an electrically analyzable one, known as a "signal" as shown in (**Figure I.4**). It comprises a chemical or biological "receptor" coupled with a "transducer" which embodies the detection method. In the context of an electrochemical sensor, the generated signal is proportional to the analyte concentration **[105].**

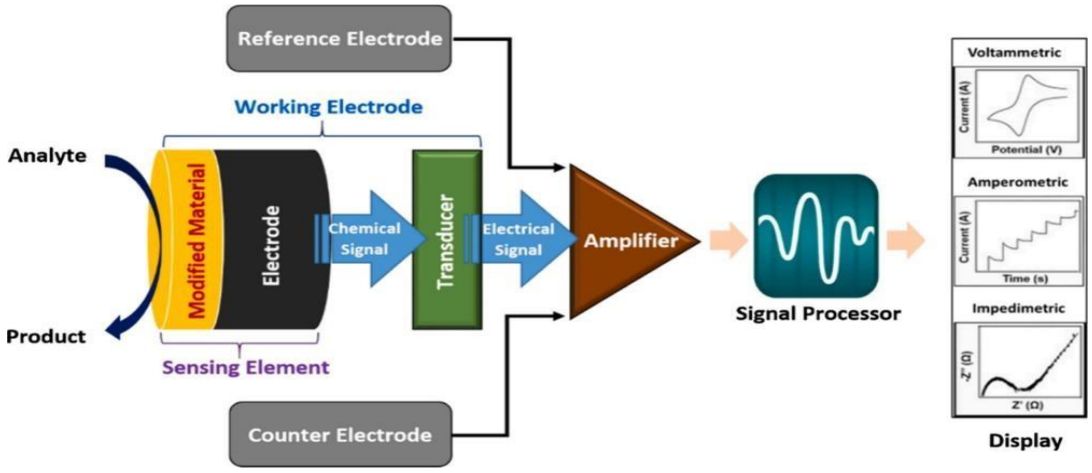

Figure I.4. Operating principle of a chemical sensor.

I.5.2. Operating principle of an electrochemical sensor

A sensor is composed of three fundamental functional components:

i. A receptor system, typically a selective layer designed for the identification of the species with which it interacts. This layer may be composed of various receptor types, including synthetic molecules, enzymes, antibodies, or cells. In electrochemical sensors, the receptor's specialized surface corresponds to the surface of an electrode that has been modified to enhance sensitivity to the analyte.

ii. A transducer system translates chemical interactions into electrical signals through various phenomena, including piezoelectric, optical, thermal, or electrochemical effects **[106, 107].**

Based on the transducer type, sensors are classified into four main categories, as illustrated in (**Figure I.5**) **[108].**

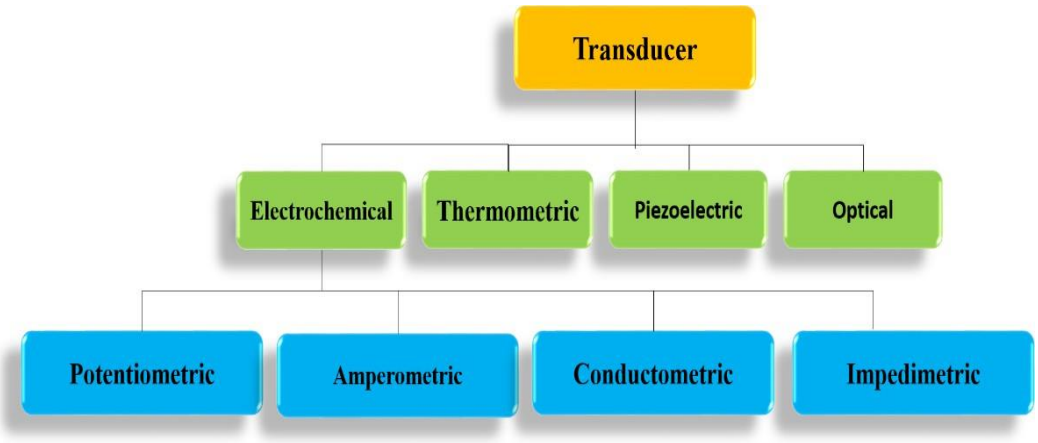

Figure I.5. Classification of transducers in the context of sensors.

iii. An analyzer system converts the signal received from the transducer into a format accessible and interpretable for the operator.

I.5.3. Measurement related characteristics of the sensor

The suitability of a sensor for a specific measurement application is assessed based on seven key characteristics. These include sensitivity, selectivity, and stability, often referred to as the "three S" alongside reversibility, reproducibility, the limit of detection, and response and recovery times **[109].**

I.5.3.1. Selectivity

A critical attribute of a sensor is its selectivity, which refers to the capacity of the receptor to discern a particular analyte from a complex mixture of other substances and potential interferents.

I.5.3.2. Sensitivity

Sensitivity (S) plays a crucial role in measurement application and interpretation. It quantifies the change in the output signal (ΔS) in relation to the corresponding change in the measured quantity (Δm), and it is mathematically represented as:

$$S_v = \frac{\Delta S}{\Delta m}$$

I.5.3.3. Stability

This parameter quantifies the temporal drift observed in the sensor signal, a phenomenon attributed to sensor aging that ultimately restricts the sensor's long term usability.

I.5.3.4. The limit of detection

The limit of detection represents the lowest concentration of an analyte that can be distinguished from background noise. It is typically defined as the minimum concentration at which the sensor can reliably detect the analyte.

I.5.3.5. Linearity

Linearity refers to the extent to which a sensor's output exhibits a direct proportional relationship with the concentration of the target analyte. A high degree of linearity suggests a consistent and predictable correlation between analyte concentration and sensor response.

I.5.3.6. Response time

This metric assesses the interval required for the sensor to attain a consistent and reliable signal following analyte exposure.

I.5.3.7. Repeatability and reproducibility

Repeatability and reproducibility arguably represent the most critical parameters for both physical and chemical sensors. These terms describe a sensor's capacity to yield highly consistent responses under specified conditions when repeatedly measuring an identical measurand value.

I.5.4. Electrochemical platforms setup

Electrochemical platforms commonly utilize a three electrode system within an electrochemical cell, comprising a working electrode, an auxiliary (or counter) electrode, and a reference electrode. These experiments necessitate an ionic substance, typically a salt solution, to act as a supporting electrolyte and ensure adequate conductivity **[110].** Various setups and equipment options are available for conducting electrochemical studies, with the standard three electrode cell being the most widely used. However, demands in the analytical field have driven the miniaturization, increased portability, and integration of components into single systems, notably leading to the development of screen printed electrode based systems.

I.5.4.1. Conventional three electrode system

Electrochemical experiments using a three electrode cell commonly involve immersing a working, reference, and auxiliary electrode in a beaker filled with a supporting electrolyte (**Figure I.6**). More sophisticated setups might also incorporate systems for controlling gas flow, temperature, and stirring. Glass is frequently chosen for constructing the cell due to its affordability and resistance to chemical reactions, though quartz and teflon are also viable options **[110,111].**

The reference electrode possesses a constant potential, though the standard hydrogen electrode is not normally utilized in practice due to its awkward handling. An auxiliary electrode facilitates charge balancing by suffering from the counter reaction compared to the working electrode. The working electrode is the sensor itself, and care must be taken for it to provide a stable and low noise signal. Selection of working electrodes is based on redox behavior, potential window, background current, cost efficiency, conductivity, and toxicity. A potentiostat or galvanostat, supported by suitable software, is essential for accurate control and data analysis. Though inexpensive laboratory setups are very convenient and versatile, their self-limiting nature prevents their application in fieldwork. Screen printed electrodes provide a more efficient and field deployable alternative **[110-112].**

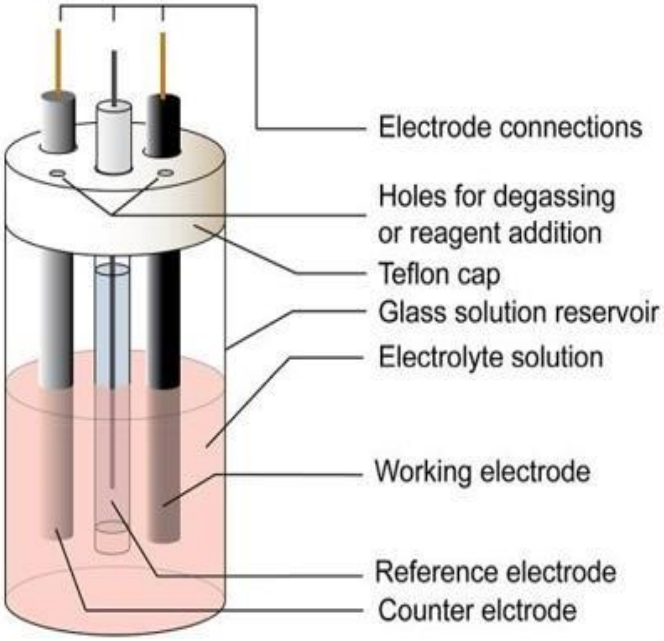

Figure I.6. Schematic representation of a standard electrochemical cell [113].

I.5.4.2. Screen-printed electrode system

The advent, in the early 1990s, of screen printed strips comprising the three electrodes assembled on the same support (**Figure I.7**), as well as the development of mini-potentiostats, considerably revived interest in the implementation of electroanalytical techniques. These strips are easily produced on a large scale with a good level of surface repeatability **[114].**

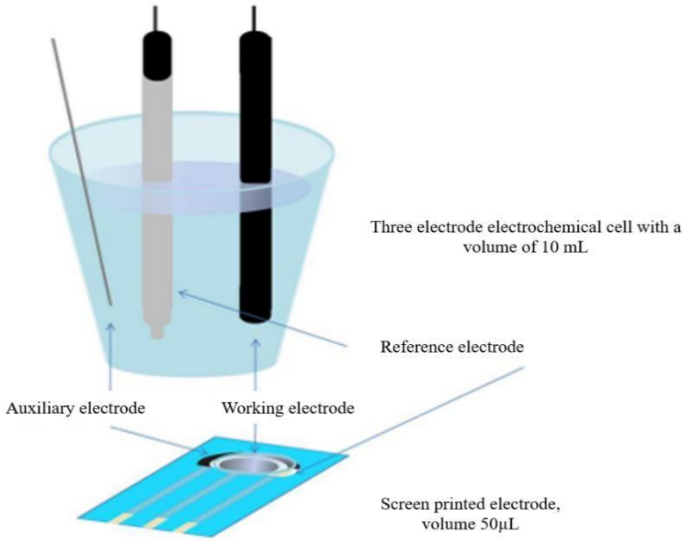

Figure I.7. Comparison between a conventional electrochemical cell and an SPE strip.

a) Screen-printed electrode fabrication

A conductive ink is applied to flat supports that can be ceramic or plastic, glass, or fabrics. The ink contains particles of carbon or metals such as gold, silver, platinum, or bismuth. After applying the ink to the support, it can be heated to allow it to solidify. Both the electrodes and the electrical connections are screen printed. Generally, the connections are made with an ink containing silver. An insulating layer covers the support and almost all of the silver contacts, while leaving the electrodes exposed **[115].**

b) Advantages of screen-printed electrodes

i. Screen printed electrodes can be manufactured in parallel with electronic components on the same production line, as they use compatible processes such as screen printing.
ii. The three electrodes required for the analysis are present on the same support, which allows for the reduction of analysis volumes and on-site analysis.
iii. The production cost of screen printed electrodes, making them cost-effective for mass production. Although equipment like a screen printing machine and drying oven are needed initially, these costs are quickly covered. The electrode materials, such as temporary binders and solvents, are cheap and readily available, lowering the final price.
iv. The great universality of the screen printed electrode is its great universality. Compatible with many industrial environments, it can be produced on a wide variety of supports (alumina, silicon, etc.). Different types of materials can be used for the electrode's manufacture, offering great flexibility in its design. This versatility facilitates the integration of the screen-printed electrode into existing industrial processes, without major modifications.
v. SPEs also offer other advantages: ease of use and portability, without the need to renew the work surface since they can be disposable.

All these advantages have allowed the development of screen-printed sensors in a large number of fields, particularly in the medical, environmental, and agri-food sectors **[116,117].**

Conclusion

After reviewing the significance and side effects of two main pharmaceuticals; dopamine and paracetamol, the need for their detection in biological fluids appears to be of utmost importance. In this context, electrochemical sensors, especially, screen-printed electrodes are an interesting means as they have several appealing characteristics, including high sensitivity, selectivity, simplicity of use, and affordability.

References

[1] A. Björklund, S.B. Dunnett, Fifty years of dopamine research, Trends Neurosci. 30 (2007).
[2] O. Hornykiewicz, Brain dopamine: a historical perspective, in: C.D. Marsden, S.J. Fahn (Eds.), Movement Disorders 3, Butterworths, London, 1994, pp. 3–10.
[3]K.A. Montagu, Catechol compounds in rat tissues and in brains of different animals, Nature 180 (1957) 244–5.
[4] A. Carlsson, M. Lindqvist, T. Magnusson, B. Waldeck, On the presence of 3-hydroxytyramine in brain, Science 127 (1958) 471.
[5] A. Carlsson, The occurrence, distribution and physiological role of catecholamines in the nervous system, Pharmacol. Rev. 11 (2, Part 2) (1959) 490–3.
[6] H. Ehringer, O. Hornykiewicz, Verteilung von Noradrenalin und Dopamin (3-Hydroxytyramin) im Gehirn des Menschen und ihr Verhalten bei Erkrankungen des extrapyramidalen Systems, Klin. Wochenschr. 38 (1960) 1236–9.
[7] W. Birkmayer, O. Hornykiewicz, Der l-Dioxyphenylalanin (l-Dopa)-Effekt bei der Parkinson-Akinese, Wien. Klin. Wochenschr. 73 (1961) 787–8.
[8] A Barbeau, Th.L. Sourkes, G.F. Murphy.Les catécholamines de la maladie de Parkinson, in: J. de Ajuriaguerra (Ed.), Monoamines et Système Nerveux Central, Georg et Cie, Genève (1962) 247–67.
[9] G.C. Cotzias, M.H. Van Woert, L.M. Schiffer, Aromatic amino acids and modification of parkinsonism, N. Engl. J. Med. 276 (1967) 374–9
[10] A. Nieoullon, Neurosciences (4e édition): À la découverte du cerveau, 1re éd., 1996.
[11] T.D. Sotnikova, J.-M. Beaulieu, R.R. Gainetdinov, M.G. Caron, Molecular Biology, Pharmacology and Functional Role of the Plasma Membrane Dopamine Transporter, Pharmacol. Ther. 111 (2006) 1–20.
[12] M.B.H. Youdim, D. Edmondson, K.F. Tipton, The therapeutic potential of monoamine oxidase inhibitors, Nat. Rev. Neurosci. 7 (2006) 295–309.
[13] M. Lebel, Rôle des protéines responsables du maintien du cytosquelette neuronal dans la maladie de Parkinson et les dyskinésies induites par la L-DOPA, PhD thesis, University of QUÉBEC À TROIS-RIVIÈRES 2010.
[14] A. Lo, Développement de méthodes de diagnostic rapide d'erreurs innées du métabolisme associées à des troubles neurologiques, PhD thesis, University of Paris-Saclay, Orsay,2017.
[15] J. Dangoumau, N. Moore, M. Molimard, A. Fourrier-Réglat, K. Latry, F. Haramburu, G. Miremont-Salamé, K. Titier, Pharmacologie generale, 2006.
[16] J.R. Hollerman, W. Schultz, Dopamine neurons report an error in the temporal prediction of reward during learning, Nat. Neurosci. 1 (1998) 304–309.
[17] W. Schultz, A neural substrate of prediction and reward, Science 275 (1997) 1593–1599.
[18] D. Centonze, B. Picconi, P. Gubellini, G. Bernardi, P. Calabresi, Dopaminergic control of synaptic plasticity in the dorsal striatum, Eur. J. Neurosci. 13 (2001) 1071–1077.
[19] T.V. Maia, M.J. Frank, From reinforcement learning models to psychiatric and neurological disorders, Nat. Neurosci. 14 (2011) 154–162.
[20] Reward without dopamine, J. Neurosci. 23 (34) (2003) 10827–10831.
[21] S. Robinson, S. M. Sandstrom, V. H. Denenberg, R. D. Palmiter, Distinguishing whether dopamine regulates liking, wanting, and/or learning about rewards, Behav. Neurosci. 119 (1) (2005) 5–15.
[22] T. S. Hnasko, B. N. Sotak, R. D. Palmiter, Morphine reward in dopamine-deficient mice, Nature 438 (2005) 854–857.
[23] M. Pessiglione, B. Seymour, G. Flandin, R. J. Dolan, C. D. Frith, Dopamine-dependent prediction errors underpin reward-seeking behaviour in humans, Nature 442 (2006) 1042–1045.

[24] V. Voon, M. Pessiglione, C. Brezing, C. Gallea, H.H. Fernandez, R.J. Dolan, M. Hallett, Mechanisms underlying dopamine-mediated reward bias in compulsive behaviors, Neuron 65 (2010) 135–142.
[25] H.H. Yin, X. Zhuang, B.W. Balleine, Instrumental learning in hyperdopaminergic mice, Neurobiol. Learn. Mem. 84 (2005) 132–139.
[26] K.C. Berridge, The debate over dopamine's role in reward: the case for incentive salience, Psychopharmacology (Berl.) 191 (2007) 391–431.
[27] K.C. Berridge, T.E. Robinson, What is the role of dopamine in reward: hedonic impact, reward learning, or incentive salience?, Brain Res. Rev. 28 (1998) 309–369.
[28] J.D. Salamone, M. Correa, Motivational views of reinforcement: implications for understanding the behavioral functions of nucleus accumbens dopamine, Behav. Brain Res. 137 (2002) 3–25.
[29] Y. Niv, Cost, benefit, tonic, phasic: What do response rates tell us about dopamine and motivation?, Neural Netw. 15 (2002) 507–520.
[30] J.D. Salamone, M. Correa, S.M. Mingote, S.M. Weber, Beyond the reward hypothesis: alternative functions of nucleus accumbens dopamine, Curr. Opin. Pharmacol. 5 (2005) 34–41.
[31] J.D. Salamone, M. Correa, S. Mingote, S.M. Weber, Nucleus accumbens dopamine and the regulation of effort in food-seeking behavior: implications for studies of natural motivation, psychiatry, and drug abuse, J. Pharmacol. Exp. Ther. 305 (2003) 1–8.
[32] Y. Niv, N.D. Daw, D. Joel, P. Dayan, Tonic dopamine: opportunity costs and the control of response vigor, Psychopharmacology (Berl.) 191 (2007) 507–520.
[33] S.J. Baloyannis, V. Costa, I.S. Baloyannis, Morphological alterations of the synapses in the locus coeruleus in Parkinson's disease, J. Neurol. Sci. 248 (2006) 35–41.
[34] P. Remy, M. Doder, A. Lees, N. Turjanski, D. Brooks, Depression in Parkinson's disease: loss of dopamine and noradrenaline innervation in the limbic system, Brain 128 (2005) 1314–1322.
[35] G.C. Cotzias, M.H. Van Woert, L.M. Schiffer, Aromatic amino acids and modification of parkinsonism, N. Engl. J. Med. 276 (1967) 374–379.
[36] R. Adam, A. Leff, N. Sinha, C. Turner, P. Bays, B. Draganski, M. Husain, Dopamine reverses reward insensitivity in apathy following globus pallidus lesions, Cortex 49 (2013) 1292–1303.
[37] B.S. Connolly, A.E. Lang, Pharmacological treatment of Parkinson disease: a review, JAMA 311 (16) (2014) 1670–1683.
[38] M.J. Frank, L.C. Seeberger, R.C. O'Reilly, By carrot or by stick: cognitive reinforcement learning in Parkinsonism, Prog. Méd. J. Médecine Chir. Pharm. 5 (2004) 43–6.
[39] N. Bódi, S. Kéri, H. Nagy, A. Moustafa, C.E. Myers, N. Daw, Gy. Dibó, A. Takáts, D. Bereczki, M.A. Gluck, Reward-learning and the novelty-seeking personality: a between- and within-subjects study of the effects of dopamine agonists on young Parkinson's patients, Brain 132 (2009) 2385–2395.
[40] O. Rascol, M. Clanet, J.L. Montastruc, M. Simonetta, M.J. Soulier-Esteve, B. Doyon, A. Rascol, Abnormal ocular movements in Parkinson's disease: evidence for involvement of dopaminergic systems, Brain 112 (1989) 1193–1214.
[41] A.W. Michell, Z. Xu, D. Fritz, S.J.G. Lewis, T. Foltynie, C.H. Williams-Gray, T.W. Robbins, R.H.S. Carpenter, R.A. Barker, Saccadic latency distributions in Parkinson's disease and the effects of L-dopa, Exp. Brain Res. 174 (2006) 7–18.
[42] A. J. Hood, S. C. Amador, A. E. Cain, K. A. Briand, A. H. Al-Refai, M. C. Schiess, A. B. Sereno, Levodopa slows prosaccades and improves antisaccades: an eye movement study in Parkinson's disease, J. Neurol. Neurosurg. Psychiatry 78 (2007) 565–570.

[43] R. Erro, K. P. Bhatia, M. Tinazzi, Parkinsonism following neuroleptic exposure: a double-hit hypothesis?, Mov. Disord. 29 (2014) 179–186.
[44] K. M. Costa, G. Schoenbaum, Dopamine, Curr. Biol. 32 (2022) R807–R827.
[45] H. Juárez Olguín, D. Calderón Guzmán, E. Hernández García, G. Barragán Mejía, The role of dopamine and its dysfunction as a consequence of oxidative stress, Oxid. Med. Cell. Longev. 2016 (2015) 9730467.
[46] S.J. Ferrando, S.J. Eisendrath, Adverse neuropsychiatric effects of dopamine antagonist medications: misdiagnosis in the medical setting, Psychosomatics 32 (1991) 300–307.
[47] A. Bertolini, A. Ferrari, A. Ottani, S. Guerzoni, R. Tacchi, S. Leone, Paracetamol: new vistas of an old drug, CNS Drug Rev. 12 (2006) 250–275.
[48] S. Bashir, Mechanisms of paracetamol (acetaminophen) induced hypothermia, PhD Thesis, University. East London, Jan. 2018.
[49] A. Chan, P. Hepp, Das Antifebrin, ein neues Fiebermittel, Centralbl. Klin. Med. 7 (1886) 561–564.
[50] H. N. Morse, Ueber eine neue Darstellungsmethode der Acetylamidophenole, Ber. Dtsch. Chem. Ges. 11 (1878) 232–233.
[51] J. von Mering, Beiträge zur Kenntniss der Antipyretica, Ther. Monatsch. 7 (1893) 577–87.
[52] B.B. Brodie, J. Axelrod, The fate of acetanilide in man, J. Pharmacol. Exp. Ther. 94 (1948) 29–38.
[53] M. Jóźwiak-Bebenista, J.Z. Nowak, Paracetamol: mechanism of action, applications and safety concern, Acta Pol. Pharm. 71 (2014) 11–23.
[54] L.F. Prescott, Paracetamol: past, present and future, Am. J. Ther. 7 (2000) 143–47.
[55] A. Autret, Paracetamol efficacy and safety in children: the first 40 years, Am. J. Ther. 7 (2000) 135–42.
[56] World Health Organization, DZA-CH-43-01-EMD-2018 fra: Liste des médicaments essentiels, WHO Platform (2018).
[57] J. C. McCrae, E. E. Morrison, I. M. MacIntyre, J. W. Dear, D. J. Webb, Long-term adverse effects of paracetamol – a review, Br. J. Clin. Pharmacol. 84 (2018) 2218–2230.
[58] Jayanand, P. Mittal, V. Sharma, J. Haria, M. Modi, Paracetamol: its efficacy, advantages & disadvantages, J. Res. Med. Dent. Sci. 10 (S1) (2022) 1–5.
[59] K. Benghazi, N. Brahmi, Synthèse, identification et caractérisation du paracétamol, thesis, University of Saad Dahlab BLIDA-1 2017.
[60] F. Medjdoub, Adsorption du paracétamol par l'utilisation des différents types d'adsorbants naturels, PhD thesis in environmental engineering, University of MHAMED BOUGARA, BOUMERDES, 2018.
[61] T. Antoine, Suivi du lancement d'un nouvel antalgique de palier 2 – Association fixe de paracétamol et tramadol, Fac. Méd. Pharm. Univ. Besançon (2005) 158.
[62] P. Lechat, G. Lagier, J. Boiteau, Le paracétamol, *Thérapie* 33 (1978) 551–585.
[63] J.E. Fairbrother, Acetaminophen, Anal. Profiles Drug Subst. 3 (1974) 109.
[64] K.T. Koshy, J.L. Lach, Stability of aqueous solutions of N-acetyl-p-aminophenol, J. Pharm. Sci. 53 (1964) 446–450.
[65] Q.G. Fogg, A.M. Summan, Stabilisation by ethylenediamine tetraacetic acid of amid and other groups in drug compound, J. Clin. Pharm. Ther. 17 (1992) 107–109.
[66] S.S. Ayoub, Paracetamol (acetaminophen): A familiar drug with an unexplained mechanism of action, Temperature (2021)
[67] D.W.J. Dippel, E.J. van Breda, H.M.A. van Gemert, H.B. van der Worp, R.J. Meijer, L.J. Kappelle, P.J. Koudstaal, Effect of paracetamol (acetaminophen) on body temperature in acute ischemic stroke: a double-blind, randomized phase II clinical trial, Stroke 32 (2001) 1607–1612.

[68] S. Bashir, B. Elegunde, W.A. Morgan, Inhibition of lipolysis: a novel explanation for the antipyretic and hypothermic actions of acetaminophen, Prog. Méd. J. Médecine Chir. Pharm. (2025)
[69] M. Ouellet, M. D. Percival, Mechanism of Acetaminophen Inhibition of Cyclooxygenase Isoforms, Arch. Biochem. Biophys. 387 (2001) 273–280.
[70] I. Popiołek, K. Piotrowicz-Wójcik, G. Porebski, Hypersensitivity reactions in serious adverse events reported for paracetamol in the EudraVigilance database, 2007–2018, Pharmacy 7 (2019) 12.
[71] A. Kwakye Agyemang, Intoxication médicamenteuse au paracétamol : une étude rétrospective sur la prise en charge aux urgences adultes du CHU de Clermont-Ferrand (étude IMPASSE), PhD thesis, University of Clermont Auvergne 2022.
[72] E. Roberts, V. Delgado Nunes, S. Buckner, S. Latchem, M. Constanti, P. Miller, M. Doherty, W. Zhang, F. Birrell, M. Porcheret, K. Dziedzic, I. Bernstein, E. Wise, P. G. Conaghan, Paracetamol: not as safe as we thought? A systematic literature review of observational studies, Ann. Rheum. Dis. (2014)
[73] A. Carvajal, J. R. Prieto, A. Alvarez Requejo, L. H. Martin Arias, Aspirin or Acetaminophen? A Comparison from Data Collected by the Spanish Drug Monitoring System, J. Clin. Epidemiol. 49 (1996) 255–261.
[74] J. Gonzalez-Valcarcel, L. Sissani, J. Labreuche, M.-G. Bousser, A. Chamorro, M. Fisher, I. Ford, K. M. Fox, M. G. Hennerici, H. P. Mattle, P. M. Rothwell, P. G. Steg, E. Vicaut, P. Amarenco, Paracetamol, Ibuprofen, and Recurrent Major Cardiovascular and Major Bleeding Events in 19 120 Patients With Recent Ischemic Stroke, Stroke 46 (2015) 3255–3262.
[75] J.T. McBride, The association of acetaminophen and asthma prevalence and severity, Pediatrics 128 (2011) 1181–1185.
[76] Acetaminophen use and risk of renal impairment: A systematic review and meta-analysis, Kidney Res. Clin. Pract. 39 (2020) 121–135.
[77] L. Tian, N. Mi, L. Wang, C. Huang, W. Fu, M. Bai, L. Gao, H. Ma, C. Zhang, Y. Lu, J. Zhao, X. Zhang, N. Jiang, Y. Lin, P. Yue, B. Xia, Q. He, J. Yuan, W. Meng, Regular use of paracetamol and risk of liver cancer: a prospective cohort study, BMC Cancer 22 (2023) 2.
[78] M. S. Jensen, C. Rebordosa, A. M. Thulstrup, G. Toft, H. T. Sørensen, J. P. Bonde, T. B. Henriksen, J. Olsen, Maternal use of acetaminophen, ibuprofen, and acetylsalicylic acid during pregnancy and risk of cryptorchidism, Epidemiology 21 (2010) 779–785.
[79] P.M. Mertes, O. Collange, S.E. Degirmenci, C. Tacquard, N. Petitpain, J.M. Malinovsky, Le choc anaphylactique, Le Congrès Médecins. Conférence d'essentiel, Sfar © (2014).
[80] D. Leong, P.E. Wu, Warfarin and acetaminophen interaction in a 47-year-old woman, CMAJ. 192 (2020) 506–8.
[81] I. Cobden, C.O. Record, M.K. Ward, D.N. Kerr, Paracetamol-induced acute renal failure in the absence of fulminant liver damage, Br. Med. J. (Clin. Res. Ed.) 284 (6308) (1982) 21–2.
[82] R.C. Dart, E. Bailey, Does therapeutic use of acetaminophen cause acute liver failure?, Pharmacotherapy 27 (2007) 1219–1230.
[83] R. Whit Curry Jr., J.D. Robinson, M.J. Sughrue, Acute renal failure after acetaminophen ingestion, JAMA 247 (1982) 1012–1014.
[84] A. Lowe, M. Abramson, S. Dharmage, K. Allen, Paracetamol as a risk factor for allergic disorders, Lancet 373 (2009) 120–121.
[85] O. Moling, E. Cairon, G. Rimenti, F. Rizza, R. Pristeri, P. Mian, On severe hepatotoxicity after therapeutic doses of paracetamol, Clin. Ther. 28 (2006) 755–760.

[86] A.R. Buckpitt, D.E. Rollins, J.R. Mitchell, On the varied effects of sulfhydryl nucleophiles on the oxidation of acetaminophen and the formation of sulfhydryl adducts, Biochem. Pharmacol. 28 (1979) 2941–2946.

[87] B.H. Lauterburg, G.B. Corcoran, J.R. Mitchell, Mechanism of action of N-acetylcysteine in the protection against the hepatotoxicity of acetaminophen in rats in vivo, J. Clin. Invest. 71 (1983) 980–991., J. Clin. Invest. 71 (1983) 980–991.

[88] D.M. Aronoff, J.A. Oates, O. Boutaud, New insights into the mechanism of action of acetaminophen: Its clinical pharmacologic characteristics reflect its inhibition of the two prostaglandin H_2 synthases, Clin. Pharmacol. Ther. 79 (2006) 9–19.

[89] D.J. Hoivik, J.E. Manautou, A. Tveit, S.G. Hart, E.A. Khairallah, S.D. Cohen, Gender-related differences in susceptibility to acetaminophen-induced protein arylation and nephrotoxicity in the CD-1 mouse, Toxicol. Appl. Pharmacol. 130 (1995) 257–271.

[90] M.E. Morris, G. Levy, Renal clearance and serum protein binding of l'acétaminophène et de ses principaux conjugués chez l'homme, J. Pharm. Sci. 73 (1984) 1033–1038.

[91] G. Ostapowicz, R.J. Fontana, F.V. Schiødt, A. Larson, T.J. Davern, S.H.B. Han, T.M. McCashland, A.O. Shakil, J.E. Hay, L. Hynan, J.S. Crippin, A.T. Blei, G. Samuel, J. Reisch, W.M. Lee, U.S. Acute Liver Failure Study Group, Results of a prospective study of acute liver failure at 17 tertiary care centers in the United States, Ann. Intern. Med. 137 (2002) 947–954.

[92] D. Casey, G. Geulayova, E. Bale, F. Brand, C. Clements, N. Kapur, J. Ness, A. Patel, K. Waters, K. Hawton, Paracetamol self-poisoning: epidemiological study of trends and patient characteristics from the multicentre study of self-harm in England, J. Affect. Disord. 276 (2020) 699–706.

[93] A.D. Manthripragada, E.H. Zhou, D.S. Budnitz, M.C. Lovegrove, M.E. Willy, Characterization of acetaminophen overdose-related emergency department visits and hospitalizations in the United States, Pharmacoepidemiol. Drug Saf 2011; 20: 819–826

[94] C. Li, B.C. Martin, Trends in emergency department visits attributable to acetaminophen overdoses in the United States: 1993–2007, Pharmacoepidemiol. Drug Saf. 18 (2009) 693–699.

[95] E. Ghodsevali, Conception et fabrication d'un biocapteur à haute sensibilité pour la détection des neurotransmetteurs, PhD thesis, University of Québec, Canada (2017).

[96] H. Fang, M.L. Pajski, A.E. Ross, B.J. Venton, Quantitation of dopamine, serotonin and adenosine content in a tissue punch from a brain slice using capillary electrophoresis with fast-scan cyclic voltammetry detection, Anal. Methods 5 (2013) 3010–3018.

[97] Q. Chu, L. Jiang, X. Tian, J. Ye, Rapid determination of acetaminophen and p-aminophenol in pharmaceutical formulations using miniaturized capillary electrophoresis with amperometric detection, Anal. Chim. Acta 606 (2008) 246–251.

[98] A.M. Domínguez-Ramírez, F.J. López-Muñoz, J.R. Medina, M. Hurtado, G. Alarcón Ángeles, A.D. Pineda, L.A. Moreno-Rocha, HPLC-PDA method for the quantification of paracetamol in plasma: application to PK/PD studies with arthritic rats, Int. J. Pharm. Pharm. Sci. 9 (2017) 168–172.

[99] Y. Wang, D.S. Fice, P.K.F. Yeung, A simple high-performance liquid chromatography assay for simultaneous determination of plasma norepinephrine, epinephrine, dopamine and 3,4-dihydroxyphenyl acetic acid, J. Pharm. Biomed. Anal. 21 (1999) 519–525.

[100] N. Gonzalez-Dieguez, A. Colina, J. Lopez-Palacios, A. Heras, Spectroelectrochemistry at screen-printed electrodes: determination of dopamine, Anal. Chem. 84 (2012) 9146–9153.

[101] P.C. Damiani, M.É. Ribone, A.C. Olivieri, Rapid determination of paracetamol in blood serum samples by first-derivative UV absorption spectroscopy, Anal. Lett. 28 (1995) 1489–1502.

[102] A. Kutluay, M. Aslanoglu, An electrochemical sensor prepared by sonochemical one-pot synthesis of multi-walled carbon nanotube-supported cobalt nanoparticles for the simultaneous determination of paracetamol and dopamine, Anal. Chim. Acta 839 (2014) 59–66

[103] S. Abdi, M.L. Chelaghmia, R. Kihal, C.E. Banks, A.G.M. Ferrari, H. Fisli, M. Nacef, A.M. Affoune, M.E.H. Benhamza, Simultaneous determination of 4-aminophenol and paracetamol based on CS-Ni nanocomposite-modified screen-printed disposable electrodes, Monatsh Chemie 154 (2023) 563–575

[104] X. Wang, Y. Ma, Z. Zhou, Z. Zhang, J. Zhang, L. Fan, X. Du, X. Lu, Ultrarapid synthesis of dumbbell-shaped carbon black-doped Ce (III, IV)-MOF composites for fabrication of simultaneous electrochemical sensor of dopamine and acetaminophen, Microchem. J. 195 (2023) 109430

[105] G. Asch, L. Blum, J. Fouletier, P. Desgoutte, B. Crétinon. Les capteurs en instrumentation industrielle, 9e éd., août 2025.

[106] A. Hulanicki, S. Geab, F. Ingman, Chemical sensors: definitions and classification, Pure Appl. Chem. 63 (1991) 1247–1250.

[107] A. Hulanicki, S. Geab, F. Ingman, Chemical sensors: definitions and classification, Pure Appl. Chem. 63 (1991) 1247–1250.

[108] M. Debliquy, Capteurs Chimiques. Techniques de l'Ingénieur, 2010, r420.

[109] D. Elbahi, Développement et modélisation de (bio) capteurs électrochimiques pour la détection de l'Amlodipine et de la Pénicilline en phase aqueuse, PhD thesis, University of Badji Mokhtar, Annaba 2019.

[110] A.J. Bard, Electrochemical Methods: Fundamentals and Applications, Wiley, New York, 1980

[111] H.C. da Silva, Development of Electrochemical Biosensors and Sensors for the Determination of Interest Analytes, PhD thesis ,University of Burgos, Burgos, 2019.

[112] E. Laviron, General expression of the linear potential sweep voltammogram in the case of diffusionless electrochemical systems, J. Electroanal. Chem. 101 (1979) 19–28.

[113] S. Hassanpour, Novel electrochemical sensors for analysis of biologically active compounds, PhD Thesis, University of PALACKÝ Olomouc 2023

[114] J.-M. Kauffmann, Électrochimie analytique : potentiels et limitations, L'Act. Chim. 400–401 (2015) 18–23.

[115] S. Patris, Développement d'immunoessais associés aux électrodes sérigraphiées : des particules superparamagnétiques aux nanobodies, PhD thesis, University of Librre de Bruxelles 2014–2015

[116] B. Riviere, Optimisation du procédé de sérigraphie pour la réalisation de capteurs de gaz en couche épaisse : étude de la compatibilité avec la technologie microélectronique, PhD thesis, University of Saint-Étienne, 2004.

[117] A.D. Ambaye, K.K. Kefeni, S. Mishra, E. Nxumalo, B. Ntsendwana, Recent developments in nanotechnology-based printing electrode systems for electrochemical sensors, Talanta 220 (2021) 121951.

Chapter II

Advances in modified screen printed sensors

II.1. Introduction

Traditionally, most of the development towards improvement of the analytical performance of detection devices has focused on the optimization of the parameters of the traditional electrodes. This is executed through the immobilization of electroactive species on their surfaces resulting in so called 'modified electrodes' for the detection of species. This modification of the surface is important because one electrode will not detect all of the desired species, especially when their oxidation or reduction potentials have a value beyond electroactive window of the electrode. To overcome this drawback, considerable research has focused on modifying the electrode surfaces with catalysts. This approach is designed to reduce overvoltage and to decrease the oxidation or reduction potential of the target species for detection in the electroactivity range of the electrolyte.

Recent developments of nanoscience and nanotechnology, more sensitive, rapid, and cost-effective sensors can be fabricated. These sensors have many applications, such as in environmental monitoring, medical diagnostics, industry, defense and security. Introduction of nanomaterials for transducers is an ideal way to engineer them since nanomaterials offer some very unique properties and they have been used greatly in the recent years. The nanostructures employed have different dimensions, forms, materials, and functions.Their appeal lies in their small size, large specific surface area, reactivity, biocompatibility, and sometimes their electrocatalytic and optical properties. The nanometric structuring of the sensitive layers has enabled the creation of miniaturized, high-performance and inexpensive sensors.

Industrial sensor manufacturing technique, such as screen printing, builds sensor by employing different materials. Screen printed electrodes allow for convenient manufacture and easy surface modification, which can improve the sensitivity and selectivity to detect the target analytes. This renders SPEs ideal for industrial monitoring, clinical diagnosis, and academic study. Nanostructure modifications are crucial to obtain better SPE performances.

This section first presents base materials of screen printed electrodes then the properties and synthesis methods of the materials commonly used for the modifications of screen printed electrodes : carbon based nanomaterials, polymeric nanomaterials, composite modifiers, metallic nanoparticles highlighting screen printed modifications using ruthenium nanomaterials as modifier. The section concludes with recent examples of the use of SPEs for the electrochemical detection of dopamine and paracetamol.

II.2. Modification of printing ink with nanomaterials of SPEs

II.2.1. Base materials of SPEs

The performance of an electrochemical device depends greatly on the nature of the working electrode used. The chosen material must show a favorable behavior to the realization of a redox reaction. A fast, reproducible reaction, without modification of the surface, is an effective selection criterion. The potential window on which the electrode can work without causing electrolysis of the electrolyte is also important; the wider it is, the more interesting the electrode used will be. The cost and the possibility of easily structuring the material are also criteria to take into account. In the literature, there is a wide variety of materials used for this purpose. Among these, some stand out for their high conductivity and robustness in the face of redox reactions. As a result, gold, platinum, and carbon are the most commonly used **[1].**

Screen printing electrodes commonly rely on functional inks, which are composed of a polymeric binder, a solvent, and conductive particles to ensure electrical conductivity.

II.2.1.1. Screen-printed carbon based electrodes (SPEs)

The use of carbon inks is more advantageous since the materials used have a wider potential window than gold or platinum electrodes. This increases the range of molecules that can be detected and analyzed. Allotropes of carbon, which include and are not limited to graphite, pearl, and diamond exhibit distinct electrochemical properties. Most popular and readily accessible is graphite, which together with diamond was traditionally regarded as a natural mineral **[1].** In addition, graphite as a material is favored in the manufacturing of screen printed electrodes due to their low cost and easy processing **[2].**

Carbon screen printed electrodes offer extensive possibilities for different application due to their excellent electrochemical properties. Besides the wide electroactivity window, carbon as a material is also chemically inert, inexpensive, easy to structure, and mechanically strong **[3].** In a microelectrode form, these properties make it appealing for all types of systems in electrochemistry.

With regards to the analysis of amino acids, the electrochemical properties of SPCEs with cysteine and tyrosine was tested using clinical pharmaceutical samples with both linear sweep and hydrodynamic voltammetry. These sensors exhibit a reduced oxidation potential in

comparison to conventional carbon and platinum electrodes **[4]** .Regarding the examination of food, *Pierini et al*. have developed a new method for measuring the flavonoid taxifolin in peanut oil samples. The method uses unmodified graphitic SPEs, making it a cost-effective, portable, and reliable option for quality control, particularly for Argentinian Cordoba peanuts. The employed GSPE platform requires minimal reagents and no electrode pretreatment, enabling decentralized and disposable analysis with a limit of detection of 0.021 μM, which is more sensitive than HPLC methods (LODs of 0.66–0.76 μM) **[5].**

II.2.1.2. Metal based SPEs

Screen-printed electrodes are commonly made using graphite inks; however, gold and platinum-based inks are also employed to construct SPEs for the analysis and determination of different elements (**Figure II.1**).

i. Platinum

Platinum is a noble metal, chemically inert, and easy to structure in various forms. It is the material that seems best suited for electrochemistry and yet, apart from its high cost, it retains a major disadvantage concerning its ability to reduce ionic hydrogen to gas in an aqueous medium, even at a very low potential, which makes it difficult to observe analytical signals for molecules that reduce at potentials lower than the reduction potential of hydrogen.

In the literature, platinum is often used as a subject of study, but also as a comparative element with new electrodes. This type of electrode is found in the detection of heavy metals, pesticides, and also as a transducer in biosensor **[6-8].**

ii. Gold

Gold electrodes have a similar behavior to that of platinum, but their surface oxidizes in a range of positive potentials. The limitation of the use of this electrode comes with the presence of sulfides in solution, whose adsorption on the gold surface is favored, thus modifying the surface state of the electrode **[9].** Its use nevertheless remains very important, particularly in the formation of assembled monolayer structures.

There is a lot of research work around gold electrodes, structured as microelectrodes, nanoparticles or as a macroscopic electrode, with or without functionalization. These

functionalized electrodes are used in multiple application domains ranging from the agri-food sector to detect pesticides or heavy metals, to medicine to identify DNA sequences, and to the environment to quantify different types of micropollutants **[6-7,10].**

Wan et al. suggest modifying gold screen printed electrodes with gold nanoparticles for the purpose of detecting the presence of lead and copper metallic cations. This approach yielded detection limits of 2.2 µg/L for lead and 1.6 µg/L for copper **[11]**.

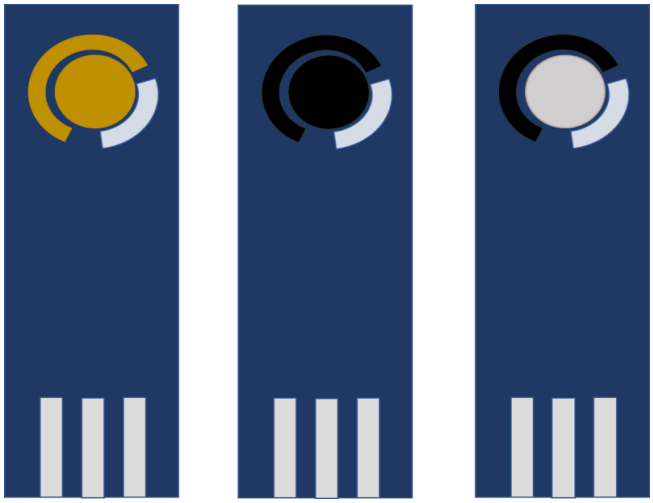

Figure II.1. Gold, graphite and platinum screen printed electrodes.

II.2.2. Different modifications of printing ink with nanomaterials

II.2.2.1. Carbon based nanomaterials

i. Graphene

Graphene is a two dimensional arrangement of monoatomic thick carbon atoms arranged in a "honeycomb" lattice. Due to its 2D structure, graphene and its derivatives, including graphene oxide and reduced graphene oxide, have attracted great interest as an electrode material since their discovery in 2004 **[12]**. This is due to its exceptional physical, chemical, and electronic properties, such as a large specific surface area, excellent electrical and thermal conductivity, excellent mechanical strength, and biochemical compatibility **[13].**

Since its discovery, numerous physical and chemical methods have also made it possible to produce graphene of variable quality depending on the number of sheets obtained or chemical defects present. One of the major challenges is to be able to generate reproducibly high quality, large area, single layer graphene sheets in significant production quantities. The main methods

of graphene synthesis for fundamental and applied research include: mechanical exfoliation **[14,15]**, chemical exfoliation **[16]**, reduction of graphene oxide **[17,18]**, and vapor phase epitaxial growth **[19,20].**

Electroanalysis and screen printed electrodes are attractive, low cost alternatives for insitu environmental monitoring. For this reason, screen printed electrodes were modified with graphene oxide nanoribbons to capitalize on their abundant edge chemistry and increased active sites. The modified electrodes were then used to detect the pesticide methyl parathion in common produce such as broccoli, beetroot, tomato, and ugli fruit. The modified SPEs showed good stability, repeatability, reproducibility, and high selectivity, enabling a detection limit of 0.5 nM **[21].** Also Graphene materials have found widespread use in the development of sensors and biosensors. For instance, in the detection and quantification of metals, *Mahendran et al.* developed a piperazine reduced graphene oxide/screen printed carbon electrode. In this design, graphene oxide was reduced using a green method, employing Hibiscus rosa sinensis flower extract, and then functionalized with piperazine to serve as the electrode material for mercury detection. The conductive properties of the reduced graphene oxide, combined with the presence of piperazine, enhance the electroactive surface area and facilitate a strong interaction with Hg, resulting in a highly sensitive electrode for the detection of the studied metal. Electrochemical biosensors are increasingly being considered for cancer diagnostics **[22]**, while CA19-9 serves as a frequently used early biomarker for pancreatic cancer, its detection methods often lack the necessary sensitivity. To address this, *Ibáñez-Redín et al.* have engineered a cost effective capacitive biosensor. This innovative sensor utilizes carbon nanodots and graphene oxide on interdigitated SPIDEs, achieving a limit of detection of 0.12 U/mL, a level promising for early cancer diagnosis **[23].**

ii. Carbon nanotubes

CNTs are presented as hollow tubes composed of sp^2 hybridized carbon atoms with a diameter on the order of a few nanometers and a length of about a few micrometers **[24]**. Based on the number of tube walls, CNTs can be classified into two main families: single walled and multi walled carbon nanotubes **[25]**, as shown in (**Figure II.2**).

Since the discovery of carbon nanotubes in 1991 by *Iijima* **[24]**, growing interest has been given to their use in a broad field of applications due to their remarkable electronic, thermal, and mechanical properties. Their excellent properties have been demonstrated by numerous

researchers. In the context of pathogens electroanalysis *Radi et al.* investigated Zearalenone's electrochemical properties, developing a method for quantifying it in cornflake samples using a carbon nanotube screen printed electrode. They achieved a detection limit of 2.5 μg/L, ten times lower than Europe's maximum permitted level **[26,27].**

The adaptability of electrode preparation is well illustrated by the screen printing method, *Araujo et al.* **[28]** introduced a cost effective and flexible screen printed electrode made from polyester sheets and conductive ink for the purpose of detecting caffeic acid in tea samples. The screen printed electrodes, decorated with multi walled carbon nanotubes, exhibited improved electrochemical performance. The study assessed the impact of acid functionalization and nanotube size, and the modified SPEs demonstrated excellent caffeic acid recovery in white, mate, and fennel tea samples.

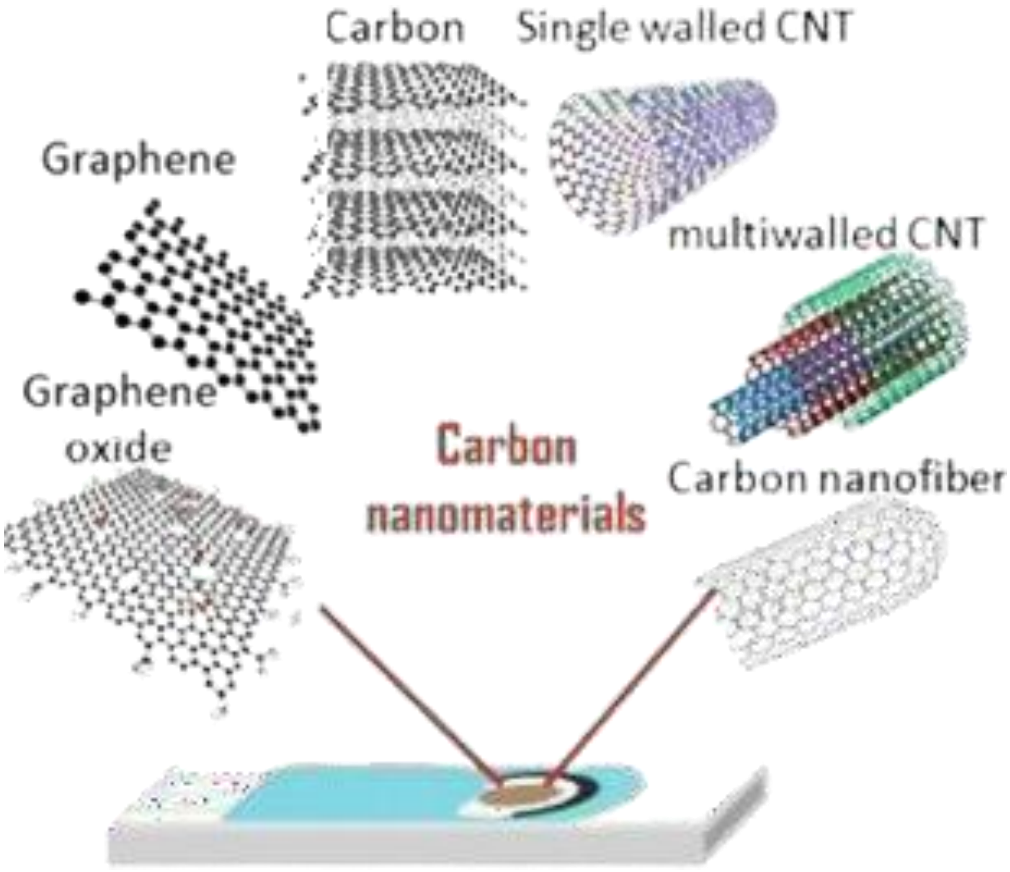

Figure II.2. 2D Carbon nanomaterials modified SPEs.

II.2.2.2. Polymeric nanomaterials

Inorganic compounds possess an advantage in catalysis and conductivity, but polymers possess excellence in malleability. Polymers were initially deemed as non-conductive due to inherent chain resistance.Conductive polypyrrole was first synthesized in 1978, negating this premise.Conductive polymers like polyaniline and polythiophene have now been utilized in chemical sensors **[29].**

Polymer materials can be synthesized with controlled molecular weights and viscosities and are therfore suitable for screen printing applications. The advancements in nanoscale control within the last few years have made it possible to develop nanostructured polymer inks, which provide even better opportunities in printing technology.

Polypyrrole (PPy), known for conductivity thanks to a π-conjugated backbone, finds far-reaching applications in batteries, sensors, and capacitors **[30].** Polymerized on the pyrrole (Py) basis, *yawale et al.* **[31]** added Py to $FeCl_3$/methanol and evaporation of methanol improved oxidation potential. 60 wt% PPy mixed with butyl carbitol and ethyl cellulose upon purification was utilized to prepare a paste ink. SEM revealed a honeycomb nanoscale architecture that can be controlled by the Py/$FeCl_3$ ratio. PPy ink was subsequently used in printed biosensors **[32].** Another method used polyvinyl alcohol, gemini surfactant, and oxidants (p-toluenesulfonate hexahydrate, $FeCl_3$), with 24h polymerization and 64h purification. Horseradish peroxidase and glucose oxidase enzymes were used to prepare PPy/enzyme inks, yielding enzyme-coated nanoparticles. Printed electrodes on flexible PET enabled rapid, stable detection of H_2O_2 and glucose.

Polyaniline, otherwise a poor conductor, can be transformed into a conducting material through protonation with salts or surfactants. Interestingly, incorporation of toluenesulfon amide can enhance its conductivity up to more than 100 S/cm **[33].** Direct screen printing of PANI is, however problematic because of particle agglomeration. For this reason, *Gill et al.* **[34]** employed a mixture of 10 wt% polyvinyl butyral, 10 wt% PS3, and ethylene glycol monobutyl ether. This new approach gave screen printed films with significantly reduced resistance, achieving values more than 1000 times smaller than those of drop-cast films. This is because nanoparticle compression is improved and more efficient electron pathways are formed.

Poly(3,4-ethylenedioxythiophene),a polythiophene derivative, has superior conductivity compared to polypyrrole and allows for enzyme immobilization through electrostatic bonds **[35].** However, poor solubility prevents nanoparticle dispersion in inks.To fight this, *Istamboulies et al.* **[33]** employed poly (sodium styrene sulfonate) as the polymerization electrolyte, allowing them to react 3,4-ethylenedioxythiophene with ammonium peroxydisulphate in water with ultrasonic for 1 hour. The print-friendly blue ink that they got was 100% conductive at 100% PEDOT. The conductivity of the ink was enhanced by PEDOT content, reaching a whopping 2420 S/cm at 100% PEDOT. Besides, the immobilized acetylcholinesterase electrode effectively oxidized choline at a low potential of 100 mV Ag/AgCl.

Although conductive polymer inks have the advantage of being flexible for application in devices like portable miniature chemical sensors, they typically have issues regarding the development of irregular nanostructures and absence of redox centers that discourage their catalytic potential.

Of special interest is the advancement of the increasing integration of electrochemical biosensors in "cancer-on-a-chip" devices to identify cancer markers at cellular, organelle, and molecular levels, *Moreira et al.* introduced a low-cost SPE biosensor for the determination of CEA, employing plastic antibodies on a polypyrrole matrix.Their method is selective adsorption of CEA on MPPy after antibody removal, with a detection limit of approximately 1 pg/mL, less than 5% deviation, and a simple and rapid process **[36].** Electrochemical techniques are generally applied in scientific research to detect amino acids. For example *Su* and *Cheng* examined the electrocatalytic cysteine oxidation on a screen printed electrode that was modified by an electrogenerated polymer film. Cyclic voltammetry determined that the modified electrode lowers the overpotential and enhances cysteine oxidation activity compared to unmodified SPEs. Besides, flow injection amperometry under optimized conditions showed good analytical performance, including high sensitivity, broad dynamic range, and low detection limit **[37].**

II.2.2.3. Composite modifiers

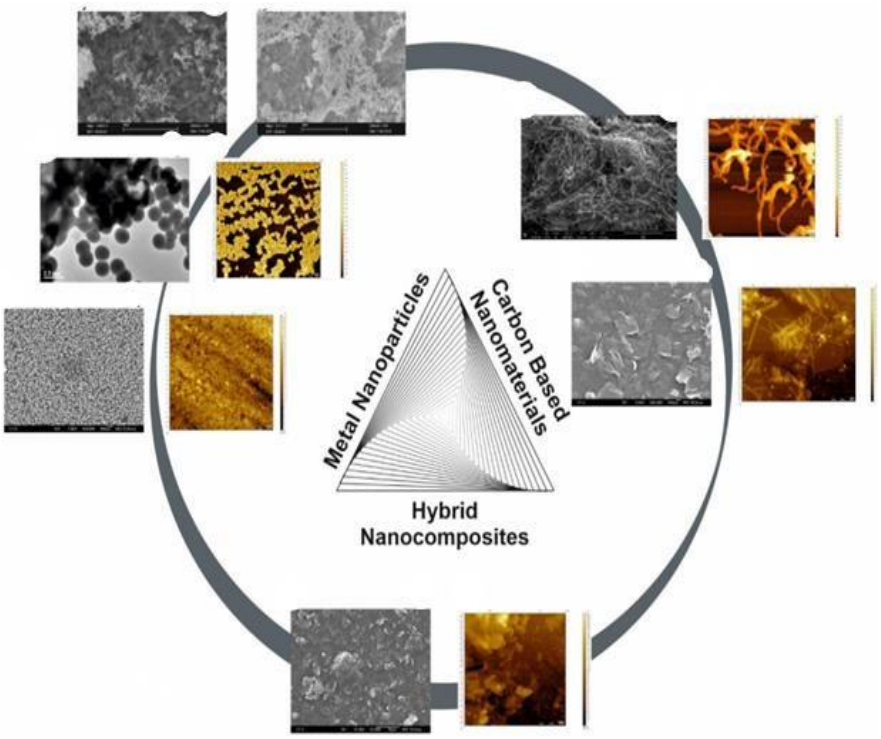

Figure II.3. Microscopic images of some : metal nanoparticles, carbon based nanomaterials and hybrid nanocomposite **[38].**

i. Carbon nanomaterials and conductive polymers

Mixing carbon nanomaterials like graphene, carbon nanotubes and carbon nanofibers with conductive polymers leads to new nanocomposites that have novel and highly promising physical and chemical behaviors. The past decade has seen wonderful progress in this area, opening new areas of application to these nanocomposites.There is plenty of work in the synthesis of the materials, the chemical and electrochemical being the most common ones used **[39].**

Functionality of synthesized nanocomposites is largely based on dispersion of carbon nanomaterials within the polymer matrix.Therfore, extreme homogeneity and dispersion of nanomaterials are required to effectively synthesize the nanocomposites. Some studies also looked at the utilization of PC/NMC nanocomposites in electrochemical sensors, identifying their employment in sensing a variety of metallic as well as organic pollutants.

ii. Metallic nanoparticles and conductive polymers

The introduction of metallic nanoparticles into conducting polymer matrices has been a successful approach to enhancing the properties of the modified electrode.The technique has demonstrated tangible gains in stability, sensitivity, and electrocatalytic activity,which has led to substantial progress in the filed **[40].**

Use of nanocomposites, prepared with conductive polymers and metal nanoparticles (more notably noble metal particles) has been extensively documented for electrochemical sensor devices. The sensors are used in the detection of an extensive variety of molecules, as documented in a recent review. *Khalifa et al.* have constructed a highly sensitive sensor for the determination of pyocyanin, a valuable marker of Pseudomonas aeruginosa infection, from corneal ulcer samples in direct method. This sensor composed of screen-printed electrode modified by polyaniline/gold nanoparticles/indium tin oxide (PANI/AuNPs/ITO) was in complete concordance with the normal phenotypic and PCR-based diagnostic test for all the diagnostic parameters studied **[41].** *Maria-Hormigos et al*. have also investigated the modification of carbon screen printed electrodes with a bismuth/polystyrene/carbon nanopowder composite material to improve lead and copper detection. These authors quote extremely low detection limits of 0.029 µg/L for Pb and 0.012 µg/L for Cu **[42].**

II.2.2.4. Metallic nanoparticle modified SPEs

Metallic nanoparticles, with sizes ranging from 1 to 100 nm, exhibit unique chemical, physical, and electronic properties. This has led to considerable interest in their use across numerous technological applications. Gold, silver, platinum, palladium, copper, bismuth, and their alloys or oxides, are among the materials being explored. In particular, their application in electrochemical sensors shows great promise for enhancing the sensitivity and selectivity of these devices, owing to their excellent electrical conductivity, large active surface area, and catalytic activities **[43].**

Metallic nanoparticles can be prepared by two main approaches, the "top-down" approach or descending route and the "bottom-up" approach or ascending route **[44,45].** For "top-down" procedures, a solid metal is systematically broken down to generate metallic nanoparticles of desired dimensions. The assembly and formation of the particles are controlled by a pattern or matrix **[46,47]**. Whereas in "bottom-up" procedures, metallic nanoparticles are obtained by

nucleation and growth processes from isolated atoms. It involves the use of physico-chemical phenomena at the atomic and molecular scale in order to chemically transform a precursor into metallic particles. The assembly and positioning of atoms, molecules or particles makes it possible to produce simple or elaborate nanostructures.

i. Gold nanoparticles

Gold nanoparticles possess better conductivity and catalytic performance **[48],** which make them highly promising for electrochemical sensing of broad-spectrum analytes **[48,49].** Moreover, AuNPs have also proven to enhance the resolution of electrochemical signals **[50].** The size dependent properties of AuNPs are strongly influenced by its preparation conditions **[51].** Gold nanoparticles are widely used as a substrate due to the fact that they can be readily functionalized and size, shape and properties can also be adjusted.These advantages have various applications in electrochemical sensors. *Titoiu et al.* built a label-free AuNP-Au-SPEs sensor for detecting lysozyme in wines. Its detection limit is similar to that of HPLC and colorimetric, and therefore has potential for allergen monitoring in wine production. The aptasensor has comparable detection performances with simpler instrumentation, multi-purpose, rapid analysis, and recyclability, especially in comparison to HPLC **[52].**

As SPE modification , *Alonso Lomillo et al*. demonstrated the feasibility of a screen printed electrode modified by gold nanoparticules for electrochemical detection of ascorbic acid in serum samples. The results showed that the electrode demonstrated linear responses to ascorbic acid in a range of 1.9-16.6 µM **[53].**

ii. Silver nanoparticles

Silver nanoparticles, can be synthesized by various chemical routes **[54].** Modified silver nanoparticle electrodes, however, possess a significant use in bioanalysis **[55,56].** Owing to the relatively small electroactivity window of silver relative to platinum and gold. Silver nanoparticles nanostructured electrodes have been used for the detection of metallic micropollutants according to numerous examples of literature, e.g.SPEs in the determination of antimony ions (Sb) with detection limit of 0.82 µg/L **[57].** *Guo et al.* prepared ternary nanocomposites of silver nanoparticles, carbon dots, and reduced graphene oxide that were electrodeposited on a glass carbon electrode. The resulting material showed improved electrocatalytic activity for the reduction of doxorubicin. They demonstrated that the modified

electrode detected doxorubicin (DOX) in the range of 0.01 to 2.5 µmol /L with a detection limit of 2 nmol/ L **[58].**

iii. Platinum nanoparticles

Platinum nanoparticles, that are electrochemically **[59,60],** chemically **[61,62],** or physically prepared **[63],** have several uses, mostly catalysis. They can even be modified easily with other biomolecules and ligands **[64].** As an example of use, *Arcos-Martínez et al.* employed electrodeposited platinum nanoparticles on SPEs in the determination of arsenic with a limit of detection of 5.68 µg/L **[65].**

A platinum/reduced graphene oxide/poly-3-aminobenzoic acid nanocomposite film was formed on a screen printed carbon electrode using a single step electropolymerization approach.The constructed modified electrode showed superior electrocatalytic activity towards hydrogen peroxide, and sensitive glucose and cholesterol biosensing was achieved. Linear detection ranges were determined to be 0.25–6.00 mM and 0.25–4.00 mM, respectively. low detection limits (LODs) of 44.3 and 40.5 µM. Moreover, the sensors demonstrated satisfactory selectivity and a recovery rate of 98.2–104.1% for serum samples **[66].**

Electrochemical immunosensors utilizing gold or platinum electroplated screen printed carbon electrodes were fabricated for the detection of cancer antigen 125 in plasma samples. The limits of detection achieved were 419 ± 31 ng/mL and 386 ± 27 ng/mL, respectively. Platinum modified SPCEs exhibited a greater surface area and enhanced antibody loading capacity. Following anti-CA125 immobilization and bovine serum albumin blocking, electron transfer rate constants decreased. Notably, only platinum modified SPCEs demonstrated a significant reduction in the electron transfer rate constant (k^o) upon CA125 binding, rendering them more effective for CA125 detection **[67].**

II.2.2.4.1. SPEs modification by physical approaches

Electrode surface modification in these devices typically occurs through three established methods, as illustrated in (**Figure II.4**).

i. Drop-Casting method

Drop casting is the simplest way to modify screen printed electrodes. Optimization is simplified to a single parameter: the final volume deposited on the electrode surface. It can be tuned by varying the size of the drop and concentration of solution for metal nanoparticules **[68].** Several metal NP solutions have been used, e.g., bismuth **[69],** platinum **[70–72],** rhodium **[73],** gold **[74],** silver **[75],** copper **[76],** and nickel **[77].**The method essentially involves the deposition of a solution onto a substrate with the subsequent drying phase.While capable of producing a high quality, thick film, it is nevertheless the most uncomplex film formation method.Its greatest advantage is the low equipment requirement. However, limitations of the method include incomplete control over film thickness, edge effects, precipitate formation upon drying, and random drying patterns. Moreover, the coating material must possess high solubility in the solvent of choice to prevent crystallization or precipitation.

ii. Ink mixing and printing method

One of the methods for modification of screen printed electrodes with nanoparticules mimics the conventional method applied to carbon paste electrodes. This involves incorporating the modifier into the carbon paste, followed by pressing and polishing. A method for screen printed electronics modification using an ink mixing technique for metals involves formulating an ink from conductive carbon particles, a solvent/binder system, and metal nanoparticles in a highly controlled manner.For best performance, several significant parameters must be addressed, including precise ink formulation, rheological property control, substrate selection, and careful control of the curing process. Screen printing is a process in which ink is placed on a mesh screen.The ink is squeezed through a stencil with a squeegee, leaving a pattern. It then dries and many layers may be applied for complex designs **[78].**

In the beginning of the 1990s, a method was developed based on conductive material in the form of metal particles mixed with screen printing inks to fabricate improved enzymatic sensors. The appeal of the method was its simplicity: available materials were combined with binding agents and solvents, reducing the process to recipe optimization primarily. Subsequently, metal particles were mixed with a conducting material and binder **[79,80].** An issue is that nanoparticle agglomeration upon mixing decreases dispersion, leading to

microsized particles with increased size.The effect constrains analytical performance and eliminates the benefit of high surface area inherent in nanoparticles, for which reason few studies have employed ink mixing with metal NPs.

A recent study investigates the optimization of ink blending to achieve high performance catalysis. The process involves inkjet printing of capped silver nanocrystals, a technique that is comparable to screen printing. The method involves printing a pre-blended ink via a nozzle, followed by a mild thermal treatment. The use of green solvents such as glycerol is one of the elements that has led to the simplicity of the procedure.

Inkjet printing on thin conductive substrates offers an advantage in the form of exposure to more metal particles by analytes, minimizing aggregation and inhibition from paste additives. Silver nanoparticles, in particular, show a higher catalytic response to hydrogen peroxide. Decapping with hydrochloric acid also enables connectivity of particles that lead to reduced resistance and improved electron transfer and overal performance.Though this method successfully solves the problem of ink mixing limitations, its, extension to other metals is undetermined **[81].**

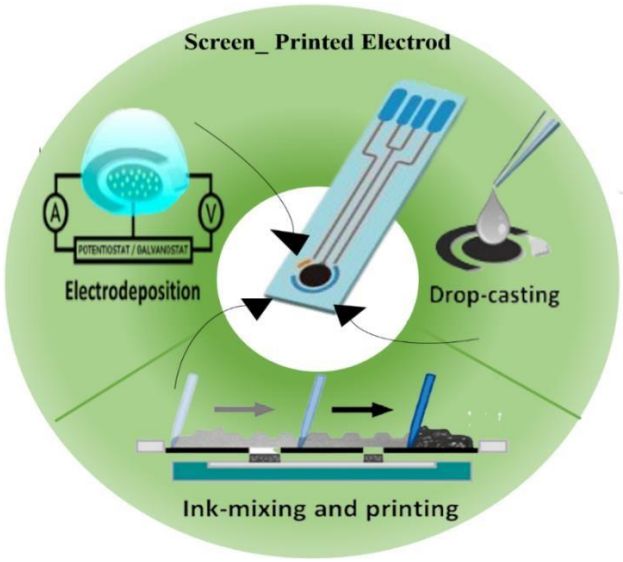

Figure II.4. Schematic illustration of the three principal approaches commonly used to modify screen printed electrodes (SPEs) with metal nanoparticles (NPs).

II.2.2.4.2. Chemical and electrochemical deposition

Electrochemical deposition is the most prevailing approach to designing solid phase extraction devices in the form of metallic nanoparticles. It allows for controlled morphology

of NPs.By reducing oxidized species, typically water soluble metal salts, at a specified potential or current, researchers can design particular metal particles on conductive surfaces. The most significant optimized parameters in electrochemical deposition are classified into two broad categories: those on the precursor solution, for instance, the salt type and concentration and those on the electrochemical deposition conditions themselves. Although higher precursor concentrations tend to form bigger particles, nanoparticle size and shape are mostly controlled electrochemically. Hence, the concentration is kept at a high level and not usually optimized **[82].** Two critical parameters influencing nanoparticle size and shape are the applied potential or current, and the deposition time. Extending the deposition time leads to an increase in both the amount and size of nanoparticles. The potential is relevant to potentiostatic techniques, whereas the current is relevant to galvanostatic techniques **[83].**

II.3. Properties and interest of ruthenium

II.3.1. History

Ruthenium was discovered in 1808 by *J.A.Sniadecki* at the University of Vilno, in Poland, then later by *G.W.Osnann* in 1828 at the University of Tartu in Russia. It was not really identified until 1844 by the Russian professor *Karl Klaus* who obtained a pure sample of oxide, and named it ruthenium in honor of Russia **[84].**

It is mostly found in its native state or in alloy with platinum. The most important mineral is laurite. Traces of ruthenium are also found in a series of nickel and copper ores. World production amounts to approximately 12 tons per year, it is often a byproduct of the extraction of precious metals from platinum mines. It is resistant to air and practically unattacked by acids, including aqua regia, unless potassium chlorate is added **[85].**

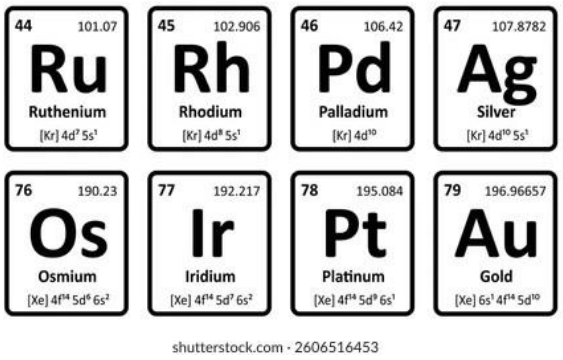

Figure II.5. Image of ruthenium in platinum group elements.

II.3.2. General properties of ruthenium

Ruthenium, a scarce element belonging to the platinum group, finds limited applications due to its inherent hardness and brittleness, rendering it challenging to machine in its pure form. Its low reactivity makes it a valuable alloying agent, enhancing the wear resistance of platinum and palladium alloys. Furthermore, it improves the corrosion resistance of titanium alloys.Ruthenium is added in amounts less than 15% to ensure the resulting alloy remains machinable. Beyond its utility in electrolysis, ruthenium, akin to other platinum group metals, exhibits significant catalytic activity, particularly in hydrogenation processes.**Table II.1** gathers some physicochemical characteristics of this element.

Table II.1. Physicochemical characteristics of ruthenium **[84]**.

Ordinary state	Solid
Melting point	2 334 °C
Boiling point	4 150 °C
Fusion energy	24 $kJ \cdot mol^{-1}$
Enthalpy of vaporization	595 $kJ \cdot mol^{-1}$
Molar volume	8.17×10^{-3} $m^3 \cdot mol^{-1}$
Vapor pressure	1.4 Pa à 2 249.85 °C
Atomic radius	131.6 pm–134pm
Covalent radius	124 pm
Density	12.2 $g.cm^{-3}$

Ruthenium is a satin white element possessing high resistance to the weather, being inert to water, air, and acids, and even to oxidation in room temperatures. It is susceptible to quick and complete corrosion upon exposure to alkaline fusion. When heated to high temperature, it gets a surface blue film of dioxide. The melting point of ruthenium is the lowest among platinum group metals **[84,86].**

II.3.3. The fields of application of ruthenium

- High-end automotive spark plugs have electrodes coated with a platinum and ruthenium alloy.
- In alloy form, ruthenium makes platinum and palladium resistant and can be used, for example, to make electrodes or pen nibs.

- It also enhances the corrosion resistance of titanium.
- It has been used in the manufacture of hard drives since 2001. It is a three-atom-thick coating between two magnetic layers. This material currently allows to store up to 25.7 Gbits/inch^2 and will allow to reach up to 400 Gbits/inch^2
- Superconductor
- Asymmetric catalysis in organic chemistry **[87].**

II.3.4. Advantages of ruthenium

- Ruthenium's capacity to shift between oxidation states, ranging from +2 to +8, makes it a distinctive catalyst for oxidative reactions **[88].**
- Ruthenium metal is notable in excited state chemistry and catalysis because of its extensively researched organometallic and coordination chemistries.
- Ruthenium compounds are being explored for their catalytic potential, particularly in drug synthesis, due to their promising applications in catalysis and generally low toxicity **[89,90].**
- Ruthenium compounds present a compelling alternative in catalysis due to their unique properties and cost-effectiveness compared to other platinum group metals. This combination of factors has led to their widespread adoption as the preferred choice for numerous catalytic reactions.
- Chemical complexes are versatile tools with applications spanning catalysis, sensor development, drug delivery, medicinal chemistry, and microscopy. Their diverse properties make them valuable in a wide range of scientific and technological fields **[91,92].**

II.3.5. State of the art of ruthenium based electrochemical sensors

i. Cations

Alkali, alkaline earth, and transition metal ions are the most common cationic analytes studied with ruthenium based sensors, especially Cu^{2+} which is a common pollutant and metallomic biomarker. A bis-phenanthroline-linked dinuclear tris complex is a biological sensor for Cu^{2+}. It exhibits high sensitivity (LOD = 3.33×10^{-8} M) and selectivity for Cu^{2+} over other metal ions, as well as water solubility, making it an excellent probe for detecting Cu^{2+} in zebrafish **[93].**

ii. Phosphates

Ruthenium based sensors interact with anions such as phosphates. These complexes are discussed based on their best selectivity or affinity for a specific anion to avoid repetitions. Phosphates are essential to living organisms and critical in forming membranes, DNA, RNA, and proteins. Selective binding of phosphate derivatives by proteins is a highly regulated event of interest for medicinal or analytical purposes **[94]**. Therefore, sensing phosphates in aqueous media has been under scrutiny for decades, and several systems have been deployed to develop sensors. Accordingly, ruthenium based sensors have been developed for the detection of phosphates, such as calixarene ruthenium bipyridyl complexes. In these systems, the phosphate anion interacts with amido groups, forming multiple hydrogen bonds. The strong affinity between the cationic complex and phosphates is highlighted by the formation of single crystals, with a stability constant between H_2PO4^- and the calixarene ruthenium complex in DMSO estimated at $2.8 \times 10^4\ M^{-1}$ **[95].**

iii. Carbohydrates

Boronic acid based sensors have emerged as a widely used method for sugar detection **[96]**, capitalizing on the reversible binding of boronic acids to diols, a common structural component of sugars. One of the earliest applications of this strategy involved a ruthenium complex designed for glucose sensing **[97,98]**, a bis-5,6-dihydroxy-1,10-phenanthroline ruthenium complex, which forms a boronic acid adduct at pH 8, undergoes disruption in the presence of glucose. This displacement assay operates on the principle that the luminescence intensity of the ruthenium/boronic acid complex diminishes as glucose is introduced **[99]**. Similarly, another ruthenium based probe detects glucose via the luminescence decay of a ruthenium tris complex, incorporating Concanavalin A, is a lectin whichspecifically bonds to mannose and glucose. The sensing mechanism is based on competitive displacement, where glucose disrupts the MLCT energy transfer process at the ruthenium center.

iv. Biomolecules

In biology, sensing is crucial for diagnostics, therapy, and understanding living organisms. Generating an interaction between a biomolecule and a metal based complex is relatively easy. However, achieving specificity and selectivity remains extremely challenging due to competition. Indeed, determining selectivity requires control experiments with competitive analytes and varying conditions. Unfortunately, it is unrealistic to test all possible conditions, but more evaluation leads

to a more robust and useful system **[100,101]**. The scientific literature contains numerous studies on this topic,especially concerning proteins and DNA/RNA

- **Proteins**

Amyloid-β accumulation is closely linked to Alzheimer's disease, making its aggregate prevention/detection critical. A dipyridophenazine ruthenium complex detects amyloid-β aggregation **[102]**, exhibiting strong photoluminescence in solution with a large Stokes shift and a long-lived photochemical process. Subsequent studies have validated ruthenium based complexes for sensing amyloid-β peptide aggregation **[103]**. An immunosensor array that uses nanorods grafted with tris ruthenium complexes as electrochemiluminescent materials has been developed for the detection of N-acetyl-β-D-glucosaminidase, a biomarker of diabetic nephropathy. The luminescent signal demonstrates a linear response to concentrations ranging from 1 $ng \cdot mL^{-1}$ to 0.5 $pg \cdot mL^{-1}$, with a detection limit of less than 0.2 $pg \cdot mL^{-1}$**[104]**.

- **DNA/RNA**

Positively charged ruthenium complexes are good for detecting nucleic acids because they strongly interact with proteins, DNA and RNA. Displacement assays use this to create a reaction when these substances are present. For example, a labeled DNA sequence can bind to polypyridyl ruthenium complexes, but this bond can be broken by a matching RNA sequence. A 3-amino-1,2,4-triazino-1,10-phenanthroline derivative was particularly effective, achieving a detection limit of 0.28 nM **[105]**.

II.3.6. State of the art of ruthenium nanoparticles based electrochemical sensors

The exploration and development of ruthenium nanomaterial based sensors is a very broad and highly promising field of scientific inquiry. Consequently, the advancement of screen printed sensors utilizing such sophisticated materials is attracting significant interest from the research community. In the context of biological species and pharmaceutical compounds analysis, different pharmacological activities have been tested on screen printed electrodes modified with different nanosized ruthenium materials through different electrochemical techniques, for example a non-enzymatic electrochemical biosensor for detecting acetaminophen in human blood was constructed on the basis of functionalized vanadium carbide and ruthenium-polyaniline nanoparticles. The sensor exhibited electrocatalytic activity and achieved a low detection limit, a broad linear range, and good

reproducibility and recovery, attributed to the material's high surface area, conductivity, π–π interactions, and abundance of electroactive sites. Real sample testing confirmed the sensor's practical applicability for effective biomonitoring **[106].**

Ruthenium/Vulcan carbon nanosensor was developed for idarubicin detection. TEM, XPS, and XRD characterized synthesized nanoparticles, showing favorable electrochemical properties when Ru@VC modified a glassy carbon electrode. The sensor had a 9.25×10^{-9} M detection limit and a 2.8×10^{-8} M quantification limit. Successful application in Idamen® IV and human serum samples, with high recovery rates and minimal interference, indicates potential for biological analysis **[107].** Also a CeO_2-Au nanofibers and RuO_2 nanowires composite, with graphene oxide and functionalized multi walled carbon nanotubes, modified a screen printed carbon electrode, enabling simultaneous electrochemical detection of serotonin, dopamine, and ascorbic acid. The modified electrode demonstrated reduced overpotentials and resolved overlapping peaks **[108].** Moreover a Ru-BCDs-modified electrode was developed by stabilizing a BPEI-coated carbon dot nanohybrid (conjugated with Ru_3^{2+}) on carbon nitride nanosheets. This electrode was used as a label-free, signal-on ECL biosensor for detecting miR133a, with a detection limit of 60 fM, and showed promise in human serum samples **[109]**. In the case of biosensing a novel composite material was developed and modified with alcohol dehydrogenase to fabricate an amperometric ethanol biosensor, designed for the detection of NADH and exhibiting enhanced electrocatalytic properties. The sensor, characterized through FE-SEM, HR-TEM, XRD, CV, and EIS techniques, demonstrated linearity within the ranges of 1–1800 µM and 1–1300 µM. Displaying favorable selectivity, precision, and accuracy in the analysis of alcoholic beverages, it presents a promising substitute for current methodologies **[110].**

Another interesting feature is that Ru may be functionalized in food analysis. Ru/V@WO_3 nanocomposites were synthesized and used to modify a glassy carbon electrode. The electrode exhibited notable sensitivity, a strong reduction peak, excellent selectivity, linearity, and long-term stability in detecting sulfonamide, and was successfully used with honey samples **[111]**. A Ru/NiFe-LDH-MXene/SPCE electrode was fabricated for nitrofurantoin detection. The synergistic effect between MXene and LDH, enhanced by Ru nanoparticles, improved the sensor's electrochemical performance, resulting in high sensitivity and a low detection limit. It was successfully applied for nitrofurantoin detection in food samples, demonstrating good recovery, suggesting its potential as a valuable tool for monitoring food safety **[112]**. A newly

developed electrochemical sensor, utilizing ruthenium nanoparticles and safranin on a carbon paste electrode, facilitates the sensitive detection of amisulpride. The Ru-Saf/CPE sensor demonstrates notable electrocatalytic activity and selectivity, proving effective across a spectrum of Amisulpride dosages and enabling the simultaneous detection of both Amisulpride and citalopram within a broad linear range **[113]**.

II.4. Applications of SPEs in the detection of dopamine and paracetamol

Table II.2. Applications of screen printed electrodes functionalized with nanoparticles in the detection of dopamine and paracetamol.

Analyte	Electrode	Method	LinearRange µM	LOD µM	Samples	Ref
DA	Pd NPs	DPV	0.35–135.35	0.056	Injection	**[114]**
DA	rGO-500 rGO-600	CV DPV	0.5–20 0.5–20	1.11 1.23	Buffer	**[115]**
DA	mMWCNTs	CV	5–8	0.43	Human blood serum	**[116]**
DA	Tyrosinase/chitosan /rGO	CV	0.4–8 and 40–500	0.022	Urine	**[117]**
DA	WO3	SWV	(-)	0.87	Urine	**[118]**
DA	Na [RuL2] /MWCNT/Nafion	CV DPV FIA	1.31–263	0.61	Dopamine hydrochloride injection	**[119]**
DA	CS/N,GQDs	CV DPV	1–100 and 100–200	0.145	Human urine	**[120]**
DA	G/PANI/PS nanofiber	SWV	0.0001–100	5×10^{-5}	Biological matrices	**[121]**
DA	AgNP	DPV	0.05–45.3	17×10^{-6}	Dopamine hydrochloride injection	**[122]**
DA **UA**	GO/Fe3O4@SiO2 core–shell	DPV	0.1–600 DA 0.75–300 UA	0.089 0.57	Dopamine injection Urine	**[123]**

TableII.2.Cont.

Analyte	Electrode	Method	LinearRange µM	LOD µM	Samples	Ref
DA **EP** **PA**	CB-ERGO	SWV	4.9–19 9.9–95 9.9–95	1.5 9.4 5.3	Buffer	**[124]**
DA **AA**	PDbS-rGO	LSV CV	0.1–300 10–1100	0.134 0.88	Ex vivo brain tissues	**[125]**
DA **UA** **EST**	RGO/AgNWs/AgNPs	LSV CV EIS DPV	0.6–50 1–100 1–90	0.16 0.58 0.58	Maternal urine	**[126]**
DA **TYR**	GQD	CV DPV	0.1–1000 1.0–900	0.05 0.5	Human urine	**[127]**
AA **DA** **UA**	GQDs/IL	DPV	25–400 0.2–10 0.5–20	6.64 0.06 0.03	Vitamin C tablets, Dopamine injection	**[128]**
DA **5-HIAA**	AuNP	SWV	0.2-100	8×10^{-6} 22×10^{-6}	the blood plasma	**[129]**
PA **IB** **CF**	SPCNTE SPCNFE SPGPHE	DPV	0.0132– 0.662 0.0097– 0.485 0.0103– 0.515	0.595 10.7 1.03	Spikes tap water and hospital wastewater	**[130]**
PA **G**	Fullerene black	DPV	1–300 0.1–300	0.01 0.005	Commercial pharmaceutical tablets urine	**[131]**
PA	carbon nanofibers	DPASV	0.002–0.05 0.1–2.0	5.4×10^{-4}	Natural water samples	**[132]**
AA **DA** **UA**	RGO, ionic liquid	CV	4.0-4500 0.5-2000 0.8-2500	0.95 0.12 0.20	Dopamine hydrochloride injection, and human urine	**[133]**
DA **CAP** **HYD**	SWCNT, Cobalt phthalocyanine microband	CV	5to 49.6	1.13 0.18 2.9	Buffer	**[134]**
DA **HQ** **CC**	MWCNT	DPV	5.0 –45 5.0 –80 5.0 – 90	0.337 0.289 0.369	Environmental monitoring and biomedical applications	**[135]**
PA **TRA**	Yb2O3 nanoplates (NPs)	DPV	0.25–2000 0.5–5400	55×10^{-6} 87×10^{-6}	Pharmaceutical dosage forms , human fluids	**[136]**

APAP **COD** **CAF**	CeO2	DPV	0.09 – 7 0.09 – 50 5 – 286	0.051 0.043 2.4	Human serum	**[137]**

LSV Linear Sweep Voltammetry ,**FIA**: Flow Injection Amperometry**,DPASV :** Diferential-Pulse Anodic Stripping Voltammetry.

Conclusion

Metallic nanoparticles are of increasing interest in science and technology because their properties differ from their bulk equivalents. Their unique physical and chemical properties make them useful for technological applications and as a fundamental model for studying the growth of matter.

Screen printed electrodes are attractive because of their advantages over other transduction systems, such as high sensitivity, ease of use, the use of a small sample volume, disposability, and low cost. In addition, electrochemical screen printed electrodes are particularly attractive for developing devices that enable rapid decentralized measurements for the diagnosis and detection of different analytes in different fields. But the greatest advantage of screen printed electrodes is the ease with which they can be modified, making them an ideal electrodes in a highly reproducible manner. In this chapter, we wanted to show the important role that nanotechnology can play in the design of screen printed electrodes.

The review of the literature on ruthenium, highlights its various relevant physical and chemical properties. Its widespread use in many fields makes it an important subject of investigation, as evidenced by the abundance of scientific publications. The bibliographic data relating to ruthenium in the context of the modification of screen-printed electrodes makes it a promising candidate for sensors elaboration.

References

[1] J. Pezard, Synthèse d'électrodes carbonées pour la détection électrochimique et insertion dans un système microfluidique, PhD thesis in chemistry, Central School of Lyon, 2015.
[2] A. Economou, Recent developments in the field of screen-printed electrodes and their related applications, Talanta 73 (2007) 347–364
[3] A. Morrin, A.J. Killard, M.R. Smyth, Electrochemical characterization of commercial and home-made screen-printed carbon electrodes, Anal. Lett. 36 (2003) 2021–2039
[4] M. Vasjari, A. Merkoçi, J.P. Hart, S. Alegret, Amino acid determination using screen-printed electrochemical sensors, Microchim. Acta 150 (2005) 233–238.
[5] G.D. Pierini, S.A. Maccio, S.N. Robledo, A.G. Ferrari, C.E. Banks, H. Fernández, M.A. Zon, Screen-printed electrochemical-based sensor for taxifolin determination in edible peanut oils, Microchem. J. 159 (2020) 105442.
[6] A. Uhlig, U. Schnakenberg, R. Hintsche, Highly sensitive heavy metal analysis on platinum- and gold-ultramicroelectrode arrays, Electroanalysis 9 (1997) 125–129.
[7] M.A. El Mhammedi, M. Achak, M. Bakasse, Evaluation of a platinum electrode modified with hydroxyapatite in the lead(II) determination in a square wave voltammetric procedure, Arab. J. Chem. 6 (2013) 299–305.
[8] J. Clavilier, R. Faure, G. Guinet, R. Durand, Preparation of monocrystalline Pt microelectrodes and electrochemical study of the plane surfaces cut in the direction of the {111} and {110} planes, J. Electroanal. Chem. Interfacial Electrochem. 107 (1979) 205–209.
[9] D.G. Wierse, M.M. Lohrengel, J.W. Schultze, Electrochemical properties of sulfur adsorbed on gold electrodes, J. Electroanal. Chem. Interfacial Electrochem. 92 (1978) 121–131.
[10] K. Wang, J. Lu, L. Zhuang, Direct determination of diffusion coefficient for borohydride anions in alkaline solutions using chronoamperometry with spherical Au electrodes, J. Electroanal. Chem. 585 (2005) 191–196.
[11] H. Wan, Q. Sun, H. Li, F. Sun, N. Hu, P. Wang, Screen-printed gold electrode with gold nanoparticles modification for simultaneous electrochemical determination of lead and copper, Sens. Actuators B Chem. 209 (2015) 336–342.
[12] K.S. Novoselov, A.K. Geim, S.V. Morozov, D. Jiang, Y. Zhang, S.V. Dubonos, I.V. Grigorieva, A.A. Firsov, Electric field effect in atomically thin carbon films, Science 306 (2004) 666–669.
[13] J. Liu, Z. Liu, C.J. Barrow, W. Yang, Molecularly engineered graphene surfaces for sensing applications: A review, Anal. Chim. Acta 859 (2015) 1–19.
[14] D.A.C. Brownson, D.K. Kampouris, C.E. Banks, Graphene electrochemistry: fundamental concepts through to prominent applications, Chem. Soc. Rev. 41 (2012) 6944–6976.
[15] D.R. Dreyer, S. Park, C.W. Bielawski, R.S. Ruoff, The chemistry of graphene oxide, Chem. Soc. Rev. 39 (2010) 228–240.
[16] D. Chen, L. Tang, J. Li, Graphene-based materials in electrochemistry, Chem. Soc. Rev. 39 (2010) 3157–3180.
[17] P.W. Sutter, J.-I. Flege, E.A. Sutter, Epitaxial graphene on ruthenium, Nat. Mater. 7 (2008) 406–411.
[18] Y. Zhu, S. Murali, W. Cai, X. Li, J.W. Suk, J.R. Potts, R.S. Ruoff, Graphene and graphene oxide: synthesis, properties, and applications, Adv. Mater. 22 (2010) 3906–3924.
[19] D.A.C. Brownson, C.E. Banks, The electrochemistry of CVD graphene: progress and prospects, Phys. Chem. Chem. Phys. 14 (2012) 8264–8281.
[20] D.A.C. Brownson, C.E. Banks, The Handbook of Graphene Electrochemistry, Springer, 2014.

[21] M. Govindasamy, R. Umamaheswari, S.-M. Chen, V. Mani, C. Su, Graphene oxide nanoribbons film modified screen-printed carbon electrode for real-time detection of methyl parathion in food samples, J. Electrochem. Soc. 164 (2017) B403–B408.
[22] G.B. Mahendran, S.J. Ramalingam, J.B.B. Rayappan, M.B. Gumpu, R.G. Kumar, M. Lakshmanakumar, N. Nesakumar, Amperometric detection of mercury ions using piperazine-functionalized reduced graphene oxide as an efficient sensing platform, ChemistrySelect 7 (2022)
[23] G. Ibáñez-Redín, R.H.M. Furuta, D. Wilson, F.M. Shimizu, E.M. Materon, L.M.R.B. Arantes, M.E. Melendez, A.L. Carvalho, R.M. Reis, M.N. Chaur, D. Gonçalves, O.N. Oliveira Jr, Screen-printed interdigitated electrodes modified with nanostructured carbon nano-onion films for detecting the cancer biomarker CA19-9, Mater. Sci. Eng. C 99 (2019) 1502–1508.
[24] S. Iijima, Helical microtubules of graphitic carbon, Nature 354 (1991) 56–58.
[25] H. Qiu, J. Yang, Structure and properties of carbon nanotubes, in: Industrial Applications of Carbon Nanotubes, Elsevier, 2017, pp. 47–69.
[26] A. Eatemadi, M. Daraee, M. Karimkhanloo, N. Kouhi, M. Zarghami, S. Akbarzadeh, R. Abasi, Y. Hanifehpour, S.W. Joo, M. Akbarzadeh, Carbon nanotubes: properties, synthesis, purification, and medical applications, Nanoscale Res. Lett. 9 (2014) 393.
[27] A.-E. Radi, A. Eissa, T. Wahdan, Voltammetric behavior of mycotoxin zearalenone at a single-walled carbon nanotube screen-printed electrode, Anal. Methods 11 (2019) 4494–4500.
[28] D.A.G. Araújo, J.R. Camargo, L.A. Pradela-Filho, A.P. Lima, R.A.A. Muñoz, R.M. Takeuchi, B.C. Janegitz, A.L. Santos, A lab-made screen-printed electrode as a platform to study the effect of the size and functionalization of carbon nanotubes on the voltammetric determination of caffeic acid, Microchem. J. 158 (2020) 105297.
[29] B. Weng, R. Shepherd, K. Crowley, A. Killard, G. Wallace, A review of wearable sensor platforms for biochemical detection, Analyst 135 (2010) 2745–2789.
[30] I.S. Chronakis, S. Grapenson, A. Jakob, Conductive polypyrrole nanofibers via electrospinning: Electrical and morphological properties, Polymer 47 (2006) 1597–1603.
[31] S.A. Waghuley, S.M. Yenorkar, S.S. Yawale, S.P. Yawale, Application of chemically synthesized conducting polymer-polypyrrole as a carbon dioxide gas sensor, Sens. Actuators B Chem. 128 (2008) 366–373.
[32] B. Weng, A. Morrin, R. Shepherd, K. Crowley, A.J. Killard, P.C. Innis, G.G. Wallace, Wholly printed polypyrrole nanoparticle-based biosensors on flexible substrate, J. Mater. Chem. B 2 (2014) 3578–3584.
[33] J. Stejskal, M. Omastová, S. Fedorova, J. Prokeš, M. Trchová, Polyaniline and polypyrrole prepared in the presence of surfactants: A comparative conductivity study, Polymer 44 (2003) 1353–1358.
[34] E. Gill, A. Arshak, K. Arshak, O. Korostynska, pH sensitivity of novel PANI/PVB/PS3 composite films, Sensors 7 (2007) 3329–3346.
[35] A. Kros, S.W.F.M. van Hövell, N.A.J.M. Sommerdijk, R.J.M. Nolte, Poly(3,4-ethylenedioxythiophene)-based glucose biosensors, Adv. Mater. 13 (2001) 1555–1557.
[36] J.S. Daniels, N. Pourmand, Label-free impedance biosensors: opportunities and challenges, Electroanalysis 19 (2007) 1239–1257.
[37] W.-Y. Su, S.-H. Cheng, Electrocatalysis and sensitive determination of cysteine at poly(3,4-ethylenedioxythiophene)-modified screen-printed electrodes, Electrochem. Commun. 10 (2008) 899–902.

[38] L. Fritea, F. Banica, T.O. Costea, L. Moldovan, L. Dobjanschi, M. Muresan, S. Cavalu, Metal nanoparticles and carbon-based nanomaterials for improved performances of electrochemical (bio)sensors with biomedical applications, Mater. 14 (2021) 6319.
[39] H.J. Salavagione, A.M. Díez-Pascual, E. Lázaro, S. Vera, M.A. Gómez-Fatou, Chemical sensors based on polymer composites with carbon nanotubes and graphene: the role of the polymer, J. Mater. Chem. A 2 (2014) 14289–14328.
[40] V.V. Kondratiev, V.V. Malev, S.N. Eliseeva, Composite electrode materials based on conducting polymers loaded with metal nanostructures, Russ. Chem. Rev. 85 (2016) 14.
[41] M.M. Khalifa, A.A. Elkhawaga, M.A. Hassan, A.M. Zahran, A.M. Fathalla, W.A. El-Said, O. El-Badawy, Highly specific electrochemical sensing of *Pseudomonas aeruginosa* in patients suffering from corneal ulcers: a comparative study, Sci. Rep. 13 (2023) 12456.
[42] R. María-Hormigos, M.J. Gismera, J.R. Procopio, M.T. Sevilla, Disposable screen-printed electrode modified with bismuth–PSS composites as high sensitive sensor for cadmium and lead determination, J. Electroanal. Chem. 767 (2016) 114–122.
[43] G. Maduraiveeran, W. Jin, Nanomaterials based electrochemical sensor and biosensor platforms for environmental applications, Trends Environ. Anal. Chem. 13 (2017) 10–23.
[44] C.-J. Jia, F. Schüth, Colloidal metal nanoparticles as a component of designed catalyst, Phys. Chem. Chem. Phys. 13 (2011) 2457–2487.
[45] A. Adlim, Preparations and application of metal nanoparticles, Indones. J. Chem. 6 (2010) 1–10.
[46] H. Asoh, F. Arai, S. Ono, Site-selective chemical etching of silicon using patterned silver catalyst, Electrochem. Commun. 9 (2007) 535–539.
[47] H. Shen, M. Liu, A. Yang, H. Yang, Enhancement of optical nonlinearity in periodic gold nanoparticle arrays, Nanotechnology 17 (2006) 4274.
[48] K. Saha, S.S. Agasti, C. Kim, X. Li, V.M. Rotello, Gold nanoparticles in chemical and biological sensing, Chem. Rev. 112 (2012) 2739–2779.
[49] M.-C. Daniel, D. Astruc, Gold nanoparticles: assembly, supramolecular chemistry, quantum-size-related properties, and applications toward biology, catalysis, and nanotechnology, Chem. Rev. 104 (2004) 293–346.
[50] X. Dai, R.G. Compton, Gold nanoparticle modified electrodes show a reduced interference by Cu(II) in the detection of As(III) using anodic stripping voltammetry, Electroanalysis 17 (2005) 1325–1330.
[51] S.A. Miscoria, G.D. Barrera, G.A. Rivas, Enzymatic biosensor based on carbon paste electrodes modified with gold nanoparticles and polyphenol oxidase, Electroanalysis 17 (2005) 1578–1582.
[52] A.M. Titoiu, R. Porumb, P. Fanjul-Bolado, P. Epure, M. Zamfir, A. Vasilescu, Detection of allergenic lysozyme during winemaking with an electrochemical aptasensor, Electroanalysis 31 (2019) 1778–1786.
[53] M.A. Alonso-Lomillo, O. Domínguez-Renedo, A. Saldaña-Botín, M.J. Arcos-Martínez, Determination of ascorbic acid in serum samples by screen-printed carbon electrodes modified with gold nanoparticles, Talanta 174 (2017) 733–737.
[54] Q.H. Tran, V.Q. Nguyen, A.-T. Le, Silver nanoparticles: synthesis, properties, toxicology, applications and perspectives, Adv. Nat. Sci.: Nanosci. Nanotechnol. 4 (2013) 1–20.
[55] W. Song, H. Li, H. Liu, Z. Wu, W. Qiang, D. Xu, Fabrication of streptavidin functionalized silver nanoparticle decorated graphene and its application in disposable electrochemical sensor for immunoglobulin E, Electrochem. Commun. 31 (2013) 16–19.
[56] J. Zhu, K. Kim, Z. Liu, H. Feng, S. Hou, Electroless deposition of silver nanoparticles on graphene oxide surface and its applications for the detection of hydrogen peroxide, Electroanalysis 26 (2014) 2513–2519.

[57] O.D. Renedo, M.J. Arcos Martínez, A novel method for the anodic stripping voltammetry determination of Sb(III) using silver nanoparticle-modified screen-printed electrodes, Electrochem. Commun. 9 (2007) 820–826.

[58] H. Guo, H. Jin, R. Gui, Z. Wang, J. Xia, F. Zhang, Electrodeposition one-step preparation of silver nanoparticles/carbon dots/reduced graphene oxide ternary dendritic nanocomposites for sensitive detection of doxorubicin, Sens. Actuators B Chem. 253 (2017) 50–57.

[59] T. You, O. Niwa, M. Tomita, S. Hirono, Characterization of platinum nanoparticle embedded carbon film electrode and its detection of hydrogen peroxide, Anal. Chem. 75 (2003) 2080–2085.

[60] T. You, O. Niwa, T. Horiuchi, M. Tomita, Y. Iwasaki, Y. Ueno, S. Hirono, Co-sputtered thin film consisting of platinum nanoparticles embedded in graphite-like carbon and its high electrocatalytic properties for electroanalysis, Chem. Mater. 14 (2002) 4796–4799

[61] L.-B. Lai, D.-H. Chen, T.-C. Huang, Preparation and characterization of Ti-supported nanostructured Pt electrodes by electrophoretic deposition, Mater. Res. Bull. 36 (2001) 1049–1055.

[62] J. Grunes, J. Zhu, E.A. Anderson, G.A. Somorjai, Ethylene hydrogenation over platinum nanoparticle array model catalysts fabricated by electron beam lithography: determination of active metal surface area, J. Phys. Chem. B 106 (2002) 11463–11468.

[63] P. Serp, R. Feurer, Y. Kihn, P. Kalck, J.L. Faria, J.L. Figueiredo, Novel carbon supported material: highly dispersed platinum particles on carbon nanospheres, J. Mater. Chem. 11 (2001) 1980–1981.

[64] S. Hrapovic, Y. Liu, K.B. Male, J.H.T. Luong, Electrochemical biosensing platforms using platinum nanoparticles and carbon nanotubes, Anal. Chem. 76 (2004) 1083–1088.

[65] S. Sanllorente-Méndez, O. Domínguez-Renedo, M.J. Arcos-Martínez, Determination of arsenic(III) using platinum nanoparticle-modified screen-printed carbon-based electrodes, Electroanalysis 21 (2009) 635–639.

[66] S. Phetsang, J. Jakmunee, P. Mungkornasawakul, R. Laocharoensuk, K. Ounnunkad, Sensitive amperometric biosensors for detection of glucose and cholesterol using a platinum/reduced graphene oxide/poly(3-aminobenzoic acid) film-modified screen-printed carbon electrode, Bioelectrochemistry 127 (2019) 125–135.

[67] A. Baradoke, B. Jose, R. Pauliukaite, R.J. Forster, Properties of anti-CA125 antibody layers on screen-printed carbon electrodes modified by gold and platinum nanostructures, Electrochim. Acta 306 (2019) 299–306.

[68] F.C. Krebs, Fabrication and processing of polymer solar cells: a review of printing and coating techniques, Sol. Energy Mater. Sol. Cells 93 (2009) 394–412.

[69] C.C. Mayorga-Martinez, M. Cadevall, M. Guix, J. Ros, A. Merkoçi, Bismuth nanoparticles for phenolic compounds biosensing application, Biosens. Bioelectron. 40 (2013) 57–62.

[70] X. Yang, Y. Ouyang, F. Wu, Y. Hu, H. Zhang, Z. Wu, In situ and controlled preparation of platinum nanoparticles doped into graphene sheets@cerium oxide nanocomposites sensitized screen-printed electrode for nonenzymatic electrochemical sensing of hydrogen peroxide, J. Electroanal. Chem. 777 (2016) 85–91.

[71] A. Popa, E.C. Abenojar, A. Vianna, C.Y.A. Buenviaje, J. Yang, C.B. Pascual, A.C.S. Samia, Fabrication of metal nanoparticle-modified screen printed carbon electrodes for the evaluation of hydrogen peroxide content in teeth whitening strips,
J. Chem. Educ. 92 (2015) 1913–1917.

[72] M.M. Pereira Silva Neves, M.B. González-García, P. Bobes-Limenes, A. Pérez-Junquera, D. Hernández Santos, F.J. Vidal-Iglesias, J. Solla-Gullón, P. Fanjul-Bolado, A non-

enzymatic ethanol sensor based on a nanostructured catalytic disposable electrode,Anal.Methods 9 (2017) 5108–5114.
[73] V.A. Gatselou, D.L. Giokas, A.G. Vlessidis, M.I. Prodromidis, Rhodium nanoparticle-modified screen-printed graphite electrodes for the determination of hydrogen peroxide in tea extracts in the presence of oxygen,Talanta 134 (2015) 482–487.
[74] A. Jirasirichote, E. Punrat, A. Suea-Ngam, O. Chailapakul, S. Chuanuwatanakul, Voltammetric detection of carbofuran using screen-printed carbon electrodes modified with gold nanoparticles and graphene oxide,Talanta 175 (2017) 331–337.
[75] H. Shamkhalichenar, J.W. Choi, An inkjet-printed non-enzymatic hydrogen peroxide sensor on paper,J. Electrochem. Soc. 164 (2017) B3101–B3106.
[76] A.V. Shabalina, V.A. Svetlichnyi, K.A. Ryzhinskaya, I.N. Lapin, Copper nanoparticles for ascorbic acid sensing in water on carbon screen printed electrodes,Anal.Sci.33 (2017)1415–1419.
[77] M. García, A. Escarpa, A class-selective and reliable electrochemical monosaccharide index in honeys, as determined using nickel and nickel-copper nanowires, Anal. Bioanal. Chem. 402 (2012) 945–953.
[78] C.W. Foster, R.O. Kadara, C.E. Banks, Fundamentals of screen-printing electrochemical architectures, Springer, Cham, Switzerland (2016).
[79] J.P. Metters, F. Tan, C.E. Banks, Screen-printed palladium electroanalytical sensors, J. Solid State Electrochem. 17 (2013) 1553–1562.
[80] W.Y. Jeon, Y.B. Choi, H.H. Kim, Disposable non-enzymatic glucose sensors using screen-printed nickel/carbon composites on indium tin oxide electrodes, Sensors 15 (2015) 31083–31091.
[81] L. Shi, M. Layani, X. Cai, H. Zhao, S. Magdassi, M. Lan, An inkjet printed Ag electrode fabricated on plastic substrate with a chemical sintering approach for the electrochemical sensing of hydrogen peroxide, Sens.Actuators B Chem. 256 (2018) 938–945.
[82] M.E. Burgoa Calvo, O. Domínguez Renedo, M.J. Arcos Martínez, Determination of lamotrigine by adsorptive stripping voltammetry using silver nanoparticle-modified carbon screen-printed electrodes,Talanta 74 (2007) 59–64.
[83] M. Chikae, K. Idegami, K. Kerman, N. Nagatani, M. Ishikawa, Y. Takamura, E. Tamiya, Direct fabrication of catalytic metal nanoparticles onto the surface of a screen-printed carbon electrode,Electrochem. Commun. 8 (2006) 1375–1380.
[84] C. Mun, Étude du comportement du produit de fission ruthénium dans l'enceinte de confinement d'un réacteur nucléaire, en cas d'accident grave, PhD thesis in radiochemistry, University of Paris-Sud,2007.
[85] A. Dali, Préparation et caractérisation de matériaux à base de ruthénium déposé sur argile à piliers d'oxydes de métaux de transition. Application aux réactions d'oxydation, PhD thesis in chemistry, University Abou-Bekr Belkaïd – Tlemcen, 2016.
[86] Pascal.P, Nouveau traité de chimie minérale. Propriétés physiques de l'analyse carbonique, volume 8 Masson, Paris, 1968
[87] B. Zadam, Synthèse de catalyseurs de type ruthénium (Ru) et iridium (Ir) supportés sur des matériaux nanostructurés. Application dans la réaction d'oxydation de l'alcool benzylique en phase liquide, PhD thesis in chemistry, University 8 Mai 1945 – Guelma, 2021.
[88] D.J. Gulliver, W. Levason, The chemistry of ruthenium, osmium, rhodium, iridium, palladium and platinum in the higher oxidation states, Coord. Chem. Rev. 46 (1982) 1−127.
[89] M.J. Clarke, Ruthenium metallopharmaceuticals, Coord. Chem. Rev. 232 (2002) 69–93.
[90] P. Crochet, V. Cadierno, Arene-ruthenium(II) complexes with hydrophilic P-donor ligands:versatile catalysts in aqueous media,Dalton Trans.43 (2014) 12447–12462.

[91] M.A. Lawrence, J.L. Bullock, A.A. Holder, Basic coordination chemistry of ruthenium, in: Ruthenium Complexes – Photochemical and Biomedical Applications,2018, pp. 25–41.
[92] O. Ablialimov, M. Kedziorek, M. Malinska, K. Wozniak, K. Grela, Synthesis, structure, and catalytic activity of new ruthenium(II) indenylidene complexes bearing unsymmetrical N-heterocyclic carbenes, Organometallics 33 (2014) 2160–2171.
[93] P. Zhang, L. Pei, Y. Chen, W. Xu, Q. Lin, J. Wang, J. Wu, Y. Shen, L. Ji, H. Chao, A dinuclear ruthenium(II) complex as a one- and two-photon luminescent probe for biological Cu^{2+} detection,Chem. Eur. J. 19 (2013) 15494–15503.
[94] S. Pal, T.K. Ghosh, R. Ghosh, S. Mondal, P. Ghosh, Recent advances in recognition, sensing and extraction of phosphates: 2015 onwards,Coord. Chem. Rev. 405 (2020) 213128.
[95] F. Szemes, D. Hesek, Z. Chen, S.W. Dent, M.G.B. Drew, A.J. Goulden, A.R. Graydon, A. Grieve, R.J. Mortimer, T. Wear, et al., Synthesis and characterization of novel acyclic, macrocyclic, and calix[4]arene ruthenium(II) bipyridyl receptor molecules that recognize and sense anions, Inorg. Chem. 35 (1996) 5868–5879.
[96] G.T. Williams, J.L. Kedge, J.S. Fossey, Molecular boronic acid-based saccharide sensors, ACS Sens. 6 (2021) 1508–1528.
[97] Z. Murtaza, J.R. Lakowicz, Lifetime-based sensing of glucose using luminescent ruthenium(II) metal complex,Proc. SPIE Adv. Fluoresc. Sens. Technol. IV 3602 (1999) 326–334.
[98] Z. Murtaza, L. Tolosa, P. Harms, J.R. Lakowicz, On the possibility of glucose sensing using boronic acid and a luminescent ruthenium metal-ligand complex, J. Fluoresc. 12 (2002) 187–192.
[99] S. Xun, G. LeClair, J. Zhang, X. Chen, J.P. Gao, Z.Y. Wang, Tuning the electrical and optical properties of dinuclear ruthenium complexes for near infrared optical sensing, Org. Lett. 8 (2006) 1697–1700.
[100] S. Kumar, R. Singh, Recent optical sensing technologies for the detection of various biomolecules: review, Opt. Laser Technol. 134 (2021) 106620.
[101] N. Dey, C.J.E. Haynes, Supramolecular coordination complexes as optical biosensors, ChemPlusChem 86 (2021) 418–433.
[102] N.P. Cook, V. Torres, D. Jain, A.A. Martí, Sensing amyloid-β aggregation using luminescent dipyridophenazine ruthenium(II) complexes,J. Am. Chem. Soc. 133 (2011).
[103] E. Babu, P.M. Mareeswaran, V. Sathish, S. Singaravadivel, S. Rajagopal, Sensing and inhibition of amyloid-β based on the simple luminescent aptamer-ruthenium complex system, Talanta 134 (2015) 343–353.
[104] H. Wang, Y. Yuan, Y. Zhuo, Y. Chai, R. Yuan, Self-enhanced electrochemiluminescence nanorods of tris(bipyridine) ruthenium(II) derivative and its sensing application for detection of N-acetyl-β-D-glucosaminidase,Anal. Chem. 88 (2016) 2258–2266.
[105] B. Sun, Z. Liang, B.-P. Xie, R.-T. Li, L.-Z. Li, Z.-H. Jiang, L.-P. Bai, J.-X. Chen, Fluorescence sensing platform based on ruthenium(II) complexes as high 3S (sensitivity, specificity, speed) and "on-off-on" sensors for the miR-185 detection,Talanta 179 (2018) 658–667.
[106] M. Duraisamy, M. Elancheziyan, M. Eswaran, S. Ganesan, A.A. Ansari, G. Rajamanickam, S.L. Lee, P.-C. Tsai, Y.-H. Chen, V.K. Ponnusamy, Novel ruthenium-doped vanadium carbide/polymeric nanohybrid sensor for acetaminophen drug detection in human blood,Int. J. Biol. Macromol. 244 (2023) 125329.
[107] S.I. Kaya, S. Kurbanoglu, E. Yavuz, S.D. Mustafov, F. Sen, S.A. Ozkan, Carbon-based ruthenium nanomaterial-based electroanalytical sensors for the detection of anticancer drug idarubicin, Sci. Rep. 10 (2020) 11160.

[108] H.A. Samie, M. Arvand, RuO_2 nanowires on electrospun CeO_2-Au nanofibers/ functionalized carbon nanotubes/graphite oxide nanocomposite modified screen-printed carbon electrode for simultaneous determination of serotonin, dopamine and ascorbic acid, J. Alloys Compd. 785 (2019) 663–672.

[109] J. Ye, G. Liu, M. Yan, Q. Zhu, L. Zhu, J. Huang, X. Yang, Highly luminescent and self-enhanced electrochemiluminescence of tris(bipyridine) ruthenium(II) nanohybrid and its sensing application for label-free detection of microRNA, Anal. Chem. 91 (2019) 13237–13243.

[110] V. Vukojević, S. Djurdjić, M. Ognjanović, B. Antić, K. Kalcher, J. Mutić, D.M. Stanković, RuO_2/graphene nanoribbon composite supported on screen printed electrode with enhanced electrocatalytic performances toward ethanol and NADH biosensing,Biosens. Bioelectron. 117 (2018) 392–397.

[111] M. Ikram, A. Munawar, A.A. Kalyar, N.A. Shad, M. Imran, Ruthenium decorated V@WO_3 nanocomposites heterostructures for selective detection of sulfonamide in honey samples,J. Food Compos. Anal. 126 (2024) 105842.

[112] M. Liu, T. Zhe, F. Li, L. Zhu, S. Ouyang, L. Wang, An ultrasensitive electrochemical sensor based on NiFe-LDH-MXene and ruthenium nanoparticles composite for detection of nitrofurantoin in food samples,Food Chem. 430 (2024) 137204.

[113] A.M. Asran, M.A. Mohamed, G.M.G. Eldin, R.K. Mishra, A. Errachid, Self-assembled ruthenium decorated electrochemical platform for sensitive and selective determination of amisulpride in presence of co-administered drugs using safranin as a mediator, Microchem. J. 164 (2021) 106061.

[114] S. Palanisamy, B. Thirumalraj, S.-M. Chen, Palladium nanoparticles decorated on activated fullerene modified screen-printed carbon electrode for enhanced electrochemical sensing of dopamine,J. Colloid Interface Sci. 449 (2015) 180–185.

[115] R.W. Leggett, The biokinetics of ruthenium in the human body, Radiat. Prot. Dosimetry 148 (2012) 389–402.

[116] Y.-M. Zhang, P.-L. Xu, Q. Zeng, Y.-M. Liu, X. Liao, M.-F. Hou, Magnetism-assisted modification of screen-printed electrode with magnetic multi-walled carbon nanotubes for electrochemical determination of dopamine, Mater. Sci. Eng. C 74 (2017) 62–69.

[117]C.-Y. Liu, Y.-C. Chou, J.-H. Tsai, T.-M. Huang, J.-Z. Chen, Y.-C. Yeh, Tyrosinase/chitosan/reduced graphene oxide modified screen-printed carbon electrode for sensitive and interference-free detection of dopamine,Appl. Sci. 9 (2019) 622.

[118] K. Ahmad, H. Kim, Design and fabrication of WO_3/SPE for dopamine sensing application, Mater. Chem. Phys. 287 (2022) 126298.

[119] S. Redžić, E. Kahrović, A. Zahirović, E. Turkušić, Electrochemical determination of dopamine with ruthenium(III)-modified glassy carbon and screen-printed electrodes, Anal. Lett. 50 (2017) 1467–1478

[120] S. BenAoun, Nanostructured carbon electrode modified with N-doped graphene quantum dots–chitosan nanocomposite: a sensitive electrochemical dopamine sensor, R. Soc. Open Sci. 4 (2017) 171199

[121] N. Rodthongkum, N. Ruecha, R. Rangkupan, R.W. Vachet, O. Chailapakul, Graphene-loaded nanofiber-modified electrodes for the ultrasensitive determination of dopamine, Anal. Chim. Acta 804 (2013) 84–91.

[122] S. Palanisamy, B. Thirumalraj, S.-M. Chen, M.A. Ali, K. Muthupandi, R. Emmanuel, P. Prakash, F.M.A. Al-Hemaid, Fabrication of silver nanoparticles decorated on activated screen printed carbon electrode and its application for ultrasensitive detection of dopamine, Electroanalysis 27 (2015) 2915–2921.

[123] H. Beitollahi, F. Garkani Nejad, S. Shakeri, GO/Fe_3O_4@SiO_2 core–shell nanocomposite modified graphite screen-printed electrode for sensitive and selective electrochemical sensing of dopamine and uric acid,Anal. Methods 7 (2015) 10066–10073.

[124] G. Ibáñez-Redín, D. Wilson, D. Gonçalves, O.N. Oliveira Jr., Low-cost screen-printed electrodes based on electrochemically reduced graphene oxide–carbon black nanocomposites for dopamine, epinephrine and paracetamol detection,J. Colloid Interface Sci. 515 (2018) 101–108.

[125] D. Thirumalai, S. Lee, M. Kwon, H.-j. Paik, J. Lee, S.-C. Chang, Disposable voltammetric sensor modified with block copolymer-dispersed graphene for simultaneous determination of dopamine and ascorbic acid in ex vivo mouse brain tissue,Biosensors 11 (2021) 368.

[126] Q. Zhao, Y. Faraj, L.-Y. Liu, W. Wang, R. Xie, Z. Liu, X.-J. Ju, J. Wei, L.-Y. Chu, Simultaneous determination of dopamine, uric acid and estriol in maternal urine samples based on the synergetic effect of reduced graphene oxide, silver nanowires and silver nanoparticles in their ternary 3D nanocomposite,Microchem. J. 158 (2020) 105185.

[127] H. Beitollahi, Z. Dourandish, M.R. Ganjali, S. Shakeri, Voltammetric determination of dopamine in the presence of tyrosine using graphite screen-printed electrode modified with graphene quantum dots,Ionics 25 (2018) 681–688.

[128] K. Kunpatee, S. Traipop, O. Chailapakul, S. Chuanuwatanakul, Simultaneous determination of ascorbic acid, dopamine, and uric acid using graphene quantum dots/ionic liquid modified screen-printed carbon electrode,Sens. Actuators B Chem. 314 (2020) 128059.

[129] P. Gupta, R.N. Goyal, Y.-B. Shim, Simultaneous analysis of dopamine and 5-hydroxyindoleacetic acid at nanogold modified screen printed carbon electrodes,Sens. Actuators B Chem. 213 (2015) 72–81.

[130] N. Serrano, Ò. Castilla, C. Ariño, M.S. Diaz-Cruz, J.M. Díaz-Cruz, Commercial screen-printed electrodes based on carbon nanomaterials for a fast and cost-effective voltammetric determination of paracetamol, ibuprofen and caffeine in water samples,Sensors 19 (2019) 4039.

[131] F. Valentini, E. Ciambella, F. Cataldo, A. Calcaterra, L. Menegatti, M. Talamo, Fullerene black modified screen-printed electrodes for the quantification of acetaminophen and guanine,Electroanalysis 29 (2017) 2744–2753.

[132] A. Sasal, K. Tyszczuk-Rotko, A. Nosal-Wiercińska, Direct determination of paracetamol in environmental samples using screen-printed carbon/carbon nanofibers sensor – experimental and theoretical studies,Electroanalysis 32 (2020) 1466–1475.

[133] J. Ping, J. Wu, Y. Wang, Y. Ying, Simultaneous determination of ascorbic acid, dopamine and uric acid using high-performance screen-printed graphene electrode, Biosens. Bioelectron. 34 (2012) 70–76.

[134] A.P. Ruas de Souza, M. Bertotti, C.W. Foster, C.E. Banks, Back-to-back screen-printed electroanalytical sensors: Extending the potential applications of the simplistic design, Electroanalysis 27 (2015) 2653–2659.

[135] S. Mu, X. Wang, Y.-T. Li, Y. Wang, D.-W. Li, Y.-T. Long, A novel screen-printed electrode array for rapid high-throughput detection, Analyst 137 (2012) 3220–3224.

[136] M. Khairy, C.E. Banks, A screen-printed electrochemical sensing platform surface modified with nanostructured ytterbium oxide nanoplates facilitating the electroanalytical sensing of the analgesic drugs acetaminophen and tramadol, Microchim. Acta 187 (2020) 126.

[137] M. Khairy, B.G. Mahmoud, C.E. Banks, Simultaneous determination of codeine and its co-formulated drugs acetaminophen and caffeine by utilising cerium oxide nanoparticles modified screen-printed electrodes, Sens. Actuators B Chem. 259 (2018) 142–154.

Chapter III

Characterisation methods and experimental protocols

III.1. Introduction

The first part of this chapter is dedicated to the different physical characterization techniques. Among the essential methods for this type of study, morphological techniques such as field emission scanning electron microscopy (FE–SEM), atomic force microscopy (AFM), and transmission electron microscopy (TEM) were used to examine the morphology of the synthesized materials. In addition, spectroscopic and structural techniques, notably Fourier-transform infrared spectroscopy (FT-IR) and X-ray diffraction (XRD),usually enable an in-depth analysis of the physicochemical properties of the samples.

The second part of the chapter focuses on electrochemical techniques, which have the advantage of being fast, sensitive, and easy to implement. In order to situate the work presented in this manuscript, a review of the main knowledge related to electrochemical analysis techniques is provided in this chapter. Only the techniques used will be detailed, namely electrochemical impedance spectroscopy (EIS), cyclic voltammetry (CV), and square wave differential voltammetry (SWV).

The third part of this chapter focuses on the description and presentation of all the experimental devices and methods used in this study, aimed at developing a new electrochemical sensor based on an activated graphite electrode modified with ruthenium nanoparticles, for the detection of pharmaceutical molecules and to ensure good reproducibility of the results.

III.2. Physical characterization of the surfaces of electrodes

There are numerous material characterization techniques based on different fundamental physical principles: radiation-matter interactions, thermodynamics, and mechanics. We distinguish between quantitative analysis, qualitative analysis (identification of compounds) and spectroscopic methods (microscopy, X-rays, neutrons), all aim at determining and identifying the nature and composition of substances. We present below the characterization techniques that we used during our work.

III.2.1. Fourier transform infrared spectroscopy

A popular chemical analysis method for determining a sample's chemical composition is Fourier-transform infrared spectroscopy (FT-IR), which uses the absorption of infrared light

(between 4000 and 400 cm^{-1}) to determine the sample's chemical composition. By comparing the incident and transmitted radiation through the sample, FT-IR can determine which functional groups are present on the surface of nanoparticles, providing comprehensive details about their chemical structure and characteristics.

The shape of a molecule, especially its symmetry, determines its capacity to absorb vibrations. The absorption bands' positions are directly correlated with the atoms' varying masses and electronegativity differences. Therefore, the observation of a particular set of distinctive absorption bands enables the accurate identification of a substance with a defined chemical composition and structure **[1].** In the current research work, a « Perkin Elmer 100 » Fourier transform spectrometer (**Figure III.1**) was utilized and dry KBr powder was employed to examine the ruthenium nanoparticles.

Figure III.1. Perkin Elmer 100 FT-IR spectrometer.

III.2.2. X-ray diffraction

X-ray diffraction is a ubiquitous materials characterization technique. It permits phase detection in a sample against the international JCPDS diffraction database, along with determination of crystal lattice parameters, interatomic distances, and atom positions. Furthermore, the Scherrer equation can be employed to estimate the average crystallite size. The technique is based on the measurement of diffraction of the rays from a sample in the parallel direction to the support relative to the radiation incidence angle to the sample as shown in **Figure III.2**.

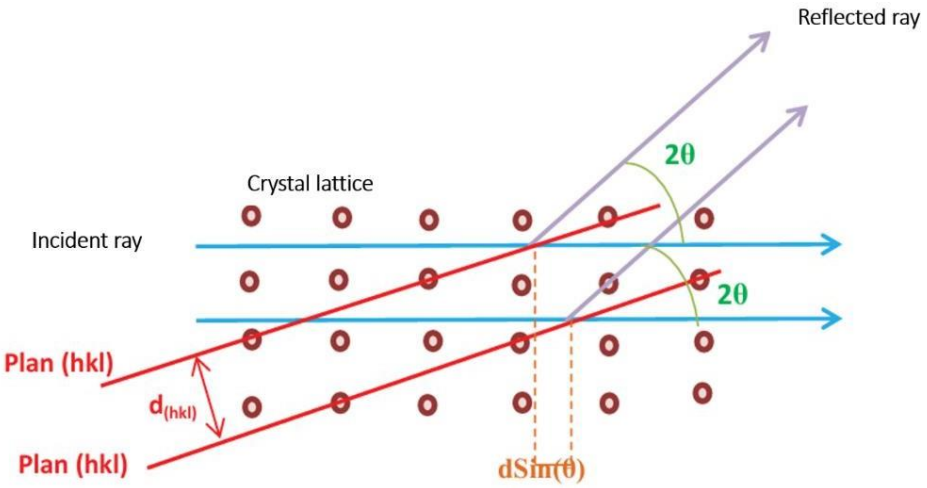

Figure III.2. X-ray diffraction.

A monochromatic X-ray beam diffracted by crystalline planes is, in accordance with Bragg's law **[2].**

$$2d_{hkl} . Sin\,(\theta_{hkl}) = n.\lambda \qquad \textbf{(III.1.)}$$

which **d** represents interatomic distance

λ is X-ray wavelength

θ is the incidence angle

n is the reflection order

In order to assess the crystalline structure of the modified electrodes, we used a Bruker D8 Discover spectrometer (Germany) to obtain X-ray diffraction data using Cu-Kα radiation (λ = 1.5418) as shown in (**Figure III.3**).

Figure III.3. Bruker D8 Discover spectrometer

III.2.3. Transmission electron microscopy

The transmission electron microscope serves as a characterization instrument that facilitates the examination of materials at the atomic level, with a focus on analyzing the distribution of nanoparticles based on their composition and structure. This enables the measurement of nanoparticle size and the execution of electron diffraction for structural identification. Additionally, the crystal lattice planes of the observed nanoparticles can be differentiated. The TEM employs a focused beam of high velocity electrons, possessing wavelengths on the order of picometers, to generate an image of a thinly prepared sample through transmission. A schematic representation of the interaction between the TEM electron beam and the analyzed material is shown in (**Figure III.4**) **[3].**

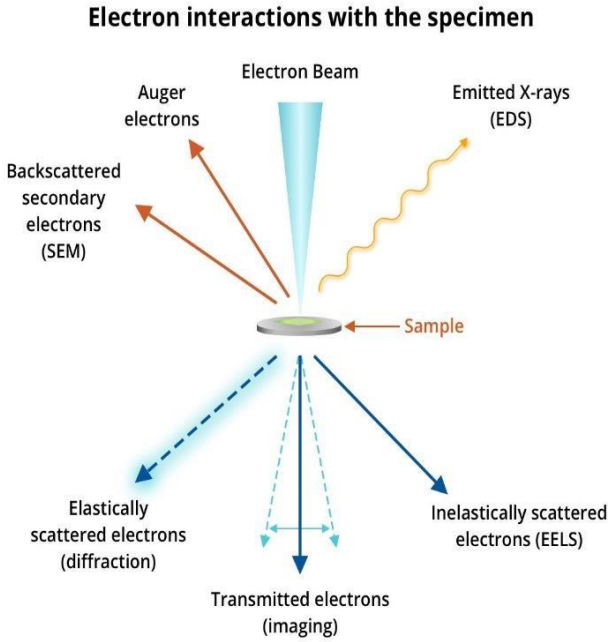

Figure III.4. Interactions between the TEM electron beam and the sample to be analyzed.

During TEM, some electrons are scattered, while others are transmitted through the material, the transmitted electrons are then utilized to create an image at the image plane of the objective lens. (**Figure III.5**) illustrates the different components of a TEM, this type of microscope is capable of generating high magnification images for high-resolution imaging.

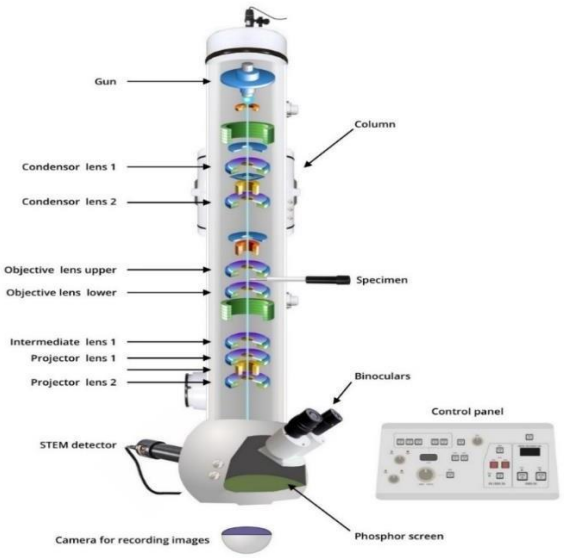

Figure III.5. Components of a transmission electron microscope.

The high resolution TEM employed in this study is with a photograph of the JEOL-JEM-1400 (Japan) model presented in (**Figure III.6**).

Figure III.6. Transmission electron microscope model JEOL JEM-1400.

III.2.4. Analysis by field emission scanning electron microscopy

Field emission scanning electron microscopy is based on electron matter interactions. It enables morphological description, obtaining high resolution images of the sample surface with greater depths of field than optical microscopy. It allows for the analysis of the composition and the study of the homogeneity of solid materials. The electron microscope involves scanning an area of the sample with an electron beam emitted by field effect and accelerated by a voltage applied in the scanning electron microscope. Subsequently, this scanning gives rise to various phenomena: diffusion and diffraction of electrons, emission of secondary electrons, Auger electrons, and backscattered electrons, as well as the emission of X-rays. FE-SEM energy-dispersive X-ray spectroscopy is based on the detection and measurement of the X-ray photons emitted due to interaction of the electrons with the sample. It allows for identification of the chemical composition of the sample surface area addressed by the beam, leading to the characterization of metallic or mineral elements present of the solid material (**Figure III.7**) **[4].**

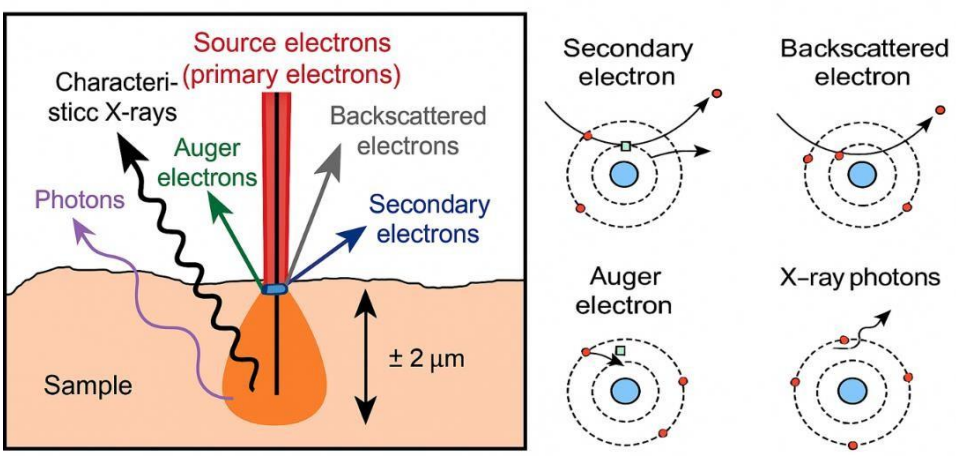

Figure III.7. The impact of an electron beam with a sample in a FE-SEM

(**Figure III.8**) shows the field emission gun scanning electron microscope equipped with a JEOL (Japan) and EDX (Energy Dispersive X-ray) analyzer, model JSM – 6301F, used in this study for taking micrographs and for analyzing the chemical composition of the deposit.

Figure III.8. JSM-6301F from JEOL, Japan model scanning electron microscope.

III.2.5. Atomic force microscopy

Atomic force microscopy (**Figure III.9**) is a technique applied in non-topographic material evaluation. Accordingly, it often serves as a complement to other characterization techniques focused on morphological sample surface analysis in two or three dimensions, including roughness.

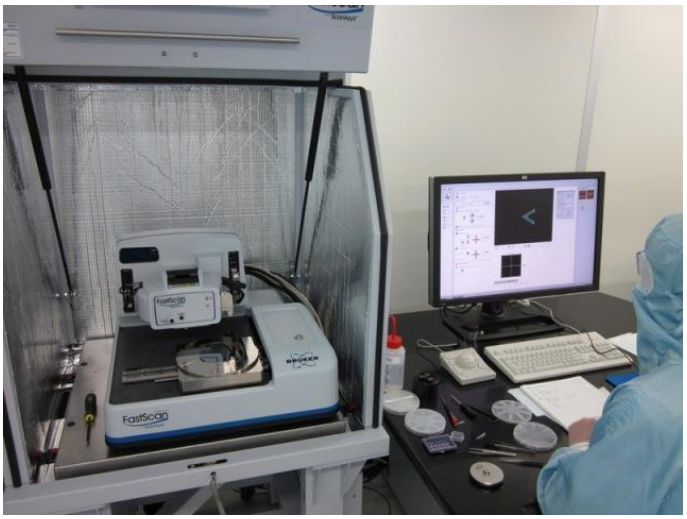

Figure III.9. Atomic force microscope Fast-Scan-Bruker.

The operation principle consists of scanning of the material surface with a needle on an elastic lever. This needle/support system is capable of moving in three directions (X, Y, and Z). The lever is deflected by a variety of forces, including Van der Waals, electrostatic, magnetic and chemical interactions. A laser diode is employed for sensing the reflectivity of the lever arm, which measures the response to these forces. The laser beam, directed at the tip end of the arm, is reflected back to a photodetector, lever deflection produces large deflection of this beam (**Figure III.10A**) **[5].**

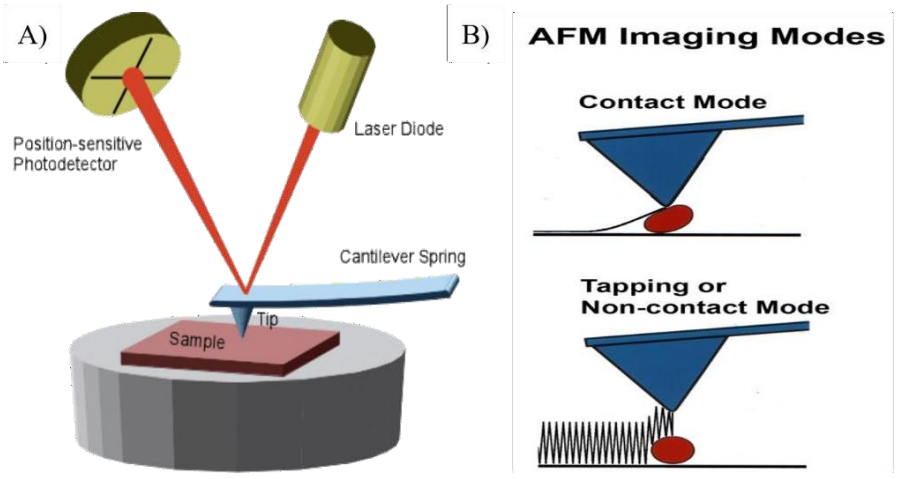

Figure III.10. Principle of an atomic force microscope (A) Illustration of the operating modes of the AFM (B).

AFM operation [6-7]

This is where the two primary operating modes of AFM are explained (**Figure III.10B**):

a) Contact mode:

Here, the sample surface is contacted physically by the tip of the detecting lever. The repulsive forces arise due to electron repulsion between tip and sample. For a weak interaction that is constant, the sample height is changed and this alteration in height is equal to the surface topography at the place being examined.

b) Non-contact mode:

Similar to contact mode, in this approach a fixed tip-sample distance is maintained, typically 50-150 Å. Attractive forces between the sample and the lever-tip assembly are also utilized.The interactions of atoms between the tip and sample are measured using microrepulsion modes. These repulsions accurately represent the sample's topography and cause lever deflection. These horizontal and vertical deviations provide images of the surface condition of the sample.

III.3. Techniques and tools for electrochemical measurements

Analytical methods play an essential role in numerous fields such as food quality control, industry, medicine, metallurgy, and environmental monitoring, to ensure compliance, safety, and process optimization. Electrochemical analysis includes quantitative analytical techniques that utilize the electrical characteristics of a solution within an electrochemical cell. These methods are focused on the characterization of redox reactions, which involve electron exchange between oxidizing and reducing agents. Electrochemical techniques are recognized for their capacity to achieve very low detection limits and offer comprehensive insights into the system under investigation. The use of electrochemical techniques presents several benefits, enabling the investigation of diverse phenomena applicable in both research and industrial contexts. They are employed in quantitative chemical assays and allow for the manipulation of non- electroactive species, as well as dilute solutions. Moreover, electrochemical methods offer data pertaining to the activities, rather than the concentrations, of chemical species.

III.3.1. Cyclic voltammetry

Cyclic voltammetry is a widely applicable electroanalytical technique for electrochemical system analysis. Its primary utility lies in elucidating potential dependent phenomena at the interface between an active surface and the electrolyte within devices, including determining the potentials and reaction kinetics **[8].** During analysis, notable fluctuations occur in the concentrations of electroactive species at the electrode surface, whereas the electrolyte concentrations remain essentially constant.

In voltammetry, a potential that changes linearly with time is applied to the working electrode at a specific forward/reverse sweep rate. This applied voltage takes the form of a triangular and symmetrical signal. The resulting current, measured as a function of the potential I = f (E), is recorded and is known as a cyclic voltammogram, a distinctive characteristic of the electroactive species under investigation **[9].**

Voltammetric analysis yields a voltammogram that is defined by multiple parameters. These parameters offer insights into the system under investigation, for instance, the half-wave potential ($E_{1/2}$) elucidates the characteristics of the electroactive species, while the diffusion current reveals information about both the concentration and the number of electrons involved in the exchange. In the context of a reversible system, a representative voltammogram, derived from cyclic voltammetry and illustrating key characteristic values is presented in (**Figure III.11**).

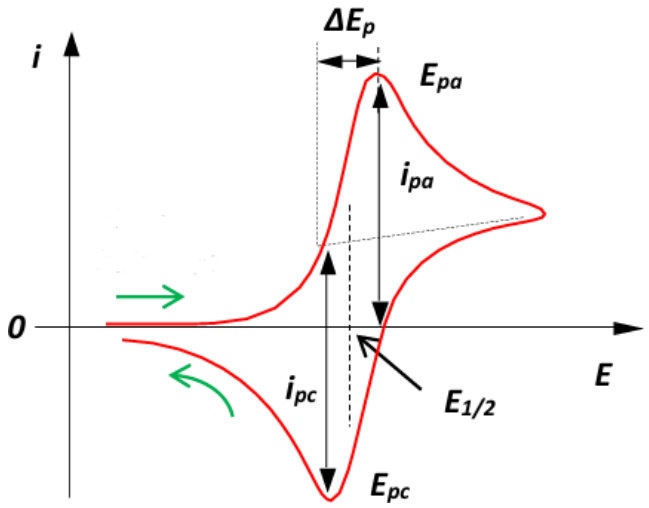

Figure III.11. Voltammogram for a reversible system.

E_{pa}, E_{pc}: Anodic and cathodic peak potentials

$E_{1/2}$: Half-wave potential

i_{pa}, i_{pc}: Anodic and cathodic peak currents

ΔEp: Anodic and cathodic peak potential difference

Cyclic voltammetry is useful in chemical sensors because it reveals information about how they work **[10].** It can also modify the electrode surface by electrografting **[11-13].** This simple technique is used in labs to study the properties of layers on the electrode surface. It can also detect species like heavy metals **[14-16],** bromine **[17],** hydrazine **[18],** nitrites **[19],** and phenol **[20].**

III.3.2. Square wave voltammetry

Square wave voltammetry is an electrochemical method that combines a potential jump (height ΔEp, duration Δt) with a symmetrical square wave (amplitude $|\Delta Es|$, duration $2\Delta t$). These elements are in phase with the frequency of the potential jumps, as illustrated in (**Figure III.12**).

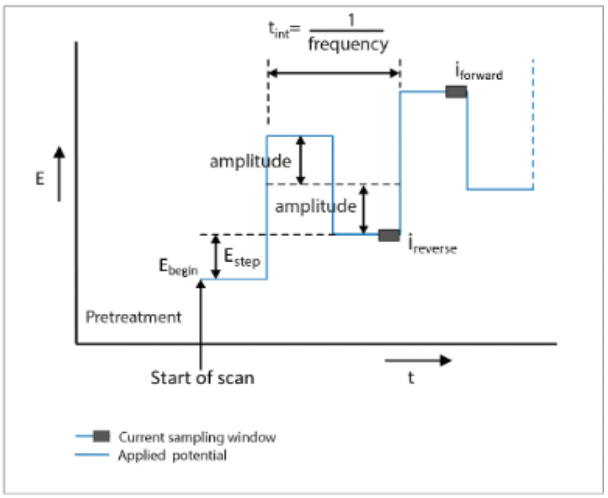

Figure III.12. Potential waveform applied to the electrode during an SWV analysis.

The current is assessed in the final microseconds of each pulse. The net response, defined as the difference in current between two consecutive pulses ($\Delta I = I_1 - I_2$), is recorded and subsequently plotted against the potential of the staircase waveform. The obtained current potential curve has a gaussian distribution, as indicated by (**Figure III.13**).

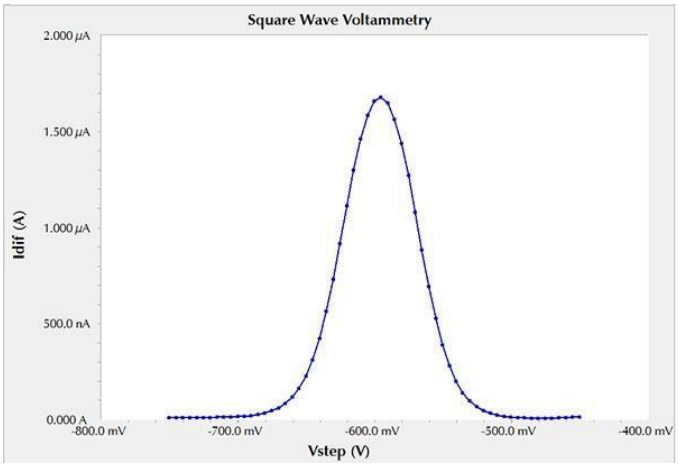

Figure III.13. Typical current response of a square wave voltammogram.

The intensity of the peak current (Ip) is directly proportional to the concentration of the corresponding analytes, while the peak potential (Ep) is identical to the half-wave potential of the usual cyclic voltammetry. The potential step (ΔEp), the period (τ), and the pulse amplitude ($|\Delta Es|$) represent the key parameters influencing the peak's width and height, which in turn affect the resolution and sensitivity of the technique **[21,22].**

Electrochemical characterization performed using square wave voltammetry, provide a rapid, accurate, and economical technique. This method is particularly valuable for the selective and sensitive determination of species in a variety of sample types, including water **[23, 24],** fly ash extracts, mineral waters **[25],** mining water **[26],** foods **[27],** wastewater **[28 ,29],** and pharmaceutical products **[30].**

III.3.3. Electrochemical impedance

Electrochemical impedance measurements are recorded with a three electrode system dipped into a supporting electrolyte within an electrochemical cell. The electrodes are connected to a potentiostat, which forms the measuring chain. The potentiostat applies a controlled potential difference between the working and reference electrodes and simultaneously measures the current flowing between the auxiliary and working electrodes. A frequency response generator generates a sinusoidal disturbance signal, and the resulting alternating current response of the system is measured in terms of the time domain characteristics of the input signal. By processing the response signal through frequency

analysis, one can determine the real and imaginary components of the electrochemical impedance system.

The non-destructive method, dedicated to research into interfacial electrical behavior **[31],** accounts for several electrochemical reactions at the metal/electrolyte interface based on frequency. Charge transfer, being a rapid process, is the prevailing one at high frequencies between the metal and the interface, whereas mass transport, being a slow process, is the dominator at low frequencies between the electrolyte and the interface. Also, the interface provides a convergence site for corrosion products, with chemical interactions that enable adsorption and desorption of molecules.

III.3.3.1. Data representation

Electrochemical impedance plots are typically displayed in two forms. One is to present the data in Cartesian coordinates on the complex Nyquist plane, where the real values Re(Z) on the x-axis and the negative imaginary (-Im) values on the y-axis are provided. Another is to employ Bode plots to present the diagrams, where the impedance modulus |Z| and phase shift φ are presented as functions of frequency on a logarithmic frequency scale. These plots are complementary to each other, each highlighting different aspects of the impedance characteristics; the Nyquist plot reveals the characteristic aspects of the diagram, but the Bode plot provides an overview over the frequency range in general, even if some phenomena are suppressed (**Figure III.14**) **[32].**

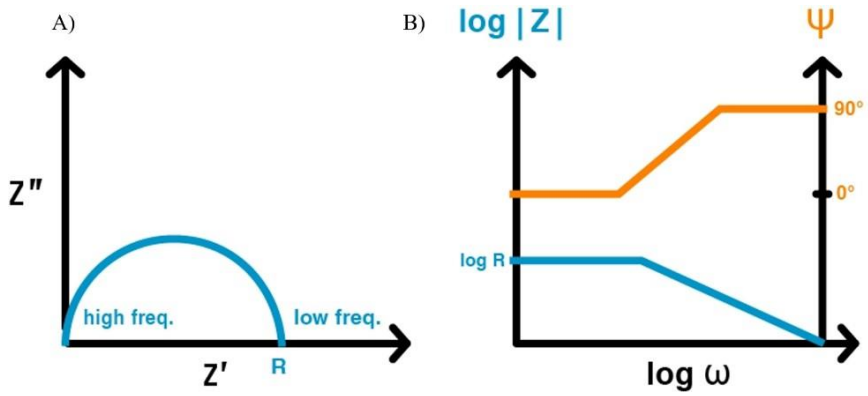

Figure III.14. Graphical representation of the diagrams: Nyquist (A), and Bode (B).

III.3.3.2. Equivalent electrical circuits

The impedance of an electrochemical system, can be compared, by analogy, with an electrical impedance. A physical component in series or parallel with other components that constitute an equivalent electrical circuit can simulate any physico-chemical process at the interface working electrode/electrolyte. These circuits allow the experimental impedance spectra to be adjusted and the physico-chemical phenomenon parameters to be obtained **[33].**

In the development of these equivalent circuits, certain of the components used are actually equivalent to real electrical components such as resistance R, capacitance C or even inductance L whose impedance is supplied by the following equation:

$$Z_L = jL\omega \qquad \textbf{(III.2.)}$$

Which becomes useful in the case of impedance measured in complex systems **[34].** There are other elements that are peculiar to electrochemical processes such as the Warburg impedance that accounts for the matter transport phenomena, which appears when the diffusing charge carrier moves through a material. Species diffusion in an electrolyte solution is a slow phenomenon, therefore observable at low frequency. For a sinusoidal perturbation of the potential, the diffusion effect induces the introduction of a resistance to the matter transfer and whose expression as a function of the angular frequency is:

$$Zw = \frac{\sqrt{2\sigma}}{\sqrt{j2\,\pi\,f}} \qquad \textbf{(III.3.)}$$

where σ is the Warburg coefficient. The Warburg impedance is represented in the complex plane, by a straight line at 45° on the axes (**Figure III.15**).

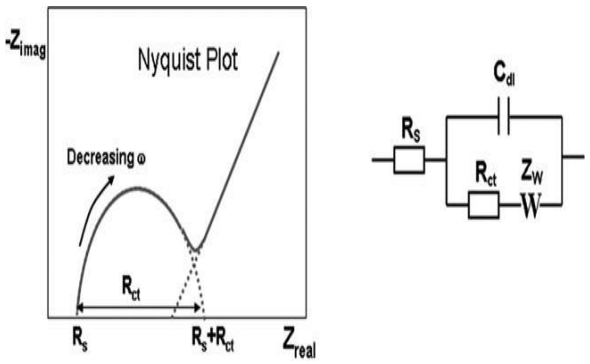

Figure III.15. Impedance of the Randles equivalent circuit: case of a diffusion layer **[35].**

Electrochemical impedance spectroscopy is the impedance spectroscopy that has found widespread use in all fields of electrochemistry, for example, to study the electrode reaction kinetics, double layer, batteries, corrosion, solid state electrochemistry.

EIS has been a fascinating technique for fuel cell characterization, analysis and study **[36],** electrodeposition **[37],** batteries **[38, 39],** and corrosion processes **[40].** It has been widely used as a tool for electrode kinetic study, conducting polymer, semiconductor, and animal and plant tissue and material study in general **[41].**

Because of its high sensitivity in eluciadation of the interfacial properties of an electrode surface as well as its capability for electrode/electrolyte interface characterization, EIS has gained widespread application on biosensors and sensors in recent years **[42- 47].** In addition, in order to track the influence of the recognition process, electrochemical impedance spectroscopy is a useful method to investigate the condition of the electrode surface after modification **[48-50].** This is an important step in developing different types of electrochemical sensors as a function of layers on conductive material surfaces **[51-57].**

III.3.3.3. Method used for fitting

There are various simulation algorithms available in the EC Lab software used for data fitting. The chosen method is called "Randomization + Levenberg–Marquardt." It occurs in two consecutive steps: first, randomization, followed by a real minimization using the Levenberg–Marquardt minimizer. The "randomize" option means that the software will choose random values for all the parameters constituting the equivalent circuit to be found, calculate the $\chi 2$ at each measurement, and keep for each parameter the value that gave the lowest $\chi 2$. Randomization is therefore used to provide initial values as close as possible to the real experimental values, in order to have a good starting point to continue with the Levenberg–Marquardt minimization, using a mathematical algorithm **[58].**

In order to show the influence of each parameter on the Nyquist diagram, different simulations are carried out from experimental data. The EC-Lab software allows us to plot simulated points from parameter values that we have chosen.

III.4. Materials and reagents

III.4.1. Chemicals

All the reagents and solvents used to prepare control solutions were provided by Sigma Aldrich and Fluka products. Electrolyts solutions used for this study were prepared using distilled water. Products quality specifications are tabulated in **table III.1**. The choice of high-quality materials is to ensure experimental results' reliability and accuracy.

Table III.1. Characteristics of chemical products.

Product name	Molecular formula	Molar mass (g/mol)	Purity (%)	Suppliers
Potassium ferrocyanide	$K_4[Fe(CN)_6]$	368.34	99 %	Fluka
Potassium ferricyanide	$K_3[Fe(CN)_6]$	329.24	99 %	Fluka
Potassium chloride	KCl	74.551	99 %	Fluka
Di-Sodium hydrogen phosphate dihydrate	$Na_2HPO_4{\cdot}2H_2O$	177.99	99.5 %	Sigma Aldrich
Sodium Di- hydrogen phosphate dihydrate	$NaH_2PO_4\,2H_2O$	156.01	99.5 %	Sigma Aldrich
Sodium hydroxide	NaOH	40	98 %	Fluka
Sulfuric acid	H_2SO_4	98.07	95-97 %	Sigma Aldrich
Dopamine	$C_8H_{11}NO_2$	153.18	99 %	Fluka
Paracetamol	$C_8H_9NO_2$	151.163	99 %	Fluka
Ruthenium chloride	$RuCl_3.3H_2O$	261.48	99 %	Sigma Aldrich
Uric acid	$C_5H_4N_4O_3$	168.110	99 %	Fluka
Sucrose	$C_{12}H_{22}O_{11}$	342.3	99 %	Fluka
Fructose	$C_6H_{12}O_6$	180.16	99 %	Fluka
Glucose	$C_6H_{12}O_6$	180.156	99.5 %	Fluka
Ascorbic acid	$C_6H_8O_6$	176.12	99 %	Fluka
Caffeine	$C_8H_{10}N_4O_2$	194.19	99 %	Fluka

III.4.2. Solutions preparation methodology

In the current investigation, a diverse range of solutions was meticulously formulated by systematically modulating their constituent composition, concentration levels, and inherent functional properties. All aqueous solutions were prepared in the LAIGM laboratory, utilizing either distilled water or phosphate buffer solution.

III.4.2.1. Electrolyte support

It is a dissociated ionic compound, 100 to 1000 times more concentrated than the electroactive species that participate in the electrode reactions **[59].** Its ions must be electroinactive, which means that under the experimental conditions, these ions do not participate in the electrode reactions and do not modify the concentration of the species that participate in them **[60].** In the presence of a supporting electrolyte, it is therefore considered that the transport of electroactive species from the solution to the electrode or from the electrode to the solution is carried out near the surface of the electrode, only by chemical diffusion or mechanical convection **[61].** In theory, the supporting electrolyte alone does not give any current and this whatever the potential applied, but in reality, a weak residual current always exists. Electrochemical measurements are always carried out in the presence of a sufficiently concentrated, non-electroactive electrolyte, therefore "not active" with respect to the reactions at the electrodes. Its aims to make the solution more conductive and to minimize the migration current. The ions of this additional substance mainly intervene to ensure the transport of electric current within the electrolytic solution, in our experiments using ferrous as an Ox/Red couple prepared in a probe solution. The electrolyte that we used is the equimolar (0.1 M) solution of the redox ($K_3Fe(CN)_6/K_4Fe(CN)_6$) in a 0.1M KCl medium. To avoid any formation of hydrocyanic acid, the solutions are kept in the dark and in tinted glass bottles. Furthermore, the use of a solution containing the redox couple $Fe(CN)_6^{3-/4-}$made it possible to see the degree of reversibility of the deposits. Equation (III.4) presents the oxidation-reduction equilibrium of the couple $Fe(CN)_6^{3-/4-}$ .It is one of the most used redox reactions in cyclic voltammetry to illustrate a reversible response.

$$[Fe(CN)_6]^{3-} + e^- \rightleftharpoons [Fe(CN)_6]^{4-} \qquad \textbf{(III.4.)}$$

III.4.2.2. Preparation and standardization of buffer solutions

As electrons move from the electrode to the analyte, ions move in solution to compensate the charge loss and close the electrical circuit. The phosphate buffer (PBS) solution serves both to maintain the pH of the solution approximately constant and to act as a supporting electrolyte.

Based on the Henderson–Hasselbalch equation:pH = pKa + log ([base]/[acid]), the pH of an equimolar combination is identical to the pKa value. A solution of equal mole amounts of Na_2HPO_4 and NaH_2PO_4 in distilled water served as a phosphate buffer, minor pH adjustments are made by the addition of small volumes of HCl or NaOH to modulate the ratio of the acidic and basic phosphate groups.

III.4.2.3. Analytical solution preparation for DA and PA

Stock solutions of the analytes, paracetamol and dopamine, were prepared carefully by weighing a known amount of each individual substance accurately and dissolving it in 50 mL of phosphate buffer solution. The solutions were then sonicated for 10 minutes in an ultrasonic bath to ensure complete homogenization. To make each electrochemical measurement, the prepared solutions of analytes and the supporting electrolyte were then poured carefully into a 75 mL electrochemical cell.

III.4.2.4. Samples preparation

The efficacy of RuNPs/ASPE for detecting DA in dopamine injectable solutions and PA in paracetamol tablets was assessed using square wave voltammetry. An appropriate volume of the commercial dopamine injectable solution (40 mg/mL) was diluted in 10 mL of 0.1 M PBS (pH 7.4). To prepare the paracetamol solution, three commercial paracetamol tablets containing 1.0 g of paracetamol tablet were finely crushed in a mortar. A tablet equivalent mass of the powder was dissolved in water using ultrasonication. After centrifugation at 3500 rpm for 20 minutes. The supernatant was filtered through a fine filter paper in order to remove insoluble excipients, the resulting solution was transferred to a 50 mL measuring flask and finally adequately diluted with 0.1 M PBS (pH 7.4) . Furthermore, the prepared electrochemical sensor was tested in biological samples. To do so, human blood serums were collected from healthy adults and pretreated according to procedures outlined in the next section.

III.4.2.5. Preparation of human blood serum

Serum is a biological fluid present in both interstitial spaces and blood. Serum is derived from blood, distinguished by the removal of blood cells, proteins, and coagulation factors, in contrast to plasma, which retains these factors. Serum samples are collected in serum gel or dry tubes. Optimal serum quality necessitates a 30-minute coagulation period at room temperature. Post centrifugation at 3000 rpm, the coagulum separates into solid and liquid phases, with the solid component comprising a dense aggregate of fibrin and blood cells (**Figure III.16**).

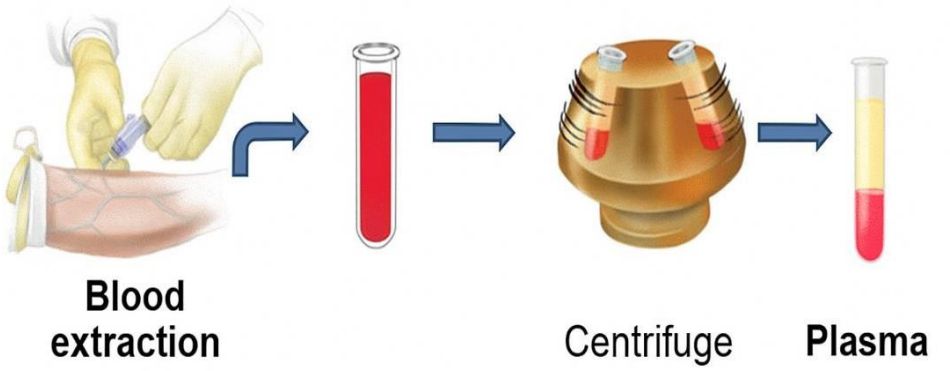

Figure III.16. Human blood serum preparation.

III.4.3. Electrodeposition

The process of electrodeposition entails applying a metallic layer from an electrolytic bath containing the metal ions to be deposited onto a conductive substrate. The goal of electrodeposited coatings is frequently to give the substrate new qualities, such as resistance to corrosion, metallic lustre, nanometric roughness, and the improvement of other qualities, among others.

Aqueous electrolytes, commonly referred to as electrodeposition baths or just baths in the industry, are typically the basis for the electrodeposition of metals in industrial finishing. The metal salt of the metal to be deposited is the precursor added with an acid or an alkali to enhance conductivity. The bath can be buffered in some situations and additives could be used to enhance the electroplating process or improve the deposit's characteristics.

The current flowing between two electrodes submerged in an aqueous conductive solution of metal salts is what causes the metal to be deposited. In industrial devices of electrodeposition,

the anode dissolves and the cathode becomes coated in metal.By altering the pace of germ development and growth, various factors (such as temperature, current density, agitation, electrolyte concentration and pH, and bath type) affect the shape of metallic deposits (**Figure III.17**) **[62].**

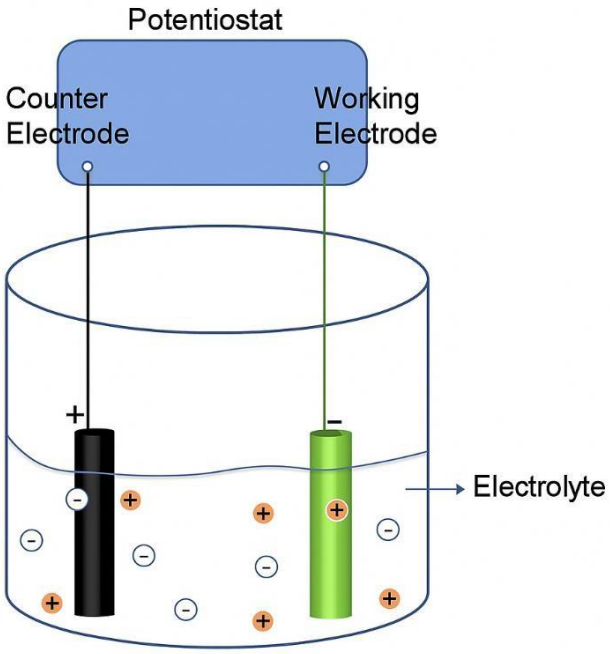

Figure III.17. Electrodeposition set-up

III.4.4. Experimental electrochemical device

The electrochemical behavior of RuNPs/ASPE was studied by cyclic voltammetry and electrochemical impedance spectroscopy, using a potentiostat VersaSTAT 3 manufactured by Princeton Applied Research (AMETEK, USA), controlled by the data acquisition software "Versa". A potentiostat is an electronic measuring device necessary to control a three electrode cell and perform most electroanalytical experiments shown in (**Figure II.18**). The study was carried out using the screen printed electrode which consists of a working electrode, where the electrochemical reactions are investigated, a reference electrode whose potential is fixed and known for the control of the working electrode's potential, and an auxiliary electrode (the counter electrode) that completes the electric circuit in the electrochemical cell.

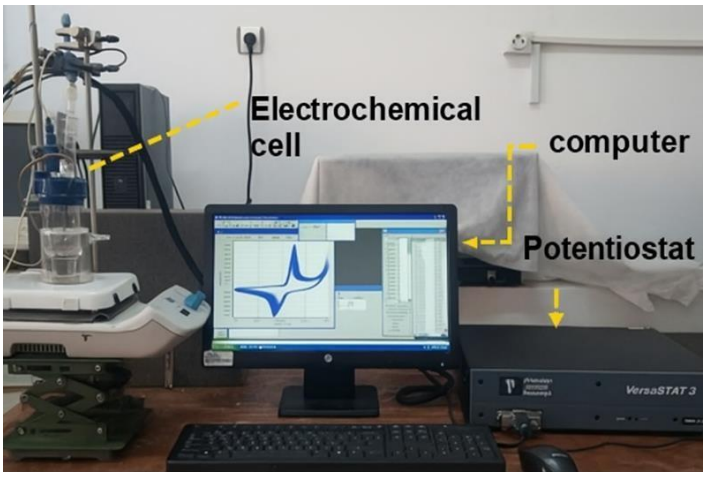

Figure III.18. Experimental setup used for kinetic studies by CV and EIS

The EC-Lab software was used for data treatment/analysis of EIS. The EC-Lab® software provides a powerful and user friendly tool for adapting successive EIS measurements called Z Fit. The latter automatically determines the successive values of the EC components for a series of impedance diagrams.

Other studies on detection with SWV were carried out using a 273A model potentiostat-galvanostat controlled by a computer using the software "Power Suite." (**Figure II.19**).

Figure III.19. Experimental setup used to characterize the sensitivity of the developed sensors developed by SWV.

III.4.5. Electrochemical cell

An electrochemical cell serves as a platform for investigating the electrical aspects of chemical reactions. In this study, the cell configuration incorporates a screen printed electrode, which integrates a reference electrode, an auxiliary electrode, and a working electrode onto a

unique strip. The electrochemical experiments were conducted within a 75 ml capacity Pyrex glass cell, equipped with a magnet positioned directly beneath the working electrode, as depicted in (**Figure III.20**). All electrochemical tests are performed at ambient temperature under aerated conditions.

Figure III.20. Electrochemical system

a) Counter electrode (CE)

The counter electrode or auxiliary electrode ensures and measures the passage of current in an electrochemical cell. The latter is kept parallel to the working electrode to ensure a good distribution of the current lines, and it usually has a large surface area compared to the working electrode. The integrated auxiliary electrode to the SPE strip used in this work is made of graphite.

b) Reference electrode (RE)

It is an electrode which potential is remarkably stable even when it delivers small currents. As its name suggests, it serves as a reference for the potentiostat in order to apply an exact potential difference between this electrode and the working electrode, and thus to vary the potential applied to the working electrode in an exact and known manner. The reference electrode used in this work is the Ag/AgCl electrode.

c) Working electrode (WE)

The working electrode, is an electrode in an electrochemical system on which the reaction (oxidation or reduction) or the equilibrium to be explored takes place.In this study, we employed three distinct working electrodes.

- Graphite
- Activated graphite
- Ruthenium deposited on activated graphite

III.4.6. Fabrication of flexible screen printed graphite electrodes

The screen printed electrodes (SPEs) were fabricated using a DEK 248 screen printing machine (DEK, Weymouth, U.K.) with the appropriate stencil. Initially, a carbon graphite layer (product code C2000802P2; Gwent Electronic Materials Ltd., U.K.) was deposited onto a polyester flexible film (Autostat, 250 μm thickness) to establish electrical contacts. After a heat treatment at 60°C for 30 minutes, the reference electrode was printed using Ag/AgCl paste (product code C2040308D2; Gwent Electronic Materials Ltd., U.K.) and then cured according to the manufacturer's instructions. Subsequently, a dielectric layer (product code D2070423D5; Gwent Electronic Materials Ltd., U.K.) was deposited and cured to define the electrode contact areas. Following a final curing process at 60°C for 30 minutes, the screen printed electrodes, featuring a graphite working electrode with a diameter of 3.1 mm, were ready for use **[63].**

In this study the screen printed electrodes were kindly furnished by Manchester Universty, UK (**Figure III.21**).

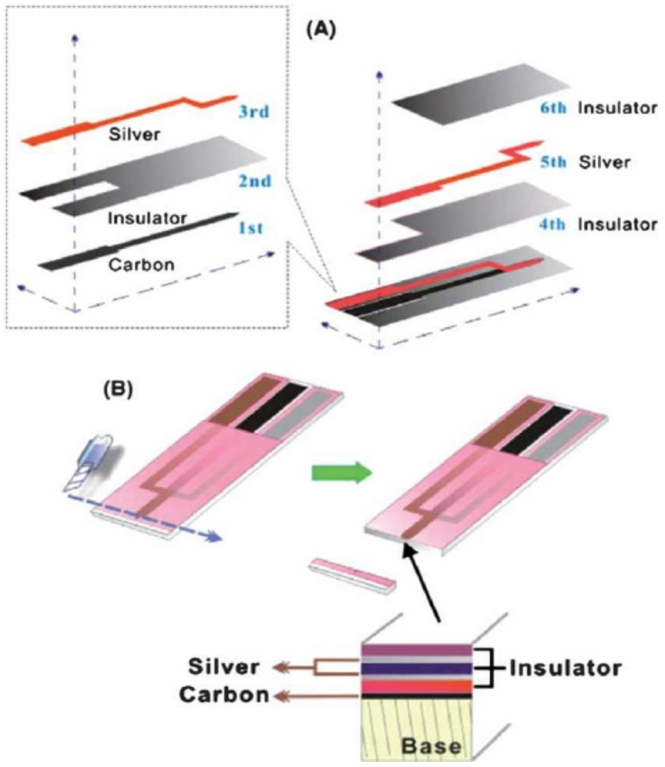

Figure III.21. An illustration of the SPE assembly's layer-by-layer structure (A).The electrode system with an integrated three electrode arrangement is shown in a cross-sectional diagram (B).

III.4.7. Electrochemical preparation of RuNPs/ASPE electrodes

The following process was used to manufacture the activated screen printed electrode (ASPE) modified by ruthenium nanoparticles:

- The graphite surface of the SPE was electrochemically activated in 1.0 M H_2SO_4 in two steps before ruthenium electrodeposition (**Figure III.22**). For five minutes, the graphite surface was polarised at a steady potential of 1.8 V. Following that, cyclic polarisation was applied to the surface. For 50 cycles, the voltage was swept at a scan rate of 50 $mV.s^{-1}$ between –0.4 V (the hydrogen evolution potential) and 1.8 V (beyond oxygen evolution potential).
- Through fifteen consecutive voltammetric cycles between -0.2 and 0.5 V at a scan rate of 50 $mV.s^{-1}$ in H_2SO_4 solution (0.1 M) containing 1.0 mM $RuCl_3$ (made in doubly distilled water), Ru nanoparticles were electrodeposited on the surface of the working electrode. During electrodeposition, temperature was maintained at 25±0.5°C.
- After its elaboration, the electrode was rinsed with distilled water and allowed to dry at room temperature. To ensure a stable peak response, at least fifty successive cyclic voltammograms were recorded for the modified RuNPs/ASPE electrode in a 0.1 M PBS

solution (pH 7.4) over a potential range of -0.4 to 0.6 V at a scan rate of 50 $mV.s^{-1}$. A similar procedure was applied to the screen printed electrode without Ru.

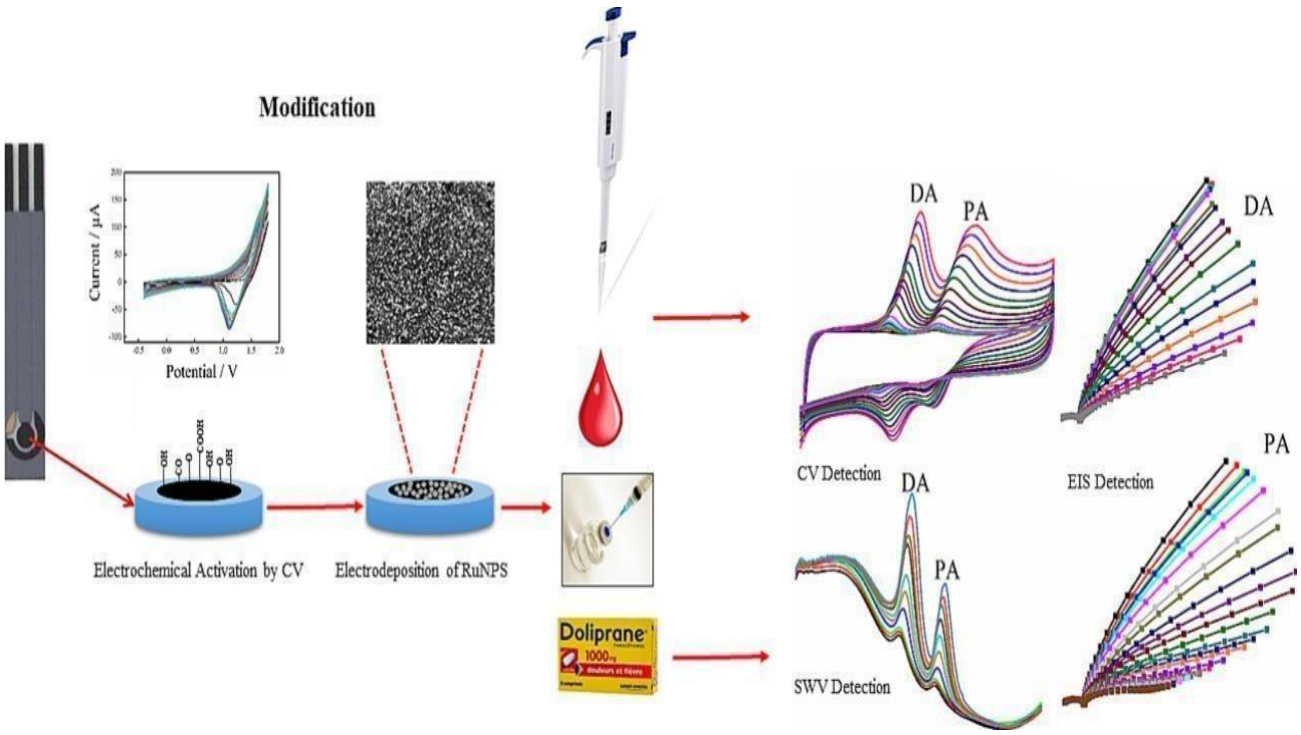

Figure III.22. Graphical overview of SPE modification and applications in dopamine and paracetamol sensing.

Conclusion

The operational procedures and experimental setup used in this study are described in depth in this chapter, which made it possible to successfully create the desired sensor meant for target molecule identification. Additionally, we have devoted the main part of this chapter to describing the several physicochemical characterisation methods. Since they offer a range of relevant information about our elaborated sensor.

In the next chapters, we report the findings from the investigation of the electrocatalytic activity of the electrode designed for dopamine and paracetamol detection as well as the physical and electrochemical characterisation of ruthenium electrodeposited on the activated graphite substrate.

References

[1] A. Bahloul, Synthèse assistée par micro-ondes, caractérisation et applications de nanoparticules de cuivre, et étude de la relation structure-activité antioxydante d'amides d'acide phénolique, PhD thesis, University of 8 Mai 1945 Guelma, 2024.

[2] B.D. Cullity, Elements of X-Ray Diffraction, 2nd ed., Addison-Wesley Publishing Company Inc., Philippines (1978).

[3] M. Gougis, Développement de capteurs électrochimiques non-enzymatiques pour la gestion du diabète, PhD thesis, University of Québec, 2014.

[4] I. Boubezari, Conception et développement de nouveaux capteurs chimiques et de (bio)capteurs à transduction électrochimique, PhD thesis, University of Claude Bernard Lyon 1, 2021.

[5] C. Herrier, Fonctionnalisation et structuration par microscopie à force atomique (AFM) de surfaces de silicium hydrogéné, PhD thesis, University of Rennes 1, 2012.

[6] HONG-QIANG Li, The common AFM modes, 1997.

[7] Atomic Force Microscopy (AFM), Techniques de l'ingénieur R1394, p. 45.

[8] C. Wolf, P. Quinn, K. Koumanov, C. Chachaty, B. Tenchov, Arrangement physique des lipides membranaires susceptibles d'être utilisés par les processus d'assemblage cellulaire des protéines, Journal de la Société de biologie, 193 (1999) 117–123.

[9] F. Bedioui, Voltampérométrie. Théorie et mise en œuvre expérimentale, Techniques de l'Ingénieur, Analyses et Caractérisations, vol. 3, no P2126, 1999.

[10] G. Cauquis, D. Serve, Quelques observations relatives aux voltammétries sur électrode de carbone vitreux dans les milieux aprotiques, J. Electroanal. Chem., 34 (1972) A1–A6.

[11] R. Bourgeois, A. Delay, Contribution de la voltammétrie à l'étude du comportement électrochimique, sur électrode de mercure, de certains ortho- et para-nitrophenylazobenzenes, Electrochim. Acta, 22 (1977) 857–865.

[12] N. Zehani, P. Fortgang, M.S. Lachgar, A. Baraket, M. Arab, S. Dzyadevych, R. Kherrat, N. Jaffrezic-Renault, Highly sensitive electrochemical biosensor for bisphenol A detection based on a diazonium-functionalized boron-doped diamond electrode modified with a multi-walled carbon nanotube-tyrosinase hybrid film, Biosens. Bioelectron., 74 (2015) 830–835.

[13] Z. Üstündağ, A.O. Solak, EDTA modified glassy carbon electrode: Preparation and characterization, Electrochim. Acta, 54 (2009) 6426–6432.

[14] N. Ruecha, N. Rodthongkum, D.M. Cate, J. Volckens, O. Chailapakul, C.S. Henry, Sensitive electrochemical sensor using a graphene–polyaniline nanocomposite for simultaneous detection of Zn(II), Cd(II), and Pb(II), Anal. Chim. Acta, 874 (2015) 40–48.

[15] M. Yüce, H. Nazır, G. Dönmez, Using of Rhizopus arrhizus as a sensor modifying component for determination of Pb(II) in aqueous media by voltammetry, Bioresource Technology, 101 (2010) 7551–7555.

[16] W. Zhang, J. Yin, F. Min, L. Jia, D. Zhang, Q. Zhang, J. Xie, Cyclic voltammetry analysis of copper electrode performance in Na_2WO_4 solution and optical property of electrochemical synthesized $CuWO_4$ nanoparticles, J. Alloys Compd., 690 (2017) 221–227.

[17] B. Bennett, J. Chang, A.J. Bard, Mechanism of the Br^-/Br_2 redox reaction on platinum and glassy carbon electrodes in nitrobenzene by cyclic voltammetry, Electrochim. Acta, 219 (2016) 1–9.

[18] H. Heydari, M.B. Gholivand, A. Abdolmaleki, Cyclic voltammetry deposition of copper nanostructure on MWCNTs modified pencil graphite electrode: An ultra-sensitive hydrazine sensor, Mater. Sci. Eng. C, 66 (2016) 16–24.

[19] A. Terbouche, S. Lameche, C. Ait-Ramdane-Terbouche, D. Guerniche, D. Lerari, K. Bachari, D. Hauchard, A new electrochemical sensor based on carbon paste electrode/Ru(III) complex for determination of nitrite: Electrochemical impedance and cyclic voltammetry measurements, Measurement, 92 (2016) 524–533.

[20] B. Idbelkas, D. Takky, Traitement électrochimique d'eaux usées chargées de phénol : étude comparative sur des électrodes de dioxyde de plomb et de platine, Ann. Chim. Sci. Mat., 26 (2001) 33–44.

[21] J. Wang, Analytical Electrochemistry, John Wiley & Sons, Inc., 3rd Ed. (2006).

[22] C. Brett, A.M. Oliveira Brett, Electrochemistry: Principles, Methods, and Applications, Oxford University Press, Oxford (1993).

[23] J.M. Zen, D.M. Tsai, H.H. Yang, Sensitive determination of Zinc(II) in real samples using a poly(4-vinylpyridine)/mercury film electrode, Chinese Chemical Society, 50 (2003) 375–380.

[24] L. Tang, X. Dai, K. Zhong, D. Wu, X. Wen, A novel 2,5-diphenyl-1,3,4-oxadiazole derived fluorescent sensor for highly selective and ratiometric recognition of Zn^{2+} in water through switching on ESIPT, Sens. Actuators B, 203 (2014) 557–564.

[25] A. Królicka, A. Bobrowski, Employing a magnetic field to amplify zinc signal obtained at bismuth film screen-printed electrodes generated using dual bismuth precursor, Electrochim. Acta, 187 (2016) 224–233.

[26] S. Uba, B.R. Horrocks, A. Uzairu, M.S. Sallau, H. Abba, Comparative studies of heavy metals in mine water by square wave stripping voltammetry and atomic spectroscopy, Int. Res. J. Pure Appl. Chem., 4 (2014) 417–429.

[27] C. Locatelli, Heavy metals in matrices of food interest: Sequential voltammetric determination at trace and ultratrace level of copper, lead, cadmium, zinc, arsenic, selenium, manganese and iron in meals, Electroanal., 16 (2004) 1478–1486.

[28] M. Á.G. Rico, M. Olivares-Marín, E.P. Gil, A novel cell design for the improved stripping voltammetric detection of Zn(II), Cd(II), and Pb(II) on commercial screen-printed strips by bismuth codeposition in stirred solutions, Electroanal., 20 (2008) 2608–2613.

[29] M. Hosseini, S.D. Abkenar, M.R. Ganjali, F. Faridbod, Determination of zinc(II) ions in wastewater samples by a novel zinc sensor based on a newly synthesized Schiff's base, Mater. Sci. Eng. C, 31 (2011) 428–433.

[30] E. Roy, S. Patra, R. Madhuri, P.K. Sharma, Development of an imprinted polymeric sensor with dual sensing property for trace level estimation of zinc and arginine, Mater. Sci. Eng. C, 49 (2015) 25–33.

[31] A.J. Bard, L.R. Faulkner, Electrochemical Methods: Fundamentals and Applications, John Wiley & Sons, Inc., New York (2001).

[32] J. Jorcin, Spectroscopie d'impédance électrochimique locale : caractérisation de la délamination des peintures et de la corrosion des alliages Al-Cu, PhD thesis, University of Toulouse-INPT, 2007.

[33] E.L. Din-Stirbu, Comportement à la corrosion des alliages d'aluminium utilisés dans l'industrie automobile pour la fabrication de radiateur de chauffage, PhD thesis, University of Lyon -INSA, 2005.

[34] S. Hong, L. Tai-Chin, Electrochemical Impedance Spectroscopy for Battery Research and Development, Technical Report 31, Solartron, 1996.

[35] C.G. Zoski, Handbook of Electrochemistry, Elsevier, Las Cruces, New Mexico, USA (2007).

[36] D. Malko, T. Lopes, E.A. Ticianelli, A. Kucernak, A catalyst layer optimisation approach using electrochemical impedance spectroscopy for PEM fuel cells operated with pyrolysed transition metal-N-C, J. Power Sources, 323 (2016) 189–200.

[37] S. Ramalingam, K. Balakrishnan, S. Shanmugasamy, A. Subramania, Electrodeposition and characterisation of Cu–MWCNTs nanocomposite coatings, Surface Engineering, 33 (2017) 369–374.

[38] A. Ganesan, A. Varzi, S. Passerini, M.M. Shaijumon, Graphene derived carbon confined sulfur cathodes for lithium-sulfur batteries: Electrochemical impedance studies, Electrochim. Acta, 214 (2016) 129–138.

[39] I.A. Jiménez Gordon, S. Grugeon, H. Takenouti, B. Tribollet, Electrochemical Impedance Spectroscopy response study of a commercial graphite-based negative electrode for Li-ion batteries as function of the cell state of charge and ageing, Electrochim. Acta, 223 (2017) 63–73.

[40] S. Ben Aoun, M. Bouklah, K.F. Khaled, B. Hammouti, Electrochemical Impedance Spectroscopy investigations of steel corrosion in acid media in the presence of thiophene derivatives, Int. J. Electrochem. Sci., 11 (2016) 7343–7358.

[41] L.A. Tobias Kogel, E. Boschmann, J. Baur, Lubricant induced metal corrosion – an electrochemical impedance spectroscopy approach, Goriva i Maziva, 55 (2016) 131–135.

[42] M.V. Riquelme, H. Zhao, V. Srinivasaraghavan, A. Pruden, P. Vikesland, M. Agah, Optimizing blocking of nonspecific bacterial attachment to impedimetric biosensors, Sensing Bio-Sensing Research, 8 (2016) 47–54.

[43] M.S. Wiederoder, I. Misri, D.L. De Voe, Impedimetric immunosensing in a porous volumetric microfluidic detector, Sens. Actuators B, 234 (2016) 493–497.

[44] E.B. Bahadır, M.K. Sezgintürk, A review on impedimetric biosensors, Artif. Cells Nanomed. Biotechnol., 44 (2016) 248–262.

[45] Z.H. Yang, Y. Zhuo, R. Yuan, Y.Q. Chai, Amplified impedimetric aptasensor combining target-induced DNA hydrogel formation with pH-stimulated signal amplification for the heparanase assay, Nanoscale, 9 (2017) 2556–2562.

[46] S.A. Jin, S. Poudyal, E.E. Marinero, R.J. Kuhn, L.A. Stanciu, Impedimetric dengue biosensor based on functionalized graphene oxide wrapped silica particles, Electrochim. Acta, 194 (2016) 422–430.

[47] A. Hushegyi, D. Pihíková, T. Bertok, V. Adam, R. Kizek, J. Tkac, Ultrasensitive detection of influenza viruses with a glycan-based impedimetric biosensor, Biosens. Bioelectron., 79 (2016) 644–649.

[48] F.S. Husairi, J. Rouhi, K.A. Eswar, C.H. Raymond Ooi, M. Rusop, S. Abdullah, Ethanol solution sensor based on ZnO/PSi nanostructures synthesized by catalytic immersion method at different molar ratio concentrations: An electrochemical impedance analysis, Sens. Actuators A, 236 (2015) 11–18.

[49] A. Sharma, J.K. Bhattarai, S.S. Nigudkar, S.G. Pistorio, A.V. Demchenko, K.J. Stine, Electrochemical impedance spectroscopy study of carbohydrate-terminated alkanethiol monolayers on nanoporous gold: Implications for pore wetting, J. Electroanal. Chem., 782 (2016) 174–181.

[50] J.K. Bhattarai, Y.H. Tan, B. Pandey, K. Fujikawa, A.V. Demchenko, K.J. Stine, Electrochemical impedance spectroscopy study of Concanavalin A binding to self-assembled monolayers of mannosides on gold wire electrodes, J. Electroanal. Chem., 780 (2016) 311–320.

[51] H. Bagheri, N. Pajooheshpour, A. Afkhami, H. Khoshsafar, Fabrication of a novel electrochemical sensing platform based on a core–shell nanostructured/molecularly imprinted polymer for sensitive and selective determination of ephedrine, RSC Adv., 6 (2016) 51135–51145.

[52] L. Mendecki, N. Callan, M. Ahern, B. Schazmann, A. Radu, Influence of ionic liquids on the selectivity of ion exchange-based polymer membrane sensing layers, Sensors, 16 (2016) 1106.
[53] G. Evtugyn, T. Hianik, Electrochemical DNA sensors and aptasensors based on electropolymerized materials and polyelectrolyte complexes, TrAC Trends Anal. Chem., 79 (2016) 168–178.
[54] B. Rezaei, M.K. Boroujeni, A.A. Ensafi, Development of Sudan II sensor based on modified treated pencil graphite electrode with DNA, o-phenylenediamine, and gold nanoparticle bioimprinted polymer, Sens. Actuators B, 222 (2016) 849–856.
[55] Y. Li, H. Song, L. Zhang, P. Zuo, B.-c. Ye, J. Yao, W. Chen, Supportless electrochemical sensor based on molecularly imprinted polymer modified nanoporous microrod for determination of dopamine at trace level, Biosens. Bioelectron., 78 (2016) 308–314.
[56] J. Bai, X. Zhang, Y. Peng, X. Hong, Y. Liu, S. Jiang, B. Ning, Z. Gao, Ultrasensitive sensing of diethylstilbestrol based on AuNPs/MWCNTs-CS composites coupling with sol-gel molecularly imprinted polymer as a recognition element of an electrochemical sensor, Sens. Actuators B, 238 (2017) 420–426.
[57] Y. Hu, B. Liang, L. Fang, G. Ma, G. Yang, Q. Zhu, S. Chen, X. Ye, Antifouling zwitterionic coating via electrochemically mediated atom transfer radical polymerization on enzyme-based glucose sensors for long-time stability in 37 °C serum, Langmuir, 32 (2016) 11763–11770.
[58] M. Devillers, Conception, évaluation et modélisation de biocapteurs pour la détection électrochimique du facteur de motilité autocrine: biomarqueur potentiel de cancers métastatiques, PhD thesis, University of Paris-Saclay, 2016.
[59] X. Diao, S. Katsuhiro, Determination of Iron Monosulfide and Iron Disulfide in Suspensions by an Electrochemical Method Using a Platinum-Silver Twin-Electrode, Analytical Sciences (2010) 681–686.
[60] A.Z. Hassan, R.G. Mohammad, F. Farnoush, S.N. Masoud, Heptadentate Schiff-base based PVC membrane sensor for Fe(III) ion determination in water samples, Materials Science and Engineering, Vol. 32, No. 3, 2012, pp. 564–568.
[61] R.A. Al-Amiery, Preparation and Spectroscopic Characterization of Iron (III) Complexes of a Functionalized Crown Ether, Journal of Thi-Qar Science, 2011,1991–8690.
[62] A.A. Pasa, M.L. Munford, Electrodeposition, Encycl. Chem. Process. (2006)
[63] C.W. Foster, R.O. Kadara, C.E. Banks, Screen-printing electrochemical architectures, Springer, Cham (2016).

Chapter IV

Results and discussion

Part A

Voltammetric detection of dopamine and paracetamol

IV.1. Introduction

In this chapter, for the first time a simple electrodeposition method was employed to develop effective, selective, and sensitive electrochemical sensor based on ruthenium nanomaterials modified activated screen-printed electrode for the determination of dopamine and paracetamol. The properties of the elaborated RuNPs/ASPE were examined using different physical and electrochemical methods.

IV.2. Electrochemical activation of RuNPs/ASPE

The preparation of the modified electrode RuNPs/ASPE, necessitates an activation step before proceeding with physical and electrochemical characterization and substances assay. This activation can be achieved through cyclic voltammetry (50 cycles), involving repeated potential sweeps within a supporting electrolyte. The potential range for these sweeps is between –0.4 V to 0.6 V in a 0.1 M PBS (pH 7.4) with a scan rate of 50 mV s^{-1}. The process continues until the voltammograms show consistent behavior across multiple cycles, with the final cycle closely matching the preceding one, as illustrated in inset of **Figure IV.1**. This voltammetric cycling serves to condition and purify the electrode surface.The obtained typical cyclic voltammogram for a RuNPs depicted in **Figure IV.1** consistent with previous finding **[1].**

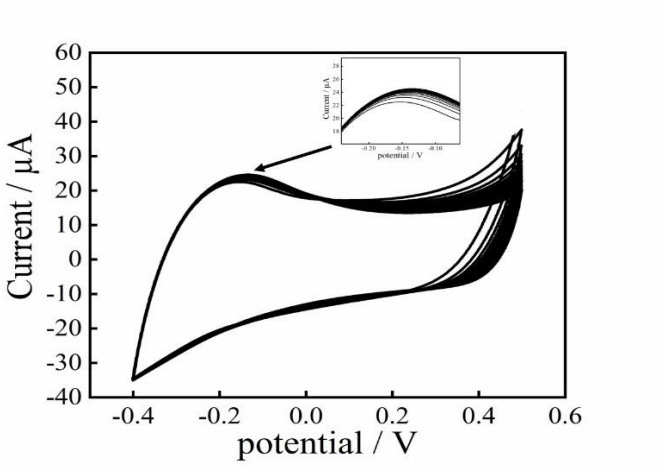

Figure IV.1. CVs of RuNPs/ASPE in PBS, 0.1 M (pH 7.4) at 50 mV s^{-1}.Inset magnification on the successive cycles.

IV.3. Evaluation of structural features and surface morphology of RuNPs/ASPE

Field emission scanning electron microscope combined with energy dispersive X-ray spectroscopy (JSM-6301F from JEOL, Japan) was used for the surface morphological analysis

of the elaborated electrodes.Transmission electron microscopy imaging was conducted utilizing a JEOL JEM-1400 TEM. Concurrently, X-ray diffraction data were amassed via a Bruker D8 Discover spectrometer, (Germany) which employed Cu-Kα radiation (λ = 1.5418) in order to clarify the cristalline structure of the electrodes. Atomic force microscopy was employed to acquire images for assessing surface morphology, utilizing a Nanoscope III system from Bruker, Germany. Morphological characterization of the sensor's surface, before and after the Ru nanoparticles modification was assessed using Fourier-transform infrared measurements, conducted using a Perkin Elmer Spectrum 100 FT-IR spectrometer.

IV.3.1. Morphological analysis of the RuNPs/ASPE by FE-SEM

To verify the deposition of ruthenium nanoparticles on the surface of the ASPE, a structural comparison between activated graphite electrode and activated graphite electrode modified with ruthenium nanoparticles was carried out using FE-SEM (field emission scanning electron microscopy). **Figure IV.2** displays the FE-SEM data, which show the elemental composition and surface morphology. A clear difference in structure can be observed from the FE-SEM images taken of the electrode surfaces. The surface of the ASPE, when examined without modification exhibits significant inhomogeneity and irregularity at a microscopic level. This observation strongly suggests that the surface of the activated screen printed graphite electrode inherently lacks uniformity in its structural composition. The second is that the ruthenium nanoparticles deposited on the surface of ASPE is much denser and more regular, with greater surface homogeneity and regularity at the microscopic level. The resulting deposit particles remained spherical in shape, which is in agreement with perevious **[2,3].** Consequently, it appears that adding ruthenium nanoparticles to the screen-printed electrode using electrodeposition technique, significantly enhances its surface texture and properties. Indeed, RuNPs directly affect the electrode surface's overall reactivity and the real electroactive surface. Electrode modification has been demonstrated as crucial for a variety of electrochemical applications. More effective electrochemical reactions can result from a well-modified surface that improves electron transfer mechanisms and the electrode's catalytic activity.

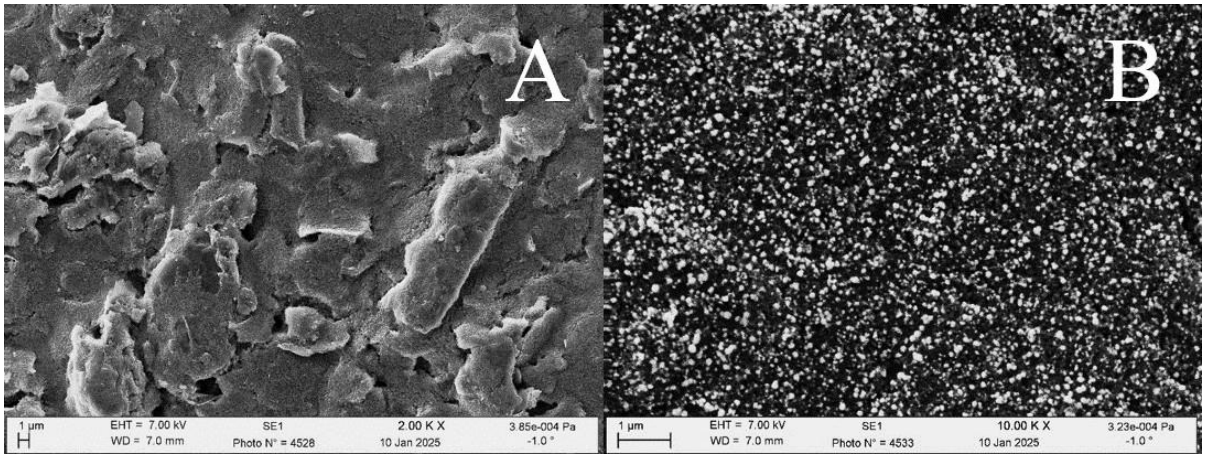

Figure IV.2. FE-SEM images of ASPE (A) and synthesized RuNPs/ASPE (B).

IV.3.2. Morphological analysis of the RuNPs/ASPE by EDX

The elemental composition of the ruthenium nanoparticles modified ASPE was ascertained by means of energy dispersive X-ray spectroscopy combined with scanning electron microscopy. The successful modification of the electrode material is indicated by the EDX results, which are displayed in **Figure IV.3**. The pattern confirm the presence of carbon, oxygen, and ruthenium.

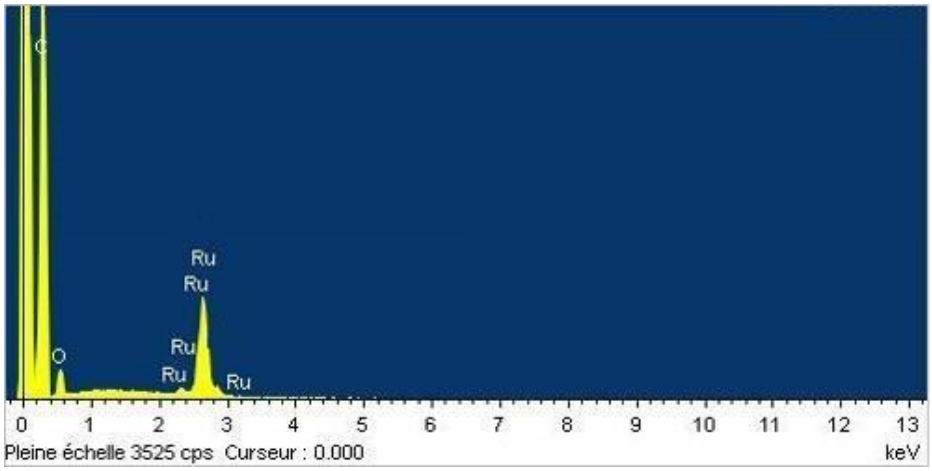

Figure IV.3. EDX analysis of RuNPs/ASPE.

IV.3.3. Morphological analysis of the RuNPs/ASPE by TEM

A detailed transmission electron microscopy image of the RuNPs based electrode's structure is shown in **Figure IV.4**. The obtained image demonstrates that these nanoparticles have highly uniform distribution and remarkably consistent structural characteristics that span the electrode's surface area. Each particle has a spherical shape, and measurements show that

its diameter is about 50 nm. This observation closely matches the information from field emission scanning electron microscopy, confirming the accuracy of both measurement methods. These nanoparticles' uniform size and dispersion are essential for improving the electrochemical performance.

Figure IV.4. TEM image of RuNPS deposited onto ASPE.

IV.3.4. X-ray diffraction analysis of the RuNPs/ASPE

By matching the experimental peaks with the JCPDS files, X-ray diffraction enables the determination of the crystalline structures and nature of samples, as well as the differentiation of phases found in modified electrodes produced by electrodeposition.

Figure IV.5 shows the X-ray diffractograms of the activated graphite electrode sample on which ruthenium nanoparticles were deposited. Thus, X-ray diffraction analysis allowed for the characterization of the nature of the crystallized mineral phases of the RuNPs/ASPE materials. The graphite diffractogram shows five diffraction peaks that correspond to the characteristic at 2θ values of 26.06°, 42.82°, 44.60°, 54.23°, and 77.29°, respectively corresponding to (0 0 2), (1 0 0), (1 0 1), (0 0 4), and (1 1 0) planes. These peaks are indexed using Miller indices based on a hexagonal cell (JCPDS No. 00- 001-0646). The crystalline peaks of Ru are represented by minor peaks at 2θ=42.82° and 44.60°, respectively, in the superposition of (0 0 2) and (1 0 1) planes **[4,5],** (JCPDS cards No. 00-006-0663) of RuNPs/ASPE diffractograms. The weakness of these peaks, however, is explained by the incorporation of Ru nanoparticles into the graphite matrix. These results are consistent with what *Subhenjit* and co-authors reported **[6].** Once again, the XRD technique allowed us to confirm the incorporation of Ru into the ASPE.

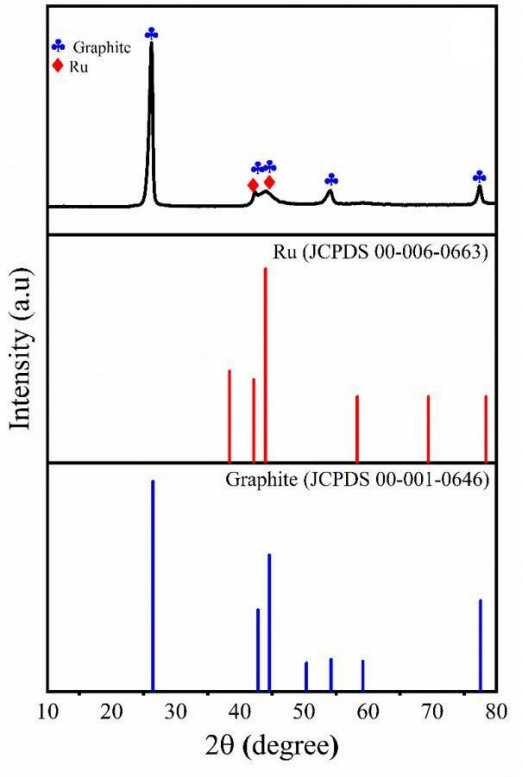

Figure IV.5. X-ray diffraction diagrams of RuNPs/ASPE.

IV.3.5. Characterization of the RuNPs/ASPE by AFM

One of the key advantages of atomic force microscopy is its ability to analyze the surface morphology and roughness of materials. The three dimensional AFM images of the activated screen printed electrode **Figure IV.6A** and ruthenium nanoparticles modified ASPE **Figure IV.6B** are represented respectively. As shown, a smoother surface was identified on the ASPE compared to the RuNPs/SPE, with average roughness of 427 nm and 582 nm for ASPE and RuNPs/ASPE, respectively. The enhanced surface roughness of RuNPs/ASPE indicates a greater exposed surface area, which is advantageous for improving the electrochemical detection of DA and PA. Also AFM analysis suggests a successful distribution of Ru nanoparticles on the surface of the screen printed electrode.

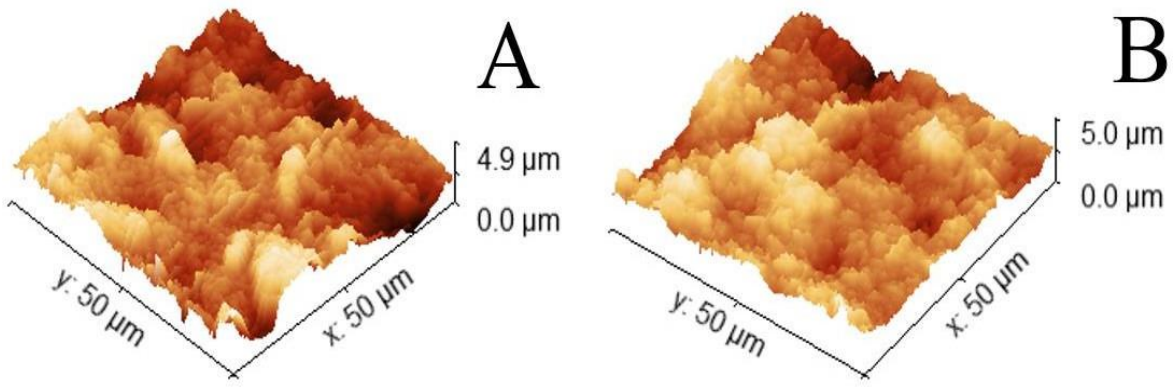

Figure IV.6. 3D AFM images of Activated SPE (A) and RuNPs deposited onto ASPE (B).

IV.3.6. Characterization of the RuNPs/ASPE by FT-IR

Infrared spectrophotometry is commonly used because it is quite rapid and does not require dissolution of the sample in an aqueous solvent **[7].** The confirmation of the chemical structures of ruthenium nanoparticles by infrared analysis, as shown in **Figure IV.7**, is a crucial step in understanding the characteristics of the studied samples.

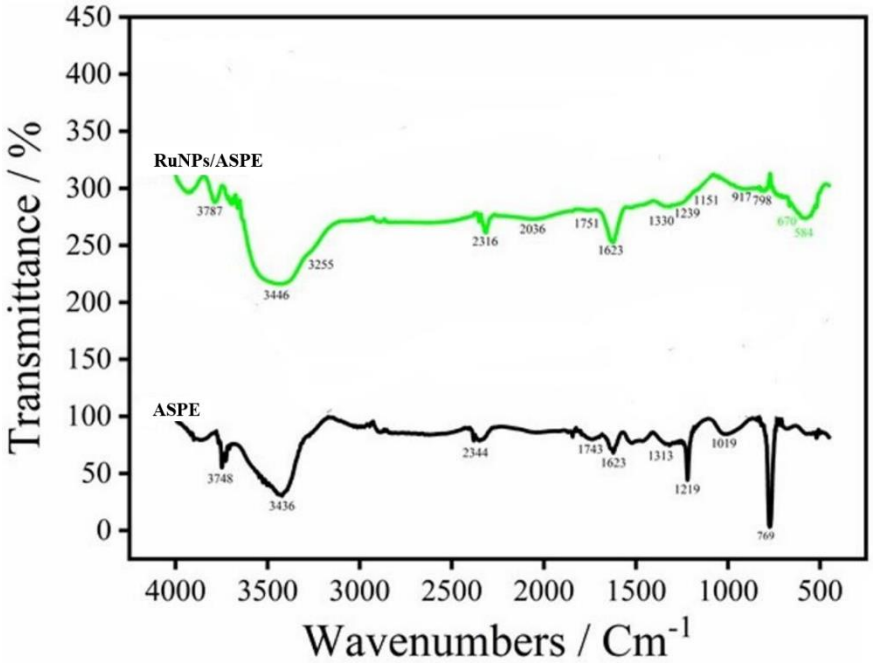

Figure IV.7. FT-IR spectra of ASPE (black curve), the modified electrode RuNPs/ASPE(green curve).

A strong absorption band at 3436 cm^{-1} is associated with O–H stretching vibration, indicating the occurrence of hydroxyl groups in the structure. A characteristic carbonyl (C=O) stretching vibration is seen at 1743 cm^{-1}. Weak absorptions seen at 1623 cm^{-1} and 1313 cm^{-1} are caused by symmetric and asymmetric stretching vibrations of C=O and O–H bonds, respectively. The

C–OH stretching vibration in the nonoxidized graphitic area appears at 1219 cm^{-1}, while the C–O stretching vibration in the alkoxy group is found at 769 cm^{-1}. These findings are consistent with previous reports of FT-IR of graphite electrodes **[8].**In addition, absorption bands of Ru–C and Ru–O groups between 584 cm^{-1} and around 670 cm^{-1} can be observed. These bands are absent in graphite, which means that ruthenium was successfully deposited after electrodeposition **[9,10].**

IV.4. Characterization of the RuNPs/ASPE using electrochemistry

Three integrated screen-printed electrodes (SPEs) were part of the electrochemical setup: a silver/silver chloride reference electrode, a graphite counter electrode, and a working electrode with a diameter of 3.1 mm decorated with Ru nanoparticles. Manchester Metropolitan University produced the SPEs. A two potentiostat/galvanostat (Versa STAT 3 and 273A) from Princeton Applied Research, AMETEK, USA, both connected to a microcomputer and managed by VersaStudio and Power Suite softwares, respectively, were used to collect all of the electrochemical data (CV, SWV, and EIS).

IV.4.1. Cyclic voltammetry analysis of the RuNPs/ASPE

Cyclic voltammetry was utilized as suitable and effective technique to evaluate the electrochemical sensing performance of the as-received SPE, activated SPE and the modified activated SPE with Ru nanoparticles. The $Fe(CN)_6^{3-/4-}$ (1.0 mM) in KCl (0.1 M) solution was chosen as the electrochemical probe. As shown in **Figure IV.8** the CV curves obtained by applying a potential scan from -0.4 to 0.6 V at a scan rate of 50 $mV.s^{-1}$, the redox peak currents increased notably when the Ru nanoparticles modified the activated SPE. On the other hand, peak potential difference (ΔEp) between the cathodic and anodic peaks for the bare SPE, ASPE, and RuNPs/ASPE were 178 mV, 121 mV and 109 mV, respectively. These results indicate that the redox reaction is becoming more reversible and the electron transfer kinetics was improved by an increase in the electroactive surface area as a result of the SPE activation and modification with ruthenium nanoparticles.

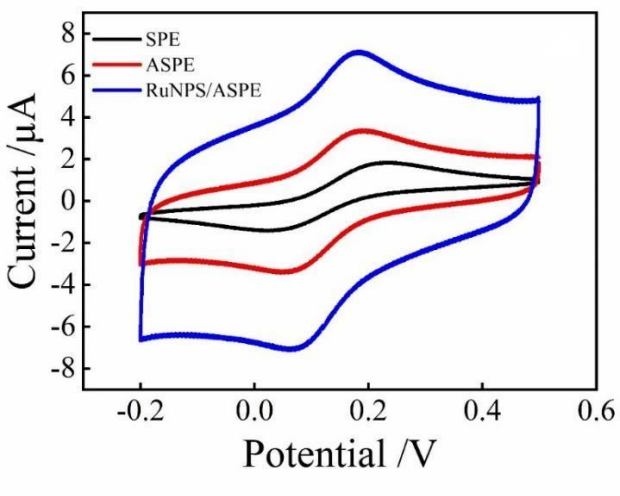

Figure IV.8. CV curves of 1.0 mM $F(CN)^{3-}_{6}/^{4-}$in 0.1 M KCl at unmodified SPE; ASPE and RuNPs/ASPE, scan rate 50 mVs^{-1}.

IV.4.2. Measurement of the functional electroactive area of the electrode surface

To illustrate the improvement of the modification in the electroactive surface area of the modified electrodes, CV experiments were conducted at scan rates ranging from 10 to 120 mV/s see **Figure IV.9.**According to Randles-Sevcik equation **[11]:**

$$Ip = \pm 0.436nFAC\sqrt{\frac{nFD\upsilon}{RT}} \qquad \textbf{(IV.1.)}$$

where:

Ip: The anodic peak current (A),

A: The electroactive surface area of the working electrode in (cm^2),

***n*:** The number of exchanged electrons,

C: The concentration of $Fe(CN)^{3-/4-}_{6}$ (mol cm^{-3}),

D: The diffusion coefficient of a 1.0mM $Fe(CN)^{3-/4-}_{6}$containing 0.1M KCL (7.6×10^{-6} cm^2 s^{-1}),

υ is the scan rate ($V\ s^{-1}$).

From Randles-Sevcik data, the electrochemical active surface areas for the bare SPE, ASPE and RuNPs/ASPE were 5.4 $\times10^{-2}$, 6.8 $\times$ 10^{-2}, and 8.79 $\times10^{-2}$ cm^2, respectively .The

finding indicated that the successful modification with Ru nanoparticles significantly enhances the electroactive surface area of SPE.

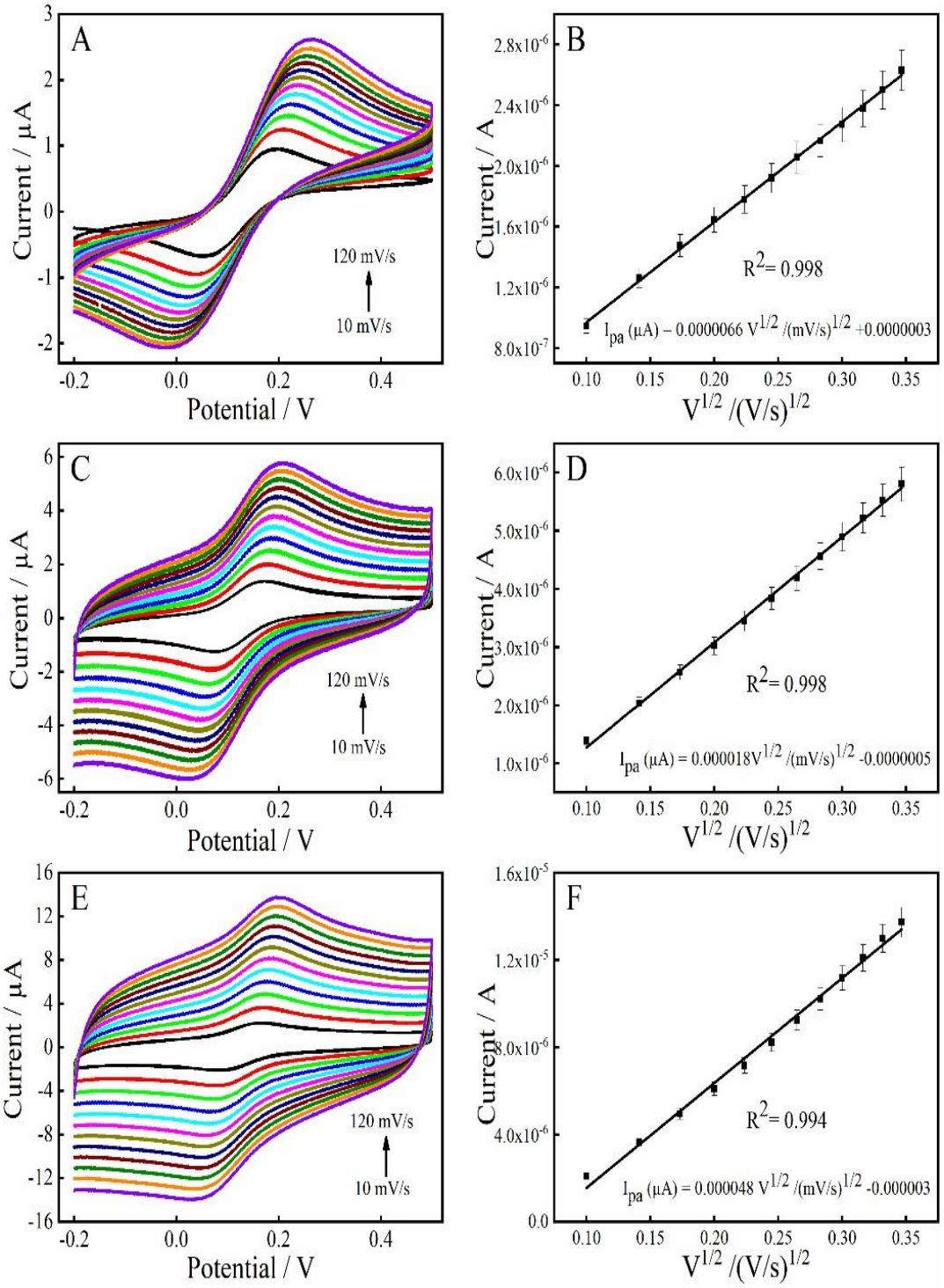

Figure IV.9. CVs of (A) bare SPE, (C) activated SPE, and (E) RuNPs/ ASPE recorded at various scan rates (10–120 mV.s^{-1}) in a 1.0 mM $Fe(CN)_6^{3-/4-}$solution containing 0.1 M KCl; (B), (D), and (F) show the corresponding plots of peak current (I_{pa}).

IV.5. Electrochemical behavior of sensors in the presence of DA and PA

The electrochemical behavior of dopamine and paracetamol at bare and modified electrodes was assessed using cyclic voltammetry. **Figure IV.10** portrays the CV curves obtained by sweeping the potential from -0.4 V to 0.6 V at a scan rate of 50 mVs^{-1} in PBS (0.1 M, pH = 7.4) containing a mixture of DA (100 µM) and PA (100 µM).

For the simultaneous determination of DA and PA to be achievable, it is necessary that the anodic peak potentials are well separated and does not interfere with each other. In the current study, the distinct separation of the anodic peak potentials as seen clearly reflects the sensor's high capability for the simultaneous determination of DA and PA.

Both the DA and PA response signals were found to be enhanced at the modified electrodes, where much sharper peaks and higher current values were registered for the RuNPs/ASPE electrode in comparison with the ASPE and SPE. The modified SPE was found to possess enhanced accumulation capacity compared with its unmodified analogue, a feature that was owed to the greater catalytic efficiency of its modifier film. Moreover, when the ASPE was decorated with Ru nanoparticles, the peak potentials of DA and PA negatively shifted on the electrode surface. The oxidation peak currents of DA and PA at the modified electrode were significantly enhanced, 1.5 times and 2.3 times, respectively, compared to those at the bare SPE electrode. All of these reveal that the RuNPs activated SPE sensor possesses excellent electrocatalytic activity for the simultaneous redox reactions of DA and PA.The higher activity of RuNPs/ASPE is likely because of the participation of OH-like functional groups on the graphite substrate that catalyze the oxidation of adsorbed intermediate species formed during DA and PA dissociation **[12,13].**

These findings, thus indicate that RuNPs/ASPE has improved electrocatalytic properties towards the detection of both DA and PA than SPE and ASPE.

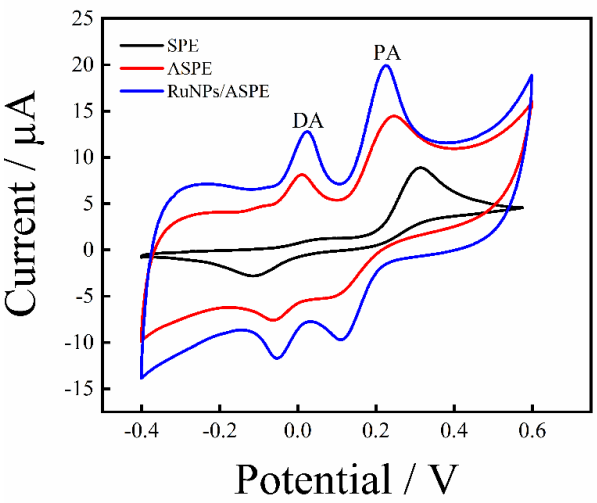

Figure IV.10.CVs responses of PA (100 µM) and DA(100 µM)mixture at bare SPE, activated SPE (ASPE), and RuNPs-modified ASPE in 0.1 M (PBS, pH 7.4), recorded 50 mVs^{-1}.

IV.6. Influence of the scan rate

The effect of scan rate on the electrocatalytic oxidation of dopamine and paracetamol onto RuNPs/ASPE was investigated using cyclic voltammetry. **Figure IV.11A** shows the cyclic voltammograms of RuNPs/ASPE recorded in a 0.1 M PBS solution at pH 7.4, containing 300 µM of each DA and PA, at scan rates ranging from 10 to 400 mV/s. As the scan rate increased, the oxidation peak currents for both DA and PA increased gradually. Meanwhile, the anodic peak potentials shift slightly toward more positive values, while the reduction peak potential shifted negatively.

Furthermore, the anodic (Ipa) and cathodic (Ipc) peak currents showed a linear relationship to the square root of the scan rate ($\nu^{1/2}$), indicating a diffusion-controlled electrochemical process for the redox reaction at RuNPs/ASPE **[14],** as shown in **Figure IV.11B** and **C** The linear regression equations are given below:

Dopamine:

$$I_{pa}(\mu A) = 2.381\, v^{1/2}\,(mVs^{-1})^{1/2} - 1.989\,(R^2 = 0.998) \quad \textbf{(IV.2.)}$$

$$I_{pc}(\mu A) = -2.545\, v^{1/2}\,(mVs^{-1})^{1/2} + 8.939\,(R^2 = 0.994) \quad \textbf{(IV.3.)}$$

Paracetamol:

$$I_{pa}(\mu A) = 2.294\, v^{1/2}(mVs^{-1})^{1/2} - 1.444\,(R^2 = 0.991) \quad \textbf{(IV.4.)}$$

$$I_{pc}(\mu A) = -1.381\, v^{1/2}\,(mVs^{-1})^{1/2} + 5.74\,(R^2 = 0.990) \quad \textbf{(IV.5.)}$$

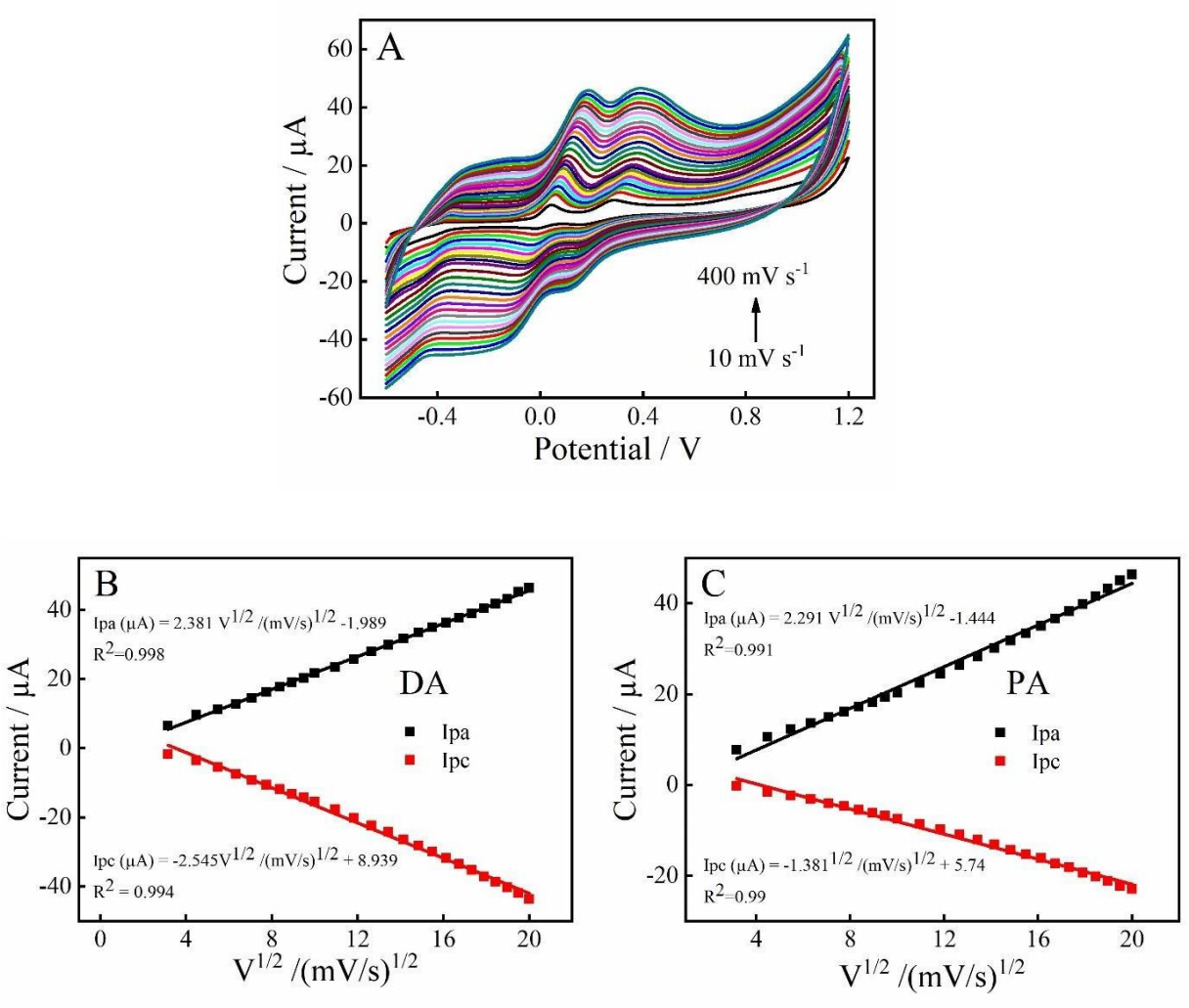

Figure IV.11. (A) CVs responses of RuNPs/ASPE in the mixture of DA (300 µM) and PA (300 µM) at various scan rates (10–400 mVs^{-1}), (B, C) dependence of anodic and cathodic peak currents of DA and PA *vs.*$v^{1/2}$

IV.7. Influence of the pH

One crucial factor that has a big impact on electrochemical performance is pH. In order to further improve the electrochemical performance of the RuNPs/ASPE sensor, the optimization of solution pH was investigated by cyclic voltammetry in different phosphate buffer solutions with pH set in the range of 5.0 to 10 and containing 100 µM of DA and 200 µM of PA.

The CV results presented in **Figure IV.12A,B**. show that the pH of the solution lead to remarkable changes in the redox peak current features.The oxidation peak currents of DA and PA gradually increased as the pH of the electrolyte solutions increased from 5.0 to 7.4. However, the current signals decreased beyond this value 7.4 to 10.0 as shown in

Figure IV.13. The observed decline is attributed to the deprotonation of the target molecules, which arises from the elevated hydroxyl ion concentration in an alkaline medium. This process subsequently induces electrostatic repulsion between the deprotonated species and the sensor surface **[15].** Consequently, a phosphate buffer electrolyte with pH 7.4 was chosen for the subsequent electrochemical experiments.

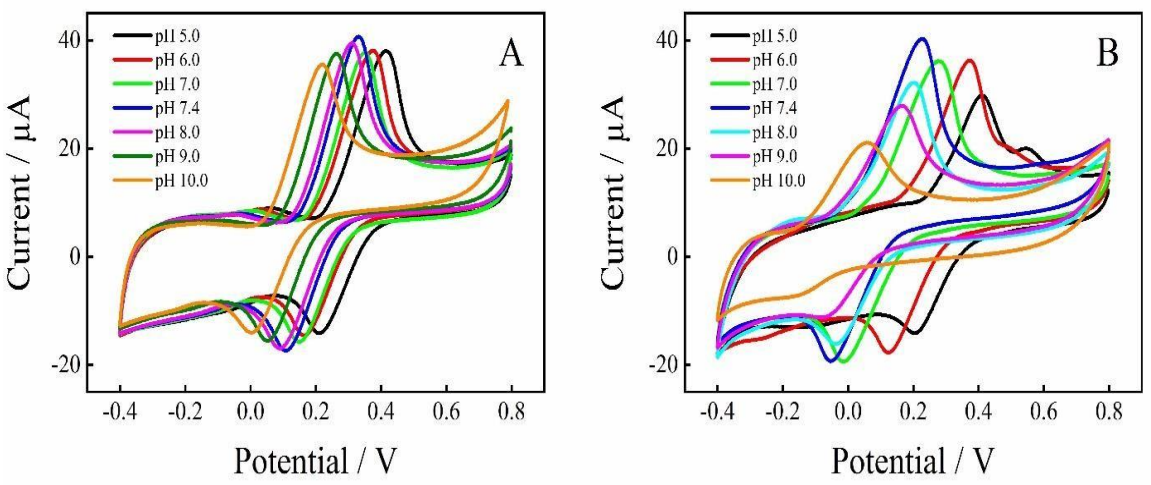

Figure IV.12. CVs response of various pH values of (A) 0.1 mM DA; (B) 0.2 mM PA, at RuNPs/ASPE in 0.1 M PBS at 50 mVs^{-1}.

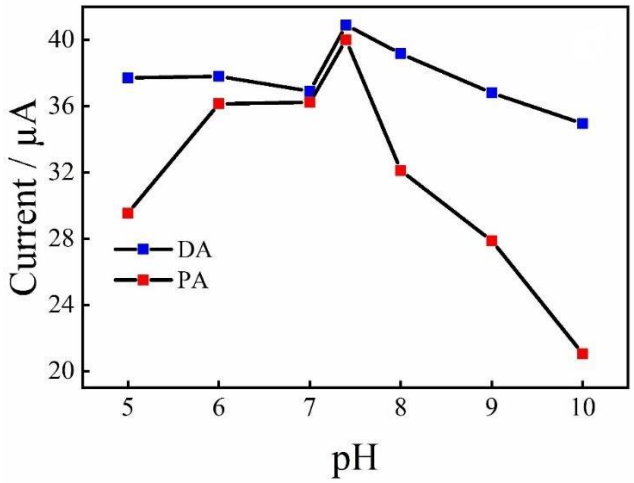

Figure IV.13. The influence of pH on the peak current oxidation of DA and PA.

On the other hand, it is important to highlight the peak potential and pH dependency. DA and PA anodic peaks potentials were shifted negatively upon rising pH (**Figure IV.14**), supporting the above statement that the electrochemical processes of DA and PA on the RuNPs/ASPE surface were directly accompanied by the transfer of protons **[**16**].**

Also, It can be noted that, within the range of 5.0 to 10, the oxidation peak potentials (Epa) plot versus pH revealed a linear relationship with the regression equations:

For DA:

$$Epa_{,DA}\,(V) = -43\ pH + 647\ (R^2 = 0.992) \qquad \textbf{(IV.6.)}$$

For PA:

$$Epa_{,PA}(V) = -56\ pH + 650\ (R^2 = 0.992) \qquad \textbf{(IV.7.)}$$

According to Nernst equation the slopes (dE_P/dpH) are 43 mV/pH and 56 mV/pH for DA and PA, respectively, which are close to the theoretical value of 59 mV/pH **[17].** This means that the same number of electrons and protons are involved in the redox reaction of both DA and PA on RuNPs/ASPE surface which is very likely to be two **[18].**

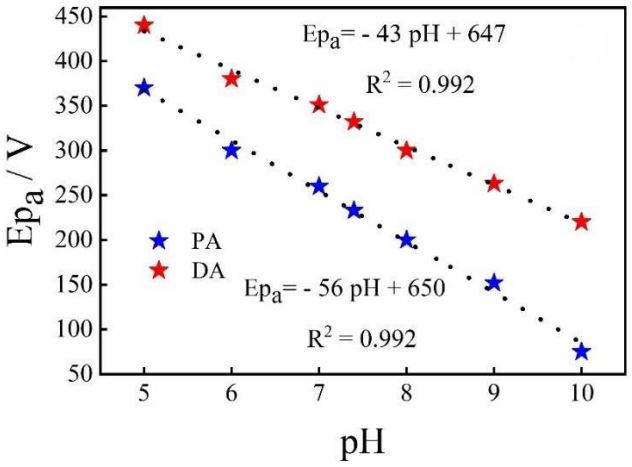

Figure IV.14. The plots of Epa of DA and PA *vs.* pH.

This is in agreement with other reported studies related to DA and PA electrochemical oxidation on various catalysts [19,20]. The electrode mechanisms of DA and PA at RuNPs/ASPE are shown in (**Figure IV.15**).

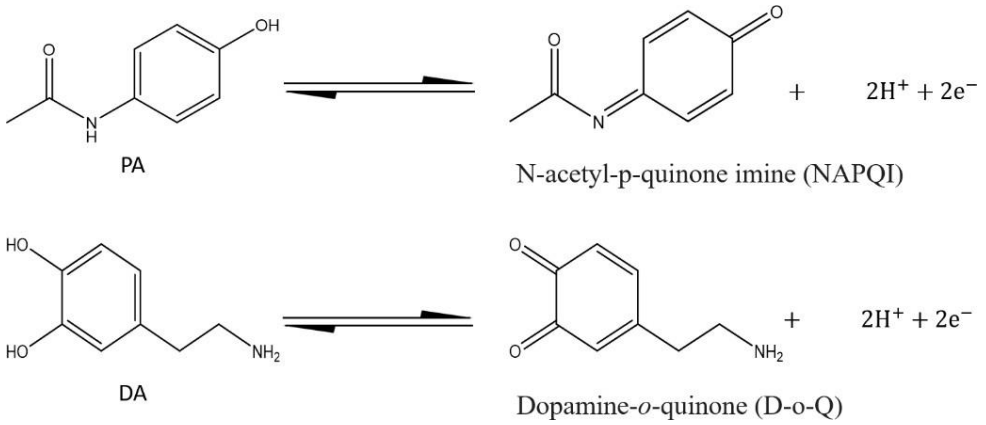

Figure IV.15. Proposed electrochemical oxidation mechanisms of (DA) and (PA) at the RuNPs/ASPE electrode surface **[20].**

IV.8. Voltammetric detection of DA and PA

Voltammetric measurements of PA and DA in optimized conditions were performed in a 0.1 M PBS solution (pH 7.4). Cyclic voltammograms were recorded by scanning the potential from –0.4 V to 0.6 V at a scan rate of 50 mVs^{-1}. Initial potential -0.6 V, final potential 0.2 V, step height 0.005 V, pulse amplitude 0.05 V, and pulse width 0.2 s were the optimised parameters used to record each SWV measurement.

IV.8.1. Individual electrochemical detection of DA and PA with RuNPs/ASPE

In order to assess DA and PA sensing performances onto RuNPs/ASPE, CV and SWV techniques were employed. First of all, CV was used to test the DA and PA concentrations effect on the elaborated RuNPs/ASPE performances. As expected, the intensity of the anodic peak currents for dopamine and paracetamol increased with the increase of the analytes concentrations.

The electrochemical response of the ruthenium nanoparticle modified activated screen printed electrode RuNPs/ASPE to dopamine is presented in **Figure IV.16A**. In the potential window of –0.4 V and +0.6 V, the sensor is able to produce a detectable response even at low concentration of 1.0 µM of dopamine.The corresponding current density response against dopamine concentration is presented in **Figure IV.16B**.

Which depicts a clear linear relationship over a wide range of concentrations (1.0 µM to 300 µM). A two segmented linear calibration plots were noted :

In the range 1.0 µM to 50 µM, the relationship of peak current to dopamine concentration is given by the equation:

$$Ip\ (\mu A) = 0.141\ C_{DA}\ (\mu M) + 6.183\ (R^2 = 0.996) \quad \textbf{(IV.8.)}$$

From 50 µM to 300 µM, the calibration curve is expressed as:

$$Ip\ (\mu A) = 0.055\ C_{DA}\ (\mu M) + 10.66\ (R^2 = 0.996) \quad \textbf{(IV.9.)}$$

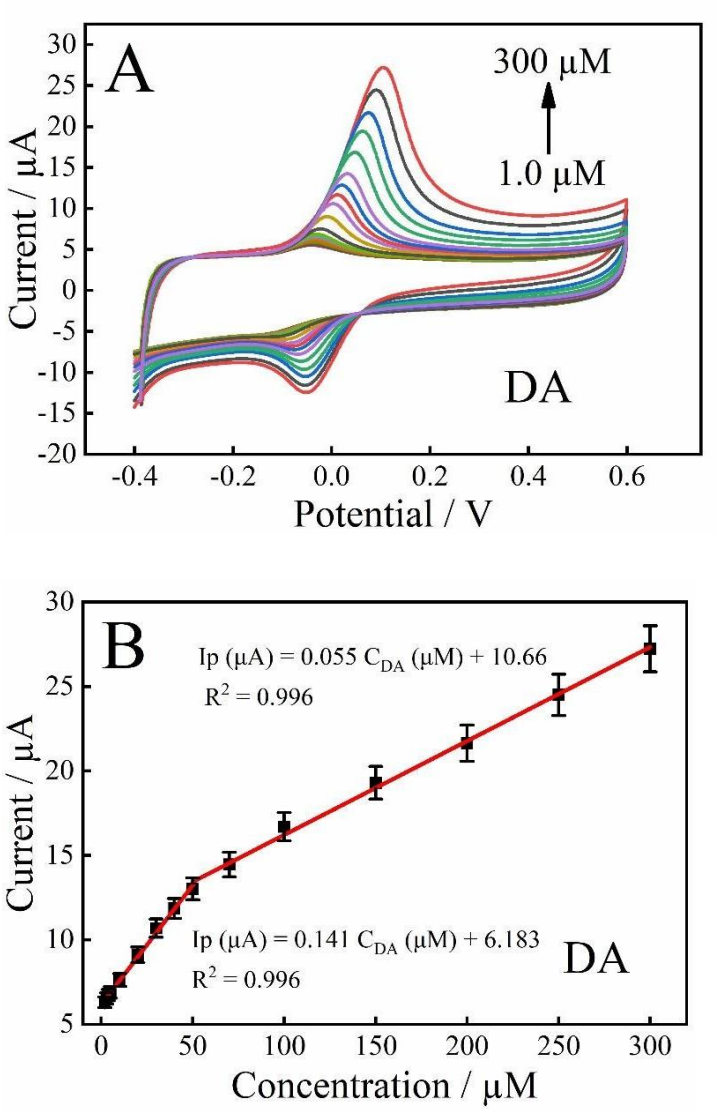

Figure IV.16. CVs of different concentrations of DA at RuNPs/ASPE in 0.1 M PBS, scan rate 50 mVs^{-1}(A), the dependence of Ipa *vs*. Concentration for DA (B)

The limit of detection (LOD) of the sensor for dopamine was estimated to be 0.8 µM and the sensitivity was equal to 1.76 µA μM^{-1} cm^{-2}**.**

The sensor fabricated was also examined for the applicability of electrochemical detection of paracetamol, as revealed in **Figure IV.17A**. It is clear from the results that the presence of paracetamol significantly affects the electrochemical response of the sensor. A successive increase in current density upon stepwise additions of paracetamol was observed up to a concentration of 400 µM. The calibration data revealed two linear dynamic ranges for the sensor response to paracetamol concentrations.

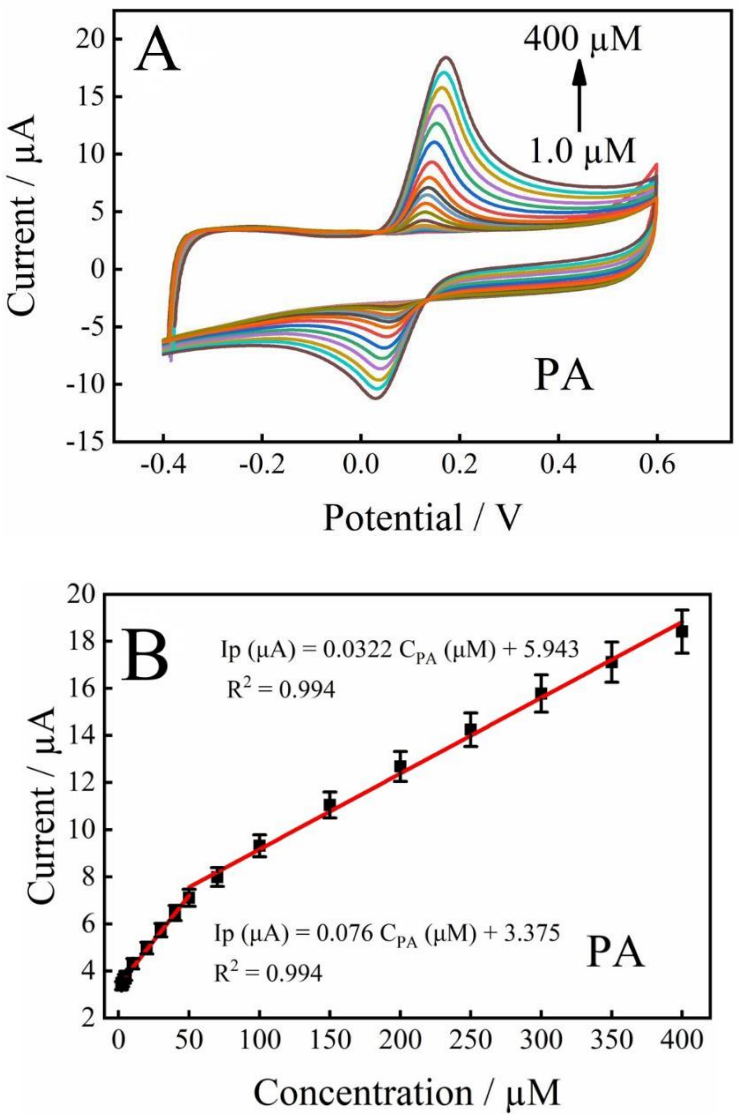

Figure IV.17. CVs of different concentrations of PA at RuNPs/ASPE in 0.1 M PBS, scan rate 50 mVs^{-1}(A), the dependence of Ipa vs. concentration for PA (B).

As shown in (**Figure IV.17B**) :

The first linear range was between 1.0 µM and 50 µM, which is controlled by the regression equation:

$$Ip\ (\mu A) = 0.076\ C_{PA}\ (\mu M) + 3.375,\ (R^2 = 0.994) \qquad \textbf{(IV.10.)}$$

The second linear range was between 50 µM and 400 µM and follows the equation:

$$Ip\ (\mu A) = 0.032\ C_{PA}\ (\mu M) + 5.943,\ (R^2 = 0.994). \quad \textbf{(IV.11.)}$$

Furthermore, the RuNPs/ASPE sensor also displayed a limit of detection of 0.7 µM with a sensitivity of 0.95 µA μM^{-1} cm^{-2}, rendering it amenable for highly selective and sensitive paracetamol detection in aqueous media, also the presence of two linear regions in both DA and PA may be attributed to the adsorption of intermediates **[21].**

In order to detect dopamine in the presence of paracetamol, the electrochemical performance of the RuNPs/ASPE sensor was systematically assessed using square wave voltammetry (SWV) in PBS at various concentrations of dopamine while maintaining a steady concentration of 20 µM for PA **Figure IV.18A**.

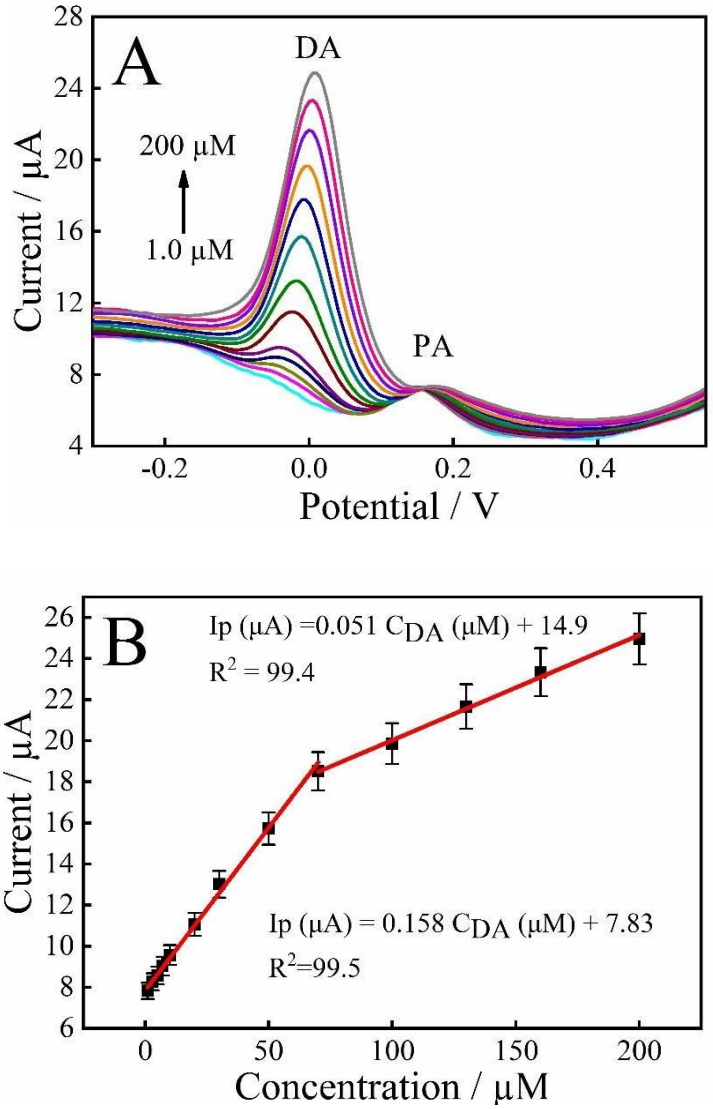

Figure IV.18. SWVs response of various concentrations of DA, at RuNPs/ASPE in 0.1 M PBS, scan rate 50 mVs^{-1}(A), the dependence of Ipa vs. concentration for DA (B).

The findings unequivocally showed that the modified electrode's electrocatalytic activity was effective since the oxidation peak current rose in direct proportion to the increase in dopamine concentration while PA's peak current (RSD = 0.95%) stayed constant. From 1.0 µM to 200 µM, the sensor showed a broad two linear dynamic range (**Figure IV.18B**).

The linear regression equation that described the relationship between the dopamine concentration and the oxidation peak current density in first linear dynamic range from 1.0 to 70 µM was :

$$Ip\ (\mu A) = 0.158\ C_{DA}\ (\mu M) + 7.83,\ R^2 = 0.995 \qquad \textbf{(IV.12.)}$$

The second from 70 to 200 µM :

$$Ip\ (\mu A) = 0.051\ C_{DA}\ (\mu M) + 14.9,\ R^2 = 0.994 \qquad \textbf{(IV.13.)}$$

The sensor exhibited excellent sensitivity of 1.93 $\mu A \cdot \mu M^{-1} \cdot cm^{-2}$ and a calculated limit of detection (LOD) of 0.11 µM, as determined by the standard signal-to-noise criterion (S/N = 3),

On the other hand, DA concentration was set to 20.0 µM in PBS solution while PA concentration was increased **Figure IV.19A**, leading to an increase in the Ipa value while the value of Ip for DA remained constant (RSD = 1.8 %). Two distinct linear response regions were observed, as shown in **Figure IV.19B** :

The first ranged from 1.0 µM to 100 µM, with the slope was calculated according to the linear equation :

$$Ip\ (\mu A) = 0.085\ C_{PA}\ (\mu M) + 4.53,\ (R^2 = 0.991) \qquad \textbf{(IV.14.)}$$

The second extended up to 330 µM, while the linear equation is

$$Ip\ (\mu A) = 0.035\ C_{PA}\ (\mu M) + 8.991,\ (R^2 = 0.997) \qquad \textbf{(IV.15.)}$$

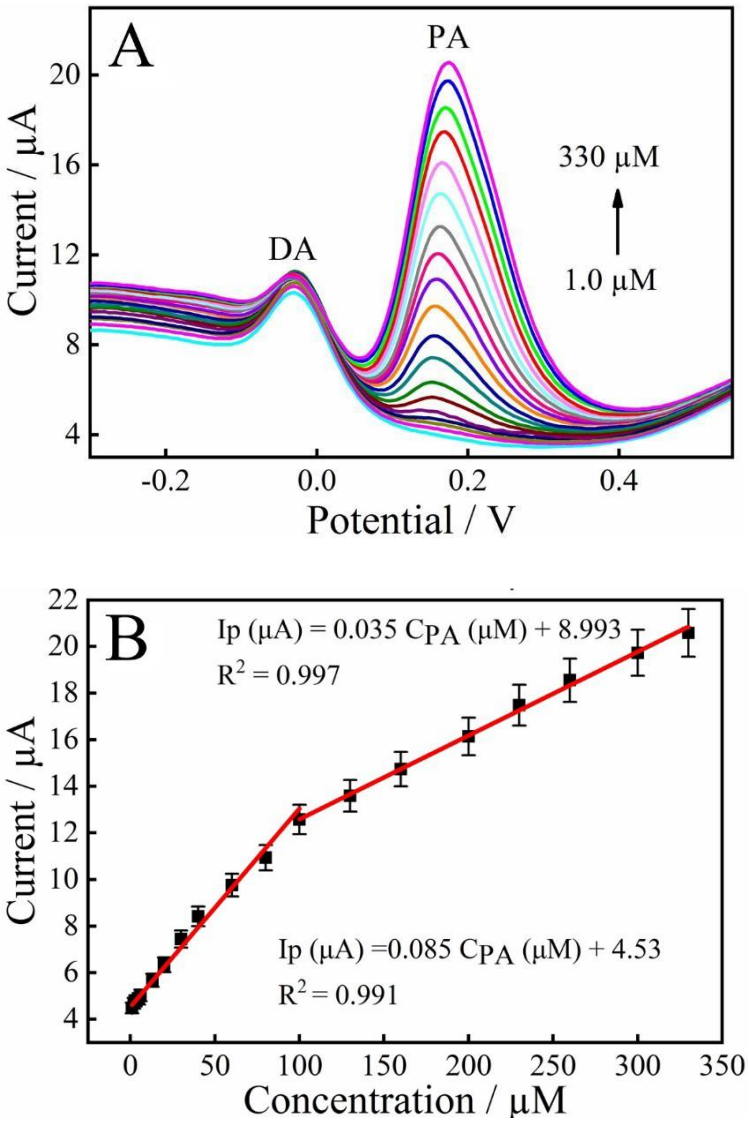

Figure IV.19. SWVs response of various concentrations of PA,at RuNPs/ASPE in 0.1 M PBS, scan rate 50 mVs^{-1}(A), the dependence of Ipa *vs*. concentration for PA (B).

The sensor sensitivity parameter is calculated from the linear part of the calibration curve, the detection limit is calculated according to the signal-to-noise ratio equal to 3 (S/N = 3). The sensitivity value is 1.06 µA $µM^{-1}$ cm^{-2} and the detection limit is equal to 0.17 µM.

These findings support the sensor's potential for accurate and sensitive dopamine and paracetamol quantification by SWV in aqueous media without loss in peak current intensity.

IV.8.2. Simultaneous electrochemical detection of DA and PA with RuNPs/ASPE

CV, as well as SWV,were performed to investigate the RuNPs/ASPE response in the case of simultaneous detection of DA and PA.

The electrochemical behavior of the RuNPs/ASPE electrode was demonstrated by plotting the cyclic voltammetry curves in the presence of dopamine and paracetamol simultaneously. The obtained curves voltammetric presented in **Figure IV.20A**.

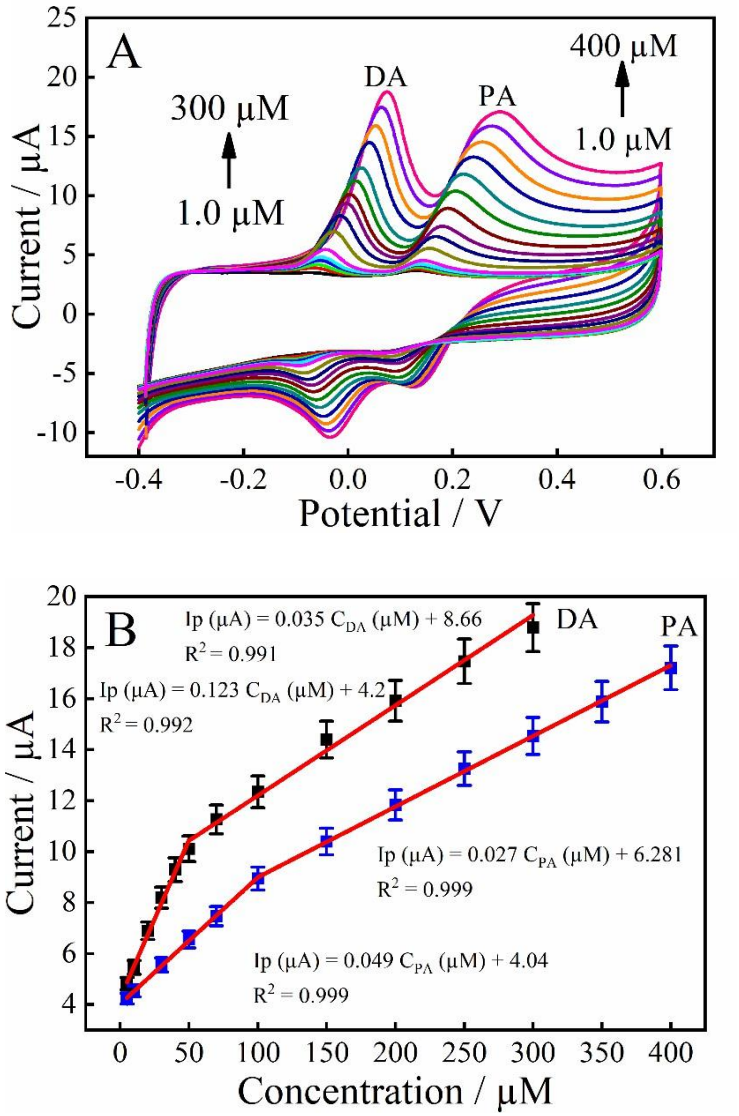

Figure IV.20. RuNPs/ASPE CV curves at different DA (1–300 µM) and PA (1–400 µM) concentrations in 0.1 M PBS (pH 7.4) at a scan rate of 50 mV s^{-1}(A), calibration curves of current *vs.* DA and PA concentrations.

In the range of the applied potential, the curve recorded when both molecules were available shows a rise in anodic current, with two distinct peaks: one at around 0.1V corresponding to dopamine and the other at 0.2V for paracetamol. These results show the enhanced effect of RuNPs on the oxidation of both DA and PA. In addition both oxidation peak

currents increased upon the concentration increase resulting in linear relationships. The linear calibration curve outlined two regions for each analyte (**Figure IV.20B**):

For DA:

From 1.0 to 50 µM and from 50 to 200 µM.

For PA:

From 1.0 to 100 µM and from 100 to 400 µM. The equations of linear regression and the associated correlation coefficients are shown in **Table IV.1**

Table IV.1. Linearity, calibration equations and correlation coefficients for DA and PA.

Target compound	Range of linearity	Calibration equations	Correlation coefficients
DA	1.0–50 µM	Ip (µA) =0.123 C_{DA} (µM) +4.268	R^2 =0.992
	50–200 µM	Ip (µA) =0.035 C_{DA} (µM) +8.666	R^2 = 0.991
PA	1.0–100 µM	Ip (µA) = 0.049 C_{PA} (µM) +4.04	R^2 =0.999
	of 100–400 µM	Ip (µA) =0.027 C_{PA} (µM) +6.282	R^2 = 0.999

For DA, the sensitivity and limits of detection (LODs) were found to be 1.5 µA μM^{-1} cm^{-2} and 1.0 µM for DA respectively, and for PA are 0.61 µA μM^{-1} cm^{-2} and 1.2 µM, respectively.

The square wave voltammograms showed that the peak current of both molecules increased with their concentration (**Figure IV.21A**) and that there is a very good linearity between the concentration and the peak current of the two molecules across two good linear ranges, as shown in **Figure IV.21B**.

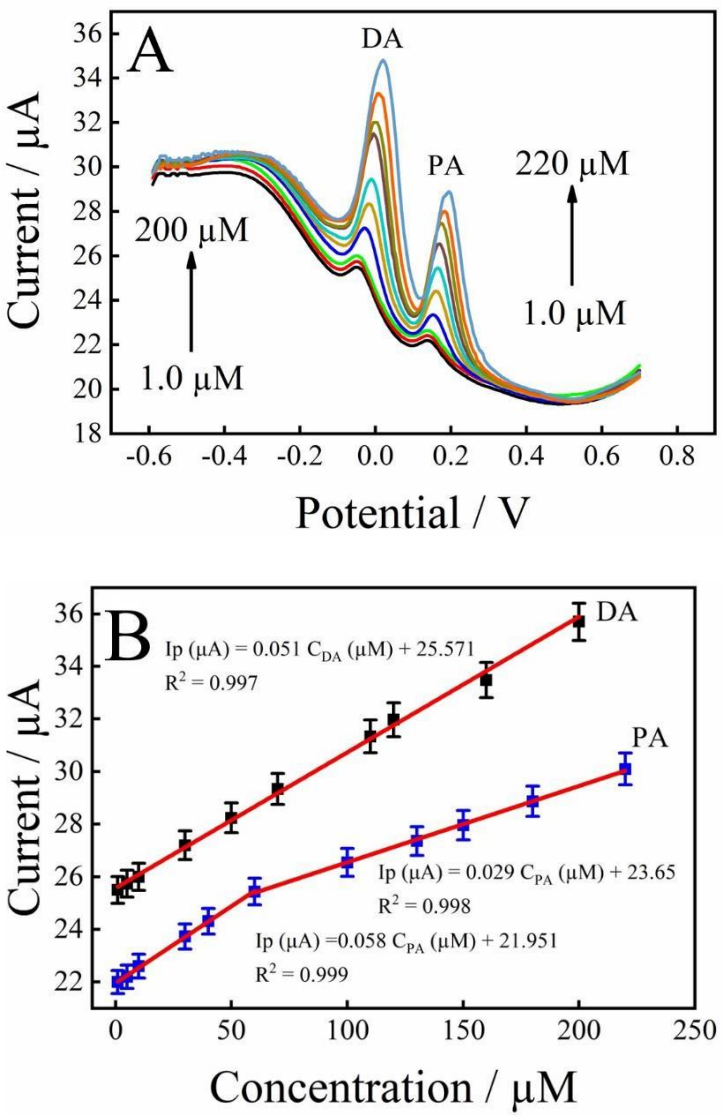

Figure IV.21. SWVs at RuNPs/ASPE at a scan rate of 50 mV s^{-1},with different concentrations of DA (1–200 µM) and PA (1–220 µM) in 0.1 M PBS (pH 7.4) (A). Plots of Ipa *vs.* DA and PA concentration (B).

The corresponding regression equations and range of linearity were gathered in (**Table IV.2**):

Table IV.2. Linearity, calibration equations and correlation coefficients for DA and PA

Target compound	Range of linearity	Calibration equations	Correlation coefficients
DA	1.0–200 µM	Ip (µA) =0.051 C_{DA} (µM) +25.571	R^2 =0.997
PA	1.0–60 µM	Ip (µA) = 0.058 C_{PA} (µM) +21.951	R^2 =0.999
	60–220 µM	Ip (µA) =0.029 C_{PA} (µM) +23.65	R^2 = 0.998

The estimated LODs values for DA and PA were determined as follows: 0.84 µM; and 0.75µM; respectively.The sensitivity were estimated as 0.65 µA μM^{-1} cm^{-2} for DA, and 0.72 µA μM^{-1} cm^{-2} for PA, respectively. Which was in accordance with the previous CV findings.

Table IV.3 illustrates a comparison of the analytical performance of the sensor developed in this study for simultaneous analysis of dopamine and paracetamol with recently published sensors in the literature. The comparison indicates that the sensor presented here has far better sensitivity and broader linear dynamic range compared to those reported systems.

Table IV.3. Comparing the effectiveness of several electrodes for DA and PA detection.

Modified electrode	Method Of detection	Linear range/µM		Detection limit/µM		Ref
		DA	PA	DA	PA	
ZIF-67[a]	DPV	2–45	2–45	1.3	1.4	**[22]**
3DRGO/MWNCTs@ZrFeOx/GCE[b]	DPV	1–180	1–190	0.23	0.212	**[23]**
Fe_2O_3/CPE[c]	DPV	2−170	2−150	0.79	1.16	**[24]**
NiO–CuO/GR/GCE[d]	DPV	0.5−20	4−400	0.17	1.33	**[25]**
3DIPC-IL/CS/GCE[e]	DPV	1–500	1–700	0.13	0.58	**[26]**
$MnFe_2O_4$/GP[f]	DPV	5–200	3–160	0.4	0.3	**[27]**
$CoFe_2O_4$/GP[g]	DPV	3–180	3–200	0.35	0.25	
f-MWCNTs/GCE[h]	DPV	3–200	3–300	0.8	0.6	**[28]**
CB-PAH/GCE[i]	LSV	1–22	2.4–27	0.55	1.3	**[29]**
GCE/ Cu^{2+}@PDA-MWCNTs[j]	DPV	4–125	5–75	0.87	0.92	**[30]**
RuNPs/ASPE	CV	1–300	1–400	0.8	0.7	**This work**
	SWV	1–200	1–330	0.11	0.17	

[a] ZIF-67: Zeolitic imidazolate framework – 67.

[b] 3D: three-dimensional structure; RGO: reduced graphene oxide; MWNCTs: multi-walled carbon nanotubes; ZrFeOx: bimetallic-organic gel; GCE: glassy carbon electrode.

[c] Fe_2O_3: iron oxide nanoparticle; CPE: carbon paste electrode.

[d] NiO: nickel oxide nanoparticles; CuO: copper oxide nanoparticles; GR: graphene.

[e] 3DIPC-IL: three-dimensional interconnected porous carbon-ionic liquid;CS: chitosan.

[f] $MnFe_2O_4$: manganese ferrite; GP: graphite.

[g] $CoFe_2O_4$: cobalt ferrite.

[h] f-MWCNTs: acid functionalized multi-wall carbon nanotubes.

[i] CB: carbon black; PAH: poly (allylamine hydrochloride) film.

[j] Cu^{2+} : copper; PDA polydopamine complex.

IV.9. Reproducibility, repeatability and stability effect

IV.9.1. Repeatability

The repeatability of the proposed RuNPs/ASPE modified electrode under these conditions was studied using SWV. Relative standard deviations (RSDs) ranged between 0.85% and 1.12% were obtained for five consecutive determinations of 100 µM dopamine and paracetamol, respectively. These results indicated that the elaborated RuNPs/ASPE exhibited excellent repeatability and was not susceptible to surface alteration by oxidation products.

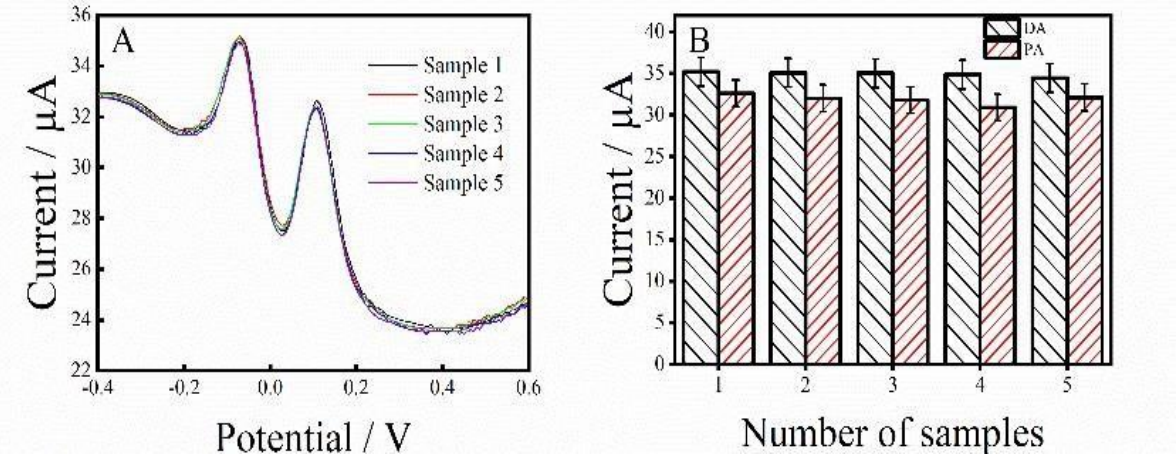

Figure IV.22. (A, B) Repeatability of RuNPs/ASPE sensor in the mixture of 100 µM DA and 100 µM PA.

IV.9.2. Reproducibility

The reproducibility of the RuNPs/ASPE signal was evaluated by detecting 100 µM DA and 100 µM PA in 0.1 M PBS using five separately prepared electrodes, the relative standard deviation (RSD) of the current response toward the detection of 100 µM DA was approximately 1.94 %. The RSD of the five different electrodes was approximated at 2.58 % for PA. These findings indicate good reproducibility of sensor response.

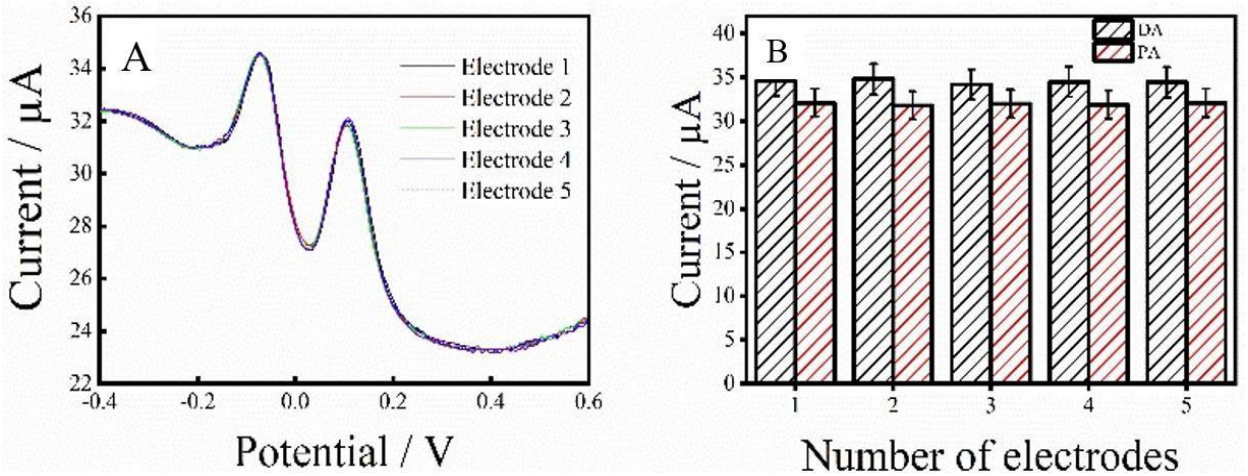

Figure IV.23. (A, B) reproducibility of RuNPs/ASPE sensor in the mixture of 100 µM DA and 100 µM PA.

IV.9.3. Stability

The stability of RuNPs/ASPE sensor was also tested, and this is revealed in (**Figure IV.24**). The sensor was stable, retaining 91% of its initial oxidation current response for both analytes. In addition, the RuNPs/ASPE sensor experienced merely a minor drop in current, revealing that the surface modification does provide a suitable platform for the dual detection of dopamine and paracetamol. The high stability of the sensor is largely attributed to the activation of the graphite substrate along with the presence of ruthenium based nanoparticles.

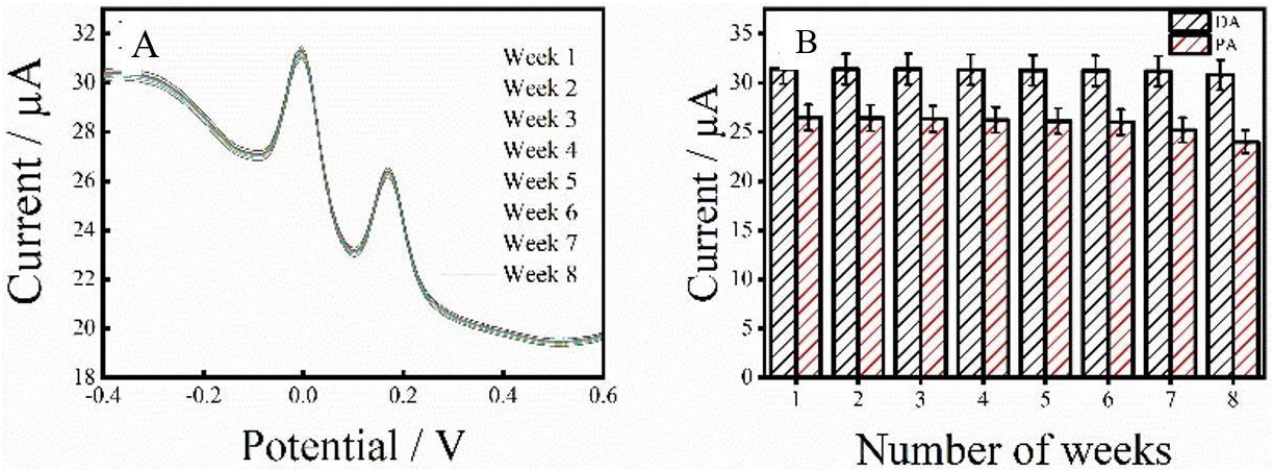

Figure IV.24. Stability of RuNPs/ASPE in the mixture of DA (100 µM) and PA (100 µM) (A, B).

IV.10. Interference studies

For assessing the selectivity of the RuNPs/ASPE towards the simultaneous determination of DA and PA, the SWV measurements were conducted in the presence of higher concentration of other interfering substances like ascorbic acid (AA) and uric acid (UA). Because of their comparable structures and near oxidation potentials, uric acid and ascorbic acid could produce interference with the electrochemical determination of paracetamol and dopamine, especially in biological fluids where these compounds are co-existent together, thereby hindering their selective and precise determination.

The DA (100 µM) and PA (100 µM) selectivity of the sensor was conducted in the presence of AA (500 µM) and UA (500 µM) in a 0.1 M PBS buffer solution. As one can observe from the **Figure IV.25**, the presence of ascorbic acid (AA) and uric acid (UA) in the solution of dopamine (DA) and paracetamol (PA) results in a positive shift of the oxidation peak potentials of DA and PA. Indeed, the figure clearly shows four distinct peaks, one corresponding to each compound present in the solution. The first peak, observed at -0.26 V, is attributed to AA, the peak for DA appears at 0.01 V; the peak for PA appears at 0.20 V and the last peak for UA appears at 0.52 V, respectively. This observation signify that the RuNPs/ASPE sensor is found to be highly selective towards AA and UA.

Also, unlike in a previous studies where UA oxidation peak is between DA and PA peaks, almost equal to that of paracetamol, RuNPs/ASPE electrode shows UA oxidation peak after the PA oxidation peak **[23].** This finding shows the high selectivity of the elaborated sensor is in the detection of DA and PA with the presence of AA and UA.

Common interferents, commonly found along with DA and PA in human blood serum or in drug preparations (with the exception of AA and UA), were investigated using square wave voltammetry. Specifically, known concentrations of significant organic interferents such as glucose, caffeine, sucrose, fructose and inorganic species NaCl, $CaCO_3$, and KNO_3 were separately added to an analytical solution made of 20 mM DA and 20 mM PA. As shown in (**Figure IV.26**), minimal variation of the peak current for all analytes was observed. These results are an explicit evidence that the RuNPs/ASPE possesses excellent selectivity and high anti-interference capability.

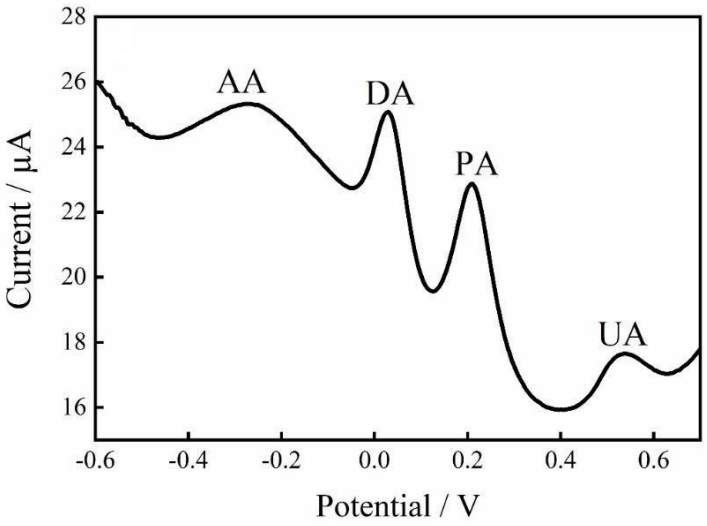

Figure IV.25. RuNPs/ASPE sensor interference with 100 µm DA, 100 µm PA, 500 µm AA, and 500 µm UA.

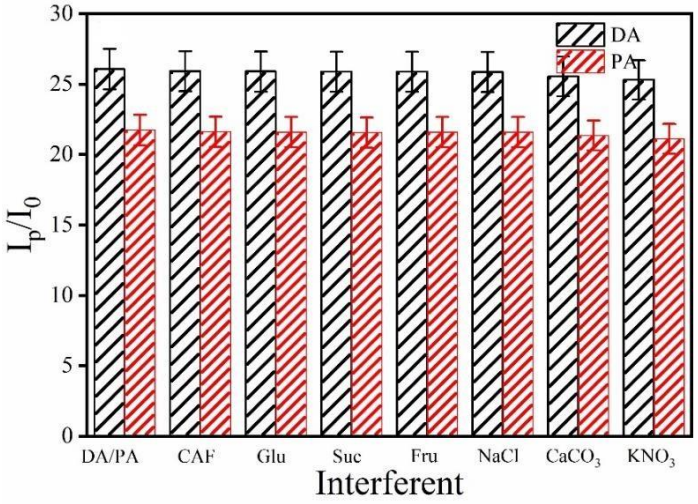

Figure IV.26. Peak current (Ip) bar diagram for DA and PA concentrations with and without interferrent minerals and biomolecules.

IV.11. Feasibility assessment in pharmaceutical and blood samples

IV.11.1.Evaluation of applicability in pharmaceutical analysis

By examining identical concentrations of PA and DA in commercial pharmaceutical samples, such as injectable dopamine solutions (40 mg/mL) and paracetamol tablets (1000 mg/tablet), as well as in standard buffer solutions, the viability of the RuNPs/ASPE was further evaluated, the SWV approach was used to conduct measurements in ideal conditions. Section III.4.2.4 provides a detailed description of the sample pretreatment procedure.

Figure IV.27.A and **B** show that the RuNPs/ASPE exhibits a current response for injectable dopamine solutions and paracetamol tablets that is close to that of the standard sample, indicating that this electrode can be used as a sensor for the detection of these molecules in real samples.

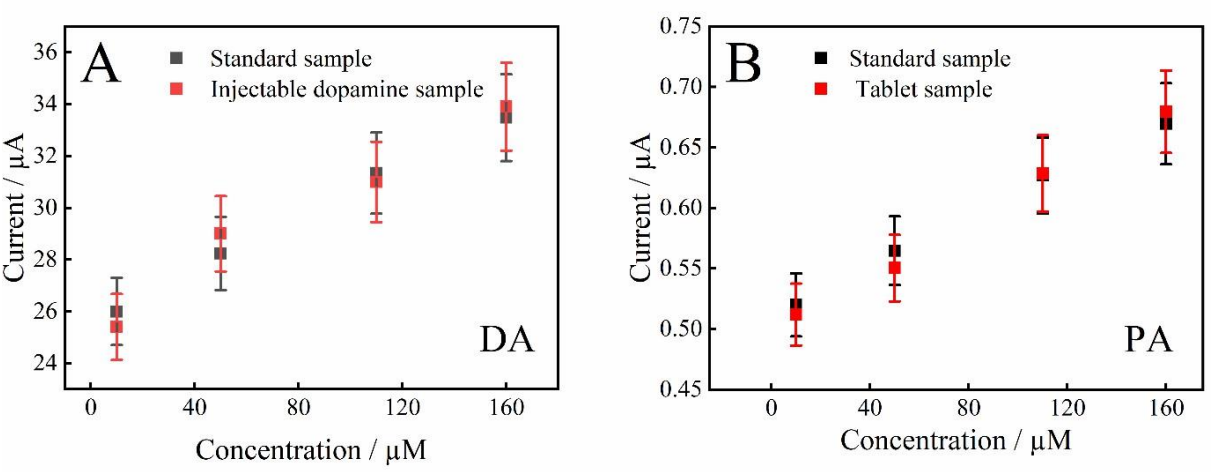

Figure IV.27. In contrast to standard solutions, sensor responses were obtained for the same analyte concentrations in injectable dopamine samples (A) and tablet samples (B).

Using the standard addition method and square wave voltammetry under optimized experimental conditions, the practical applicability of the RuNPs/ASPE sensor was proved by precisely determining the concentrations of various analytes in pharmaceutical tablets.

The experimental results, meticulously summarized and presented in table IV.4, demonstrated a good agreement of concordance with the manufacturer's pre-established target contents. Specifically, the obtained recovery rates, which spanned from 98.02% to 103.84%, underscore the high accuracy and efficiency of the analytical method employed.Furthermore, the relative standard deviation values, determined from triplicate parallel measurements for each sample, consistently fell below 3.26 %. Significantly, excipients present in tablet formulations did not exhibit interference with the detection of analytes in commercially available samples. Consequently, these results validate the reliability and accuracy of the developed RuNPs/ASPE sensor for the quantitative determination of DA and PA within pharmaceutical matrices.

Table IV.4. Quantification of DA and PA using RuNPs/ASPE in dopamine hydrochloride injections and pharmaceutical tablets (n = 3).

Pharmaceutical preparation	Sample	Reported values		Determined		Recovery (%)		RSD (%)	
		DA	PA	DA	PA	DA	PA	DA	PA
Dopamine hydrochloride injection (mg/ml)	1	20	–	20.76±0.17	ND	103.84	–	1.58	–
	2	40	–	40.66±0.64	ND	101.65	–	1.34	–
Paracetamol tablet (mg)	1	–	500	ND	490.1±84		98.02	–	2.04
	2	–	1000	ND	992.9±0.76		99.29	–	3.26

IV.11.2.Evaluation of applicability in blood serum samples

To evaluate its commercial applicability and accuracy, the developed RuNPs/ASPE sensor was also applied to the detection of dopamine and paracetamol in human blood serum samples. By following the same experimental protocol and working under the same conditions, for the purposes of analysis, human blood samples were individually supplemented with dopamine at concentrations of 2.0 and 4.0 µM, and paracetamol at 50 and 100 µM.

As can be observed in **Table IV.5**, recovery of the modified RuNPs/ASPE sensor was in the range of 97.37% to 102.27% for co-detection of dopamine and paracetamol, exhibiting excellent correlation with the theoretical values. Further, the relative standard deviation of all of these measurements was comfortably within 3%, thus demonstrating the high precision and good repeatability of the technique. These results cumulatively highlight the excellent analytical performance of the modified sensor, especially in terms of its accuracy, reproducibility, and reliability. The ability of the sensor to maintain.

Table IV.5. Quantitative analysis of DA and PA mixtures in human serum samples (n = 3).

Sample	Analyte (µM)				Recovery (%)		RSD(%)	
	Added		Found					
	DA	PA	DA	PA	DA	PA	DA	PA
Serum 1	–	–	0.97±0.48	21.6±0.22	–	–	1.45	1.63
Serum 2	2	50	3.05±0.83	72.54±0.45	97.37	98.71	1.89	2.01
Serum 3	4	100	5.07±0.71	118.9±0.68	98.02	102.27	2.1	2.98

Conclusion

A novel electrochemical sensor has been developed for the determination of DA and PA using a very simple, fast and cost-effective electrodeposition method of ruthenium nanoparticles on the activated surface of graphitic screen printed electrodes. The main methods applied for characterization were field emission scanning electron microscopy (FE-SEM), energy dispersive spectroscopy (EDX), X-ray diffraction (XRD), transmission electron microscopy (TEM), atomic force microscopy (AFM) and Fourier-transform infrared spectroscopy (FTIR) for monitoring the process of elaboration and modification of SPE.These methods provided rich and relevant information on the structure, morphology, topography, and crystallography of the modified electrode.

The modified electrode displayed an excellent electrocatalytic activity and a large active surface. Moreover, the developed sensor gave excellent results in individual and simultaneous electrocatalytic detection of dopamine and paracetamol using both CV and SWV techniques with an extensive linear concentration ranges and low detection limits.

Furthermore, the RuNPs/ASPE showed a good repeatability, excellent reproducibility, strong anti-interference and high stability. Furthermore, the sensor was successfully applied for the quantification of dopamine in injections, paracetamol in pharmaceutical tablets and for the simultaneous measurement of dopamine and paracetamol in human serum samples.

References

[1] B. Łosiewicz, M. Martin, C. Lebouin, A. Lasia, Kinetics of hydrogen underpotential depositon at ruthenium in acidic solutions, J. Electroanal. Chem. 649 (2010) 198–205.

[2] V.B. Saptal, T. Sasaki, B.M. Bhanage, Ru@PsIL-catalyzed synthesis of N-formamides and benzimidazole by using carbon dioxide and dimethylamine borane, ChemCatChem 9 (2017) 1188–1193.

[3] P. Hao, P. Song, Z. Yang, Q. Wang, Synthesis of novel $RuO_2/LaFeO_3$ porous microspheres and its gas sensing performances towards triethylamine, J. Alloys Compd. 806 (2019) 960–967.

[4] H. Xiong, Y. Zhang, S. Wang, K. Liew and J. Li,Preparation and catalytic activity for Fischer−Tropschsynthesis of Ru Nanoparticles confined in the channels of mesoporous SBA-15, The Journal of Physical Chemistry C, 112 (2008) 9706.

[5] H. Li, R. Wang, Q. Hong, L. Chen, Z. Zhong, Y. Koltypin,J. Calderon-Moreno and A. Gedanken,Ultrasound-assisted polyol method for the preparation of SBA-15 supported ruthenium nanoparticles and the study of their catalytic activity on the partial oxidation of methane, Langmuir, 20 (2004) 8352.

[6] S. Hazra, H. Joshi, B.K. Ghosh, A. Ahmed, T. Gibson, P. Millner and N.N. Ghosh,Development of a novel and efficient H2O2 sensor by simple modification of a screen printed Au electrode with Ru nanoparticle loaded functionalized mesoporous SBA15, RSC Advances, 5 (2015) 34390.

[7] M. Fernández Cervera, J. Heinämäki, M. Räsänen, S.L. Maunu, M. Karjalainen, O.M. Nieto Acosta, A. Iraizoz Colarte, J. Yliruusi, Solid-state characterization of chitosans derived from lobster chitin, Carbohydr. Polym. 58 (2004) 401–408.

[8] W.S. Cardoso, V.L.N. Dias, W.M. Costa, I. de Araujo Rodrigues, E.P. Marques, A.G. Sousa, J. Boaventura, C.W.B. Bezerra, C. Song, H. Liu, J. Zhang, A.L.B. Marques, Nickel-dimethylglyoxime complex modified graphite and carbon paste electrodes: preparation and catalytic activity towards methanol/ethanol oxidation, J. Appl. Electrochem. 39 (2009) 55–64

[9] C. Potvin, J.M. Manoli, A. Dereigne, G. Pannetier, Complexes oléfiniques du ruthénium: II. Préparation et propriétés physico-chimiques du bis-(acetyl-acetonato) norbornadiène ruthénium, Journal of the Less Common Metals 25 (1971) 373–378.

[10] J.S. Jeng, Y.T. Lin, J.S. Chen, Preparation and characterization of transparent semiconductor RuO_2–SiO_2 films synthesized by sol–gel route, Thin Solid Films 518 (2010) 5416–5420.

[11] A.G.M. Ferrari, C.W. Foster, P.J. Kelly, D.A.C. Brownson, C.E. Banks, Determination of the electrochemical area of screen-printed electrochemical sensing platforms, Biosensors 8 (2018) 53–63.

[12] A. Jirasirichote, E. Punrat, A. Suea-Ngam, O. Chailapakul, S. Chuanuwatanakul, Voltammetric detection of carbofuran determination using screen-printed carbon electrodes modified with gold nanoparticles and graphene oxide, Talanta 175 (2017) 331–337.

[13] M.L. Chelaghmia, M. Nacef, A.M. Affoune, Ethanol electrooxidation on activated graphite supported platinum–nickel in alkaline medium, J. Appl. Electrochem. 42 (2012) 819–826.

[14] X. Kang, Y. Song, J. Zhao, Y. Li, Simultaneous determination of paracetamol and dopamine, and detection of bisphenol A using three-dimensional interconnected porous carbon functionalized with ionic liquid, J. Electroanal. Chem. 895 (2021) 115482.

[15] T. Kokab, A. Shah, M.A. Khan, M. Arshad, J. Nisar, M.N. Ashiq, M.A. Zia, Simultaneous femtomolar detection of paracetamol, diclofenac, and orphenadrine using a carbon

nanotube/zinc oxide nanoparticle-based electrochemical sensor, ACS Appl. Nano Mater. 5 (2021) 4699–4712.

[16] M.R. Majidi, M.H. Pournaghi-Azar, R.F. Bajeh Baj, Graphene nanoplatelets like structures formed on ionic liquid modified carbon-ceramic electrode: As a sensing platform for simultaneous determination of dopamine and acetaminophen, J. Mol. Liq. 220 (2016) 778–787.

[17] M. Achache, G.E. Idrissi, N. Ben Seddik, S. El Boumlasy, I. Kouda, I. Raissouni, F. Chaouket, K. Draoui, D. Bouchta, M. Choukairi, Innovative use of shrimp shell powder in carbon paste electrode for the electrochemical detection of dopamine and paracetamol: valorization, characterization and application, Microchem. J. 202 (2024) 110754.

[18] J. Tang, Y. Liu, J. Hu, S. Zheng, Co-based metal-organic framework nanopinnas composite doped with Ag nanoparticles: A sensitive electrochemical sensing platform for simultaneous determination of dopamine and acetaminophen, Microchem. J. 155 (2020) 104759**.**

[19] B. Ranjani, J. Kalaiyarasi, D.M. Soundari, K. Pandian, S.C.B. Gopinath, Synthesis of novel nanostructured copper tungstate/GCE electrochemical system in deep eutectic solvent medium for simultaneous detection of dopamine and paracetamol, Inorg. Chem. Commun. 145 (2022) 109879.

[20] X. Liu, E. Shangguan, J. Li, S. Ning, L. Guo, Q. Li, A novel electrochemical sensor based on FeS anchored reduced graphene oxide nanosheets for simultaneous determination of dopamine and acetaminophen, Mater. Sci. Eng. C 70 (2017) 628–636.

[21] M.L. Chelaghmia, H. Fisli, M. Nacef, D.A.C. Brownson, A.M. Affoune, H. Satha, C. E. Banks, Disposable non-enzymatic electrochemical glucose sensors based on screen-printed graphite macroelectrodes modified via a facile methodology with Ni, Cu, and Ni/Cu hydroxides are shown to accurately determine glucose in real human serum blood samples, Anal. Methods 25 (2021) 2812–2822.

[22] N.T.T. Tu, P.C. Sy, T.V. Thien, et al., Microwave-assisted synthesis and simultaneous electrochemical determination of dopamine and paracetamol using ZIF-67-modified electrode, J. Mater. Sci. 54 (2019) 11654–11670.

[23] A. Xie, H. Wang, J. Lin, J. Pan, M. Li, J. Wang, S. Jiang, S. Luo, 3D RGO/MWCNTs-loaded bimetallic-organic gel derived ZrFeOx as an electrochemical sensor for simultaneous detection of dopamine and paracetamol, J. Alloy. Compd. 938 (2023) 168647.

[24] M.M. Vinay, Y. Arthoba Nayaka, Iron oxide (Fe 2 O 3) nanoparticles modified carbon paste electrode as an advanced material for electrochemical investigation of paracetamol and dopamine, J. Sci. -Adv. Mater. Dev. 4 (2019) 442–450.

[25] B.D. Liu, X.Q. Ouyang, Y.P. Ding, et al., Electrochemical preparation of nickel and copper oxides decorated graphene composite for simultaneous determination of dopamine, acetaminophen and tryptophan, Talanta 146 (2016) 114–121.

[26] X. Kang, Y. Song, J. Zhao, Y. Li, Simultaneous determination of paracetamol and dopamine, and detection of bisphenol a using three-dimensional interconnected porous carbon functionalized with ionic liquid, J. Electroanal. Chem. 895 (2021) 115482.

[27] Y. Kumar, P. Pramanik, D.K. Das, Electrochemical detection of paracetamol and dopamine molecules using nano-particles of cobalt ferrite and manganese ferrite modified with graphite, Heliyon 5 (2019) e02031.

[28] Z.A. Alothman, N. Bukhari, S.M. Wabaidur, S. Haider, Simultaneous electrochemical determination of dopamine and acetaminophen using multiwall carbon nanotubes modified glassy carbon electrode, Sens. Actuat. B Chem. 146 (2010) 314–320.

[29] J. Scremin, G.J. Mattos, R.D. Crapnell, S.J. Rowley-Neale, C.E. Banks, E.R. Sartori, Glassy carbon electrode modified with layering of carbon black/poly(allylamine hydrochloride) composite for multianalyte determination, Electroanalysis 33 (2021) 526–536.

[30] M. Shahbakhsh, M. Noroozifar, Copper polydopamine complex/multiwalled carbon nanotubes as novel modifier for simultaneous electrochemical determination of ascorbic acid, dopamine, acetaminophen, nitrite and xanthine, J. Solid State Electrochem. 22 (2018) 3049–3057.

Part B

Impedimetric detection of dopamine and paracetamol

IV.1. Introduction

Electrochemical impedance spectroscopy (EIS) is a powerful and informative technique. **[1]** Recently, it became much more attractive than other electrochemical methods **[2,3]** due to its remarkably strong operability, excellent selectivity, and enhanced sensitivity **[4].** In a preliminary research, *Boumya et al.* employed azo coupling reaction with oxidized 2,4-dinitrophenylhydrazine (DNPH) as a new method for DA and PA sensing using the EIS **[5].**

Herein and for the first time, an impedimetric sensor was elaborated by the modification of activated screen printed graphite electrode using ruthenium nanoparticules for the quantification of dopamine and paracetamol.

The principal objective in this part is to study the sensors' responses to obtain complete knowledge of impedance changes in the analyte detection and to appraise the analytical performance of the RuNPs/ASPE electrode.

IV.2. Electrochemical impedance spectroscopy analysis of the RuNPs/ASPE

Electrochemical impedance spectroscopy was performed to evaluate the electrocatalytic performance of the modified SPEs at the frequency range from 100 kHz to 0.1 Hz with an amplitude of 10 mV. Data analysis and fitting was performed using EC-Lab software.

Electrochemical impedance spectroscopy was implemented to examine the charge transfer characteristics. To simplify the analysis of the impedance data, Randles equivalent circuit model was employed as shown in **Figure IV.1** including a charge transfer resistance (Rp) which is the resistance between the redox probe and the electrode surface, (Rs) electrolyte solution resistance, (Zw) Warburg impedance and (C_{PE}) constant phase element **[6].**

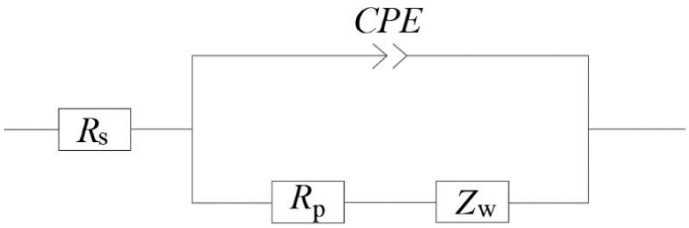

Figure IV.1. Equivalent circuit based on the Randles model

Figure IV.2 shows the typical Nyquist spectra of bare SPE, ASPE and RuNPs/ASPE, in the frequency range from 100 kHz to 0.1 Hz. Spectra comprise a linear part at lower frequencies corresponding to the diffusion process while the semicircle impedance response at higher frequencies corresponds to the charge transfer resistance.

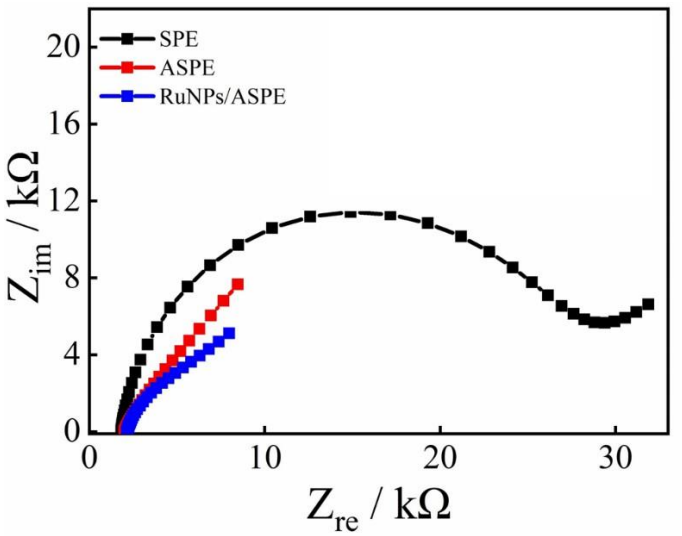

Figure IV.2. Nyquist plots of 1.0 mM $F(CN)_6^{3-/4-}$in 0.1 M KCl at unmodified SPE; ASPE and RuNPs/ASPE.

The charge transfer resistance values estimated by the Randles equivalent electrical circuit fitting are illustrated in **table IV.1**.

Table IV.1. The Randles equivalent electrical circuit fitting

Electrode	**Charge transfer resistance**	**Fits**	**Color**
SPE	25.1 KΩ	(χ2 =0.044)	black
ASPE	11.8 KΩ	(χ2 = 0.046)	red
RuNPs/ASPE	3.14 KΩ	(χ2 =0.044)	blue

The outcome appearing in (**Table IV.1**) reveals that the RuNPs/ASPE sensor has the lowest charge transfer resistance. This is indicated graphically by a smaller semicircle in the corresponding Nyquist plot, which is a direct measure of an improved electron transfer mechanism at the electrode interface. This enhanced electron mobility thus testifies to the improved electrochemical conductivity and catalytic performance of RuNPs/ASPE compared

to the other materials evaluated in this study.This result is consistent with the above cyclic voltammetry results.

IV.3. Electrochemical impedimetric detection of DA and PA on RuNPs/ASPE

The new RuNPs/ASPE electrode's electrochemical characteristics were described using electrochemical impedance spectroscopy. With an amplitude of 10 mV, the impedance spectra were acquired throughout a frequency range of 100 kHz to 0.1 Hz. The ideal working potentials for paracetamol and dopamine were found to be +0.2 V and +0.1 V, respectively. Fitting and data analysis were done using EC-Lab software.

IV.3.1. The representation of Nyquist diagrams

Dopamine and paracetamol concentrations increase is depicted by a change in the Nyquist plots illustrated by a gradual decrease in impedance values. This is seemingly due to a reduced charge transfer resistance which is attributed to the chemical reaction of DA or PA on the high-valence Ru species along with the higher quantity of electroactive molecules present on the electrode surface [7-9]. Both DA and PA are capable of participating in sequential redox reactions, releasing two protons and two electrons ($2H^{+}/2e^{-}$). This process enables electron transfer between the electrode and the target molecules, a phenomenon also observed in the work of *M. Emadoddin et al* [10]. To the best of our knowledge, a limited number of reports have utilized EIS analysis for dopamine or paracetamol detection [5].

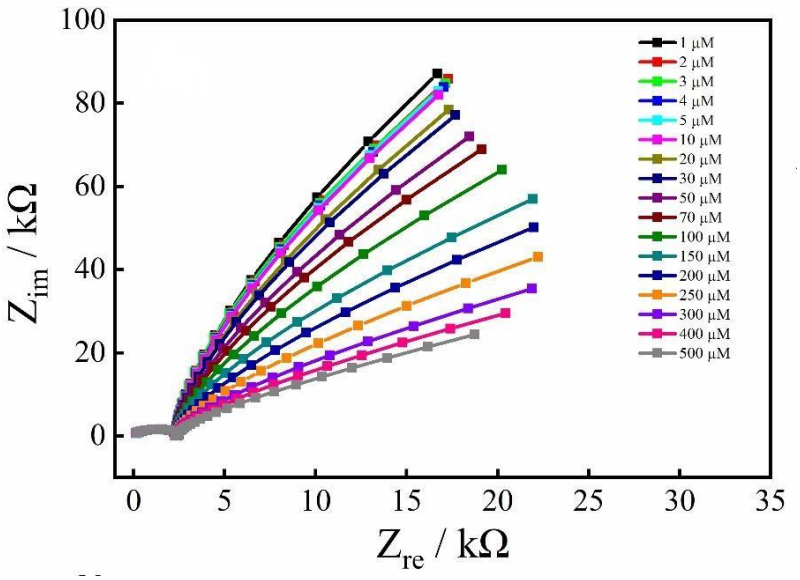

Figure IV.3. Influence of dopamine concentration in the range of 1–500 µM on the response of the RuNPs/ASPE impedimetric sensor.

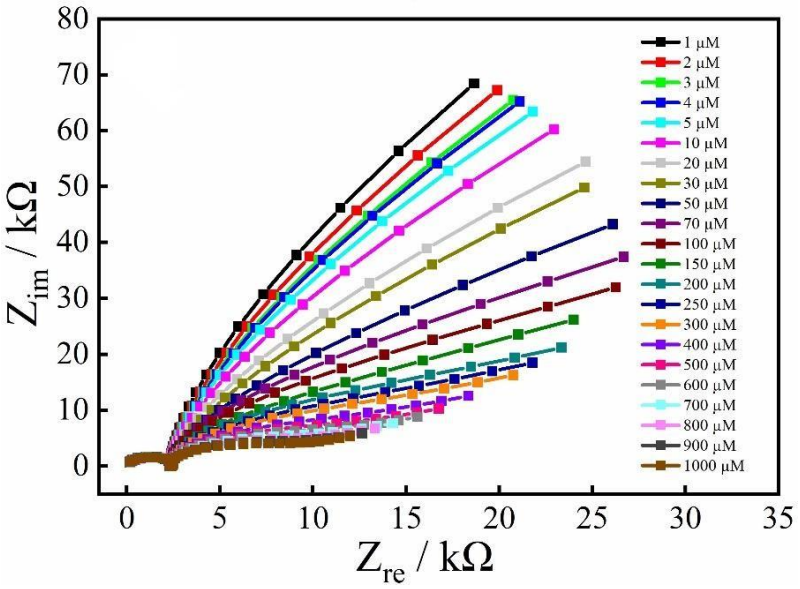

Figure IV.4. Influence of paracetamol concentration in the range of 1–1000 µM on the response of the RuNPs/ASPE impedimetric sensor.

Fitting the EIS results

In order to understand the surface phenomena between dopamine , as well as paracetamol and the electrode material, the obtained EIS spectra were analyzed by building the corresponding equivalent circuit shown in (**Figure IV.5**).The fitting was performed using EC Lab analysis software, resulting in good fits ($\chi^2=10^{-2}$). The electrical circuit can be divided into several components:

i. The ohmic resistance of the electrolyte solution is represented by R_1 in the equivalent circuit of the RuNPs/ASPE

ii. C_1 indicated the rated capacitance that represents the distribution of charge in the frequency domain, which is associated with the slow adsorption mechanism [11,12] and the electrode surface morphology [13,14]

iii. Q_2 defined the constant phase element

iv. The double-layer capacitance C_3 was connected in parallel with the charge-transfer resistance R_4

v. The Warburg impedance (W_4) represents the diffusion of the molecules from the bulk electrolyte to the electrode interface and is associated with the charge-transfer resistance and the double-layer capacitance [15].

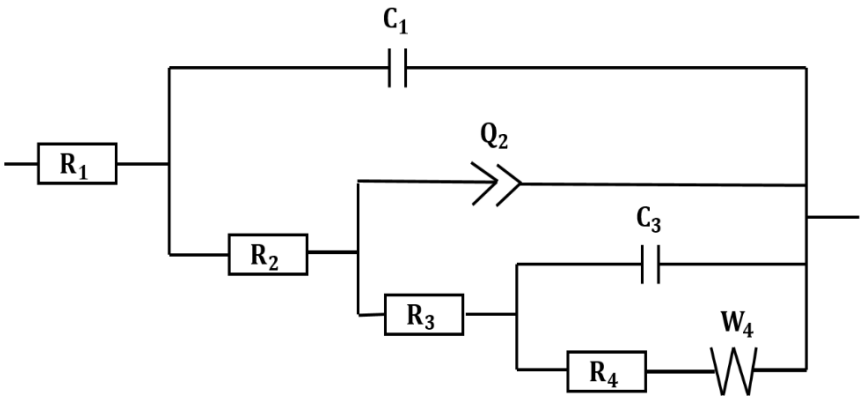

Figure IV.5. Equivalent circuit model.

IV.3.2. The representation of Bode diagrams

The initial analysis of the impedance spectra, presented in the Bode representation, reveals a notable pattern. The magnitude of the impedance variations induced by the individual addition of the two molecular species is significantly more pronounced at lower frequencies **Figure IV.6A** and **B**.

Conversely, the modulus of the impedance at higher frequencies remains largely unaffected by variation in molar concentration. However, at frequencies below 1 Hz, a distinct divergence in the impedance moduli becomes clearly apparent, indicating a concentration dependent effect.

Further investigation demonstrated a direct correlation between the inverse impedance modulus and amounts of the species present in the solution, specifically, an increase in molecular concentration leads to a decrease in the impedance. This observation is consistent with the principle that higher concentrations of charge carriers or intervening species typically result in lower overall resistance or impedance in an electrochemical system.

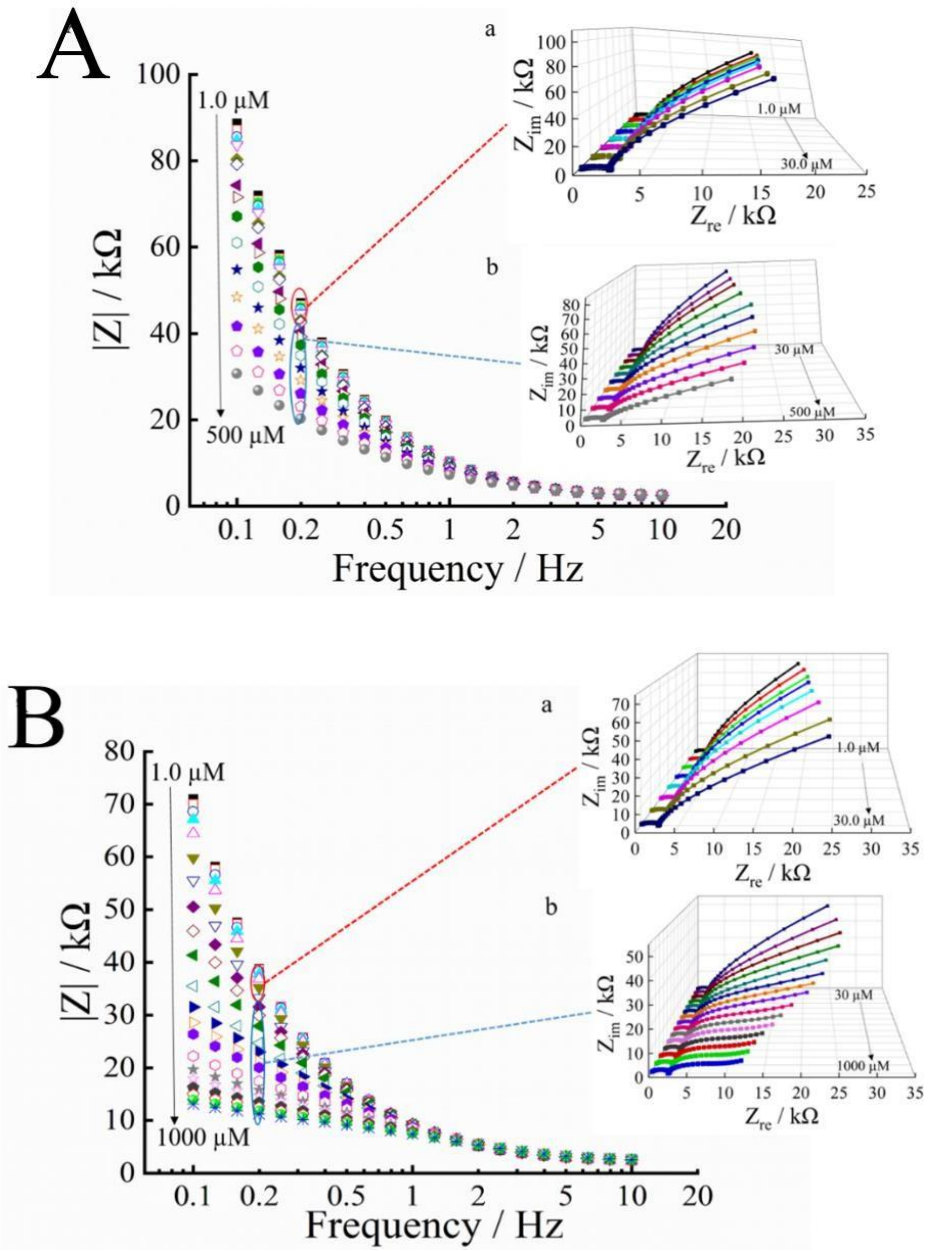

Figure IV.6. Bode plots achieved for different concentrations of DA from 1.0 µM to 500 µM (A) PA from 1.0 µM to 1000 µM at RuNPs/ASPE electrode; insets show the related Nyquist plots.

IV.3.3. Calibration curve and analytical characteristics

In this way, the variation of 1/|Z| as a function of DA and PA concentrations was analyzed at frequency of 0.2 Hz for DA and PA frequency, as shown in **Figure IV.7** and **Figure IV.8**, respectively.

The calibration plot showed excellent linearity from 1 µM to 500 µM, with a correlation coefficient $R^2 = 0.998$ according to the following linear regression equation for DA:

$$1/|Z|\ (kohm^{-1}) = 5.4\ E\text{-}5\ C_{DA}\ (\mu M) + 0.02\ (R^2 = 0.993) \quad \textbf{(IV.1.)}$$

Whereas, calibration curves for PA showed two segments**:**

From 1 µM to 150 µM:

$$1/|Z|\ (kohm^{-1}) = 5.695\ E\text{-}5\ C_{PA}\ (\mu M) + 0.038\ (R^2 = 0.995) \quad \textbf{(IV.2.)}$$

From 150 µM to 1000 µM:

$$1/|Z|\ (kohm^{-1}) = 9.56\ E\text{-}5\ C_{PA}\ (\mu M) + 0.0312\ (R^2 = 0.993) \quad \textbf{(IV.3.)}$$

A low detection limit of 0.92 µM for DA and 1.1 µM for PA was calculated, confirming the capability and the ultrahigh sensitivity of RuNPs/ASPE as an impedimetric sensor.

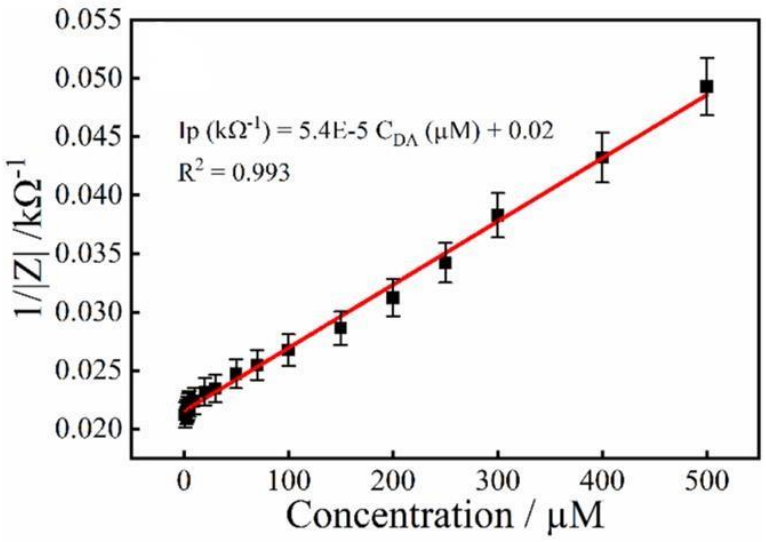

Figure IV.7. RuNPs/ASPE Plot of 1/|Z| *vs*. Concentration for DA in 0.1 M PBS

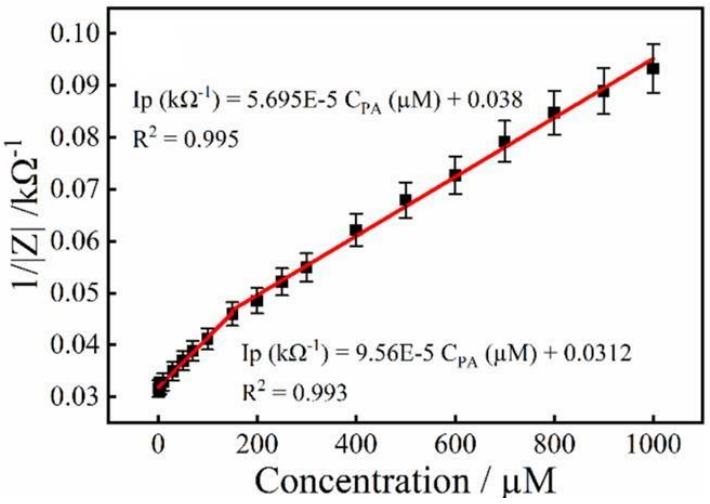

Figure IV.8. RuNPs/ASPE Plot of 1/|Z| *vs.* Concentration for PA in 0.1 M PBS.

Conclusion

For the first time a novel electrochemical impedimetric sensor was constructed in two steps for the detection of paracetamol and dopamine using a quick, easy, and effective electrochemical method. In this part of chapter, electrochemical impedance spectroscopy was given to the identification of mechanisms responsible for the impedance variation at the modified electrode/electrolyte interface. Surface modification of the ASPE led to a marked alteration in charge transfer resistance, and this has been attributed to structural changes that take place in the RuNPs layer.

Impedance responses acquired with the synthesized impedimetric sensor for the detection of dopamine and paracetamol indicated a clear reduction in diameter of the semicircle of the Nyquist plot. Moreover, the sensor was found to have 1.0–500 µM and 1.0–1000 µM ranges for sensing dopamine and paracetamol, respectively.

Cumulatively, the results highlight the excellent potential of the prepared impedimetric platform as an excellent contender for routine analysis uses. Charge transfer kinetic improvements pave the way for future optimization strategies that have the potential to access lower detection limits 0.92 µM for dopamine and 1.1µM for paracetamol, respectively.Overall, the synthesized RuNPs/ASPE sensor is a significant improvement towards the practical, high performance electrochemical sensors useful for advanced sensing applications.

References

[1] R.K. Shervedani, M. Bagherzadeh, S.A. Mozaffari, Determination of dopamine in the presence of high concentration of ascorbic acid by using gold cysteamine self-assembled monolayers as a nanosensor, Sens. Actuators B Chem. 115 (2006) 614–621.

[2] H.D. Ertuğrul Uygun, M.N. Demir, A Novel Fullerene-Pyrrole-Pyrrole-3-Carboxylic Acid Nanocomposite Modified Molecularly Imprinted Impedimetric Sensor for Dopamine Determination in Urine, Electroanalysis 32 (2020) 1971–1976.

[3] S. Chandra, K. Arora, D. Bahadur, Impedimetric biosensor based on magnetic nanoparticles for electrochemical detection of dopamine, Mater. Sci. Eng. B 177 (2012) 1531–1537.

[4] M. Dervisevic, M. Senel, E. Cevik, Novel impedimetric dopamine biosensor based on boronic acid functional polythiophene modified electrodes, Mater. Sci. Eng. C 72 (2017) 641–649.

[5] W. Boumya, M. Achak, M. Bakasse, M.A. El Mhammedi, Indirect determination of dopamine and paracetamol by electrochemical impedance spectroscopy using azo coupling reaction with oxidized 2,4-dinitrophenylhydrazine (DNPH): Application in commercial tablets, J. Sci: Adv. Mater. Devices 5 (2020) 218–223.

[6] N.K. Sharma, A. Nain, K. Singh, N. Rani, A. Singa, Impedimetric sensors: principles, applications and recent trends, Int. J. Innov. Technol. Explor. Eng. 8 (2019) 2278−3075.

[7] A.L. Rinaldi, R. Carballo, Impedimetric non-enzymatic glucose sensor based on nickel hydroxide thin film onto gold electrode, Sens. Actuators B Chem. 228 (2016) 43−52.

[8] A.L. Rinaldi, S. Sobral, R. Carballo, Nickel hydroxide nanoparticles on screen-printed electrodes as an impedimetric non-enzymatic glucose sensor, Electroanalysis 29 (2017) 1−9.

[9] M.L. Chelaghmia, H. Fisli, M. Nacef, D.A.C. Brownson, A.M. Affoune, H. Satha, C.E. Banks, Disposable non-enzymatic electrochemical glucose sensors based on screen-printed graphite macroelectrodes modified with Ni, Cu and Ni/Cu hydroxides for glucose detection in human serum, Anal. Methods 13 (2021) 2740−2749.

[10] M. Emadoddin, S.A. Mozaffari, F. Ebrahimi, An antifouling impedimetric sensor based on zinc oxide embedded polyvinyl alcohol nanoplatelets for wide range dopamine determination in the presence of high concentration ascorbic acid, J. Pharm. Biomed. Anal. 205 (2021) 114278.

[11] R. Signorelli, D.C. Ku, J.G. Kassakian, J.E. Schindall, Electrochemical double-layer capacitors using carbon nanotube electrode structures, Proc. IEEE 97 (2009) 1837−1847.

[12] D.B. Bonham, M.E. Orazem, A mathematical model for the AC impedance of semiconducting electrodes, AIChE J. 34 (1988) 495−502.

[13] Z. Zhang, P. Cui, X.Y. Chen, J.W. Liu, The production of activated carbon from cation exchange resin for high-performance supercapacitor, J. Solid State Electrochem. 17 (2013) 1749−1758

[14] W. Xing, S.Z. Qiao, R.G. Ding, F. Li, G.Q. Lu, Z.F. Yan, H.M. Cheng, Superior electric double layer capacitors using ordered mesoporous carbons, Carbon 44 (2006) 216−224.

[15] D. Thomas, N.B. Fernandez, M.D. Mullassery, R. Surya, Iron oxide loaded biochar/polyaniline nanocomposite: synthesis, characterization and electrochemical analysis, Inorg. Chem. Commun. 119 (2020) 108097.

[16] M. Emadoddin, S.A. Mozaffari, F. Ebrahimi, An antifouling impedimetric sensor based on zinc oxide embedded polyvinyl alcohol nanoplatelets for wide range dopamine determination in the presence of high concentration ascorbic acid, J. Pharm. Biomed. Anal. 205 (2021) 114278.

[17] W. , M. Achak, M. Bakasse, M.A. El Mhammedi, Indirect determination of dopamine and paracetamol by electrochemical impedance spectroscopy using azo coupling reaction with

oxidized 2,4-dinitrophenylhydrazine (DNPH): Application in commercial tablets, J. Sci: Adv. Mater. Devices 5 (2020) 218–223

[18] H.D. Ertuğrul Uygun, M.N. Demir, A Novel Fullerene-Pyrrole-Pyrrole-3-Carboxylic Acid Nanocomposite Modified Molecularly Imprinted Impedimetric Sensor for Dopamine Determination in Urine, Electroanalysis 32 (2020) 1971–1976.

[19] S. Chandra, K. Arora, D. Bahadur, Impedimetric biosensor based on magnetic nanoparticles for electrochemical detection of dopamine, Mater. Sci. Eng. B 177 (2012) 1531–1537.

[20] M. Dervisevic, M. Senel, E. Cevik, Novel impedimetric dopamine biosensor based on boronic acid functional polythiophene modified electrodes, Mater. Sci. Eng. C 72 (2017) 641–649.

[21] N. Plesu, A. Kellenberger, I. Taranu, B.O. Taranu, I. Popa, Impedimetric detection of dopamine on poly(3-aminophenylboronic acid) modified skeleton nickel electrodes, React. Funct. Poly. 73 (2013) 772–778.

[22] B. Zheng, X. He, Q. Zhang, M. Duan, A Novel Molecularly Imprinted Membrane for Highly Sensitive Electrochemical Detection of Paracetamol, Int. J. Electrochem. Sci. 17 (2022) 220736.

[23] H. Dolas, B. SayiNli, A. sezai Sarac, A Determination Method of Dopamine or Epinephrine by Conducting Polymers : The Electrochemical Impedance Spectroscopy, J. Eng. Technol. Appl. Sci. 1 (2016) 89

General conclusion

General conclusion

The objective of this thesis is the exploration of new ruthenium-based nanomaterials deposited on activated screen-printed electrodes and their application as electrochemical sensors for dopamine and paracetamol detection. The development of the ruthenium nanomaterial is done by the initial activation of the graphite surface of SPE in H_2SO_4 solution, followed by the deposition of ruthenium nanoparticles onto the ASPE through cyclic voltammetry method.

Numerous techniques, such as scanning electron microscopy, energy dispersive spectroscopy, X-ray diffraction, transmission electron microscopy, Fourier-transform infrared spectroscopy, and atomic force microscopy, were used to examine the structural characteristics of the synthesized ruthenium nanoparticles and bare SPEs. The formation of uniformly distributed ruthenium nanoparticles on the ASPE was shown by SEM and TEM analyses, which also revealed a spherical structure that is consistent with ruthenium's inherent characteristics. The successful formation of ruthenium nanoparticles on the ASPE electrode was validated by the EDX results, while hexagonal crystal planes of ruthenium were revealed by X-ray diffraction patterns. Ru nanoparticles formed on the ASPE were further identified by Fourier transform infrared spectroscopy.

Electrochemical properties were also studied by voltammetric and impedimetric methods. The results obtained by CV and EIS showed that the synthesized Ru nanoparticles on ASPEs have excellent electrical properties, as well as a significantly larger active surface area than bare graphite electrodes. Furthermore, cyclic voltammetry and square wave voltammetry were used to characterise the new RuNPs/ASPE for the individual and simultaneous detection of trace amounts of paracetamol and dopamine, the obtained limits of detection were 0.11 µM and 0.17 µM for DA and PA, respectively. A wide linear range from 1 µM to 200 µM for DA, and from 1 to 330 µM for PA,respectively, while electrochemical impedance spectroscopy was used for their individual detection.

The versatile RuNPs/ASPE is a promising sensor as three different electrochemical methods can be employed to quantify dopamine and paracetamol , in addition under the best experimental conditions had good analytical performance in sensing these analytes with impressive low limit of detection, very good sensitivity , with outstanding selectivity as well.

This research proved the efficiency and solidity of the elaborated sensor for identifying paracetamol and dopamine in complex environments (hydrochloride injection , pharmaceutical

tablet and human serum samples) with excellent repeatability and reproducibility, and satisfactory selectivity.

Lastly, new electrochemical sensors were prepared for the detection of dopamine and paracetamol. The sensors are inexpensive, simple to prepare, responsive, reproducible, and stable, thus feasible devices for the detection of paracetamol and dopamine. The findings demonstrated that ruthenium nanoparticles are an interesting material for the improvement of the electrochemical properties of activated screen printed graphite electrodes. Furthermore, the incorporation of ruthenium nanoparticles to the sensor synthesis, allows the formation of nanostructured films with high conductivity.

The work conducted in the scope of this thesis opens new avenues, which will be pursued, in an attempt to widen the field of application of the obtained nanomaterials.

- The detection of other pharmaceuticals or pollutants like phenols and pesticides,
- The application of the synthesized ruthenium nanoparticles as supercapacitors or in fuel cells,
- The development of new methods for deposition of RuNPs on SPEs using additives for achieving better performance,
- To consider co-deposits involving other metals, such as transition metals (Ni, Cu, etc.), especially for their low cost for pharmaceutical sensors applications.